

UNIVERSITAT POLITÈCNICA DE CATALUNYA

DEPARTAMENT D'ENGINYERIA ELÈCTRICA



Departament d'Enginyeria Elèctrica



UNIVERSITAT POLITÈCNICA DE CATALUNYA



CITCEA - Centre d'Innovació Tecnològica
en Convertidors Estàtics i Accionaments

PhD Thesis

Feeder flow control and operation in large scale photovoltaic power plants and microgrids

**Part I. Feeder flow control in large scale photovoltaic
power plants**

**Part II. Multi-microgrids and optimal feeder flow
operation of microgrids**

Autor: **Eduard Bullich-Massagué**

Directors: **Andreas Sumper**
Mònica Aragüés-Peñalba

Barcelona, July 2018

Universitat Politècnica de Catalunya
Departament d'Enginyeria Elèctrica
Centre d'Innovació Tecnològica en Convertidors Estàtics i Accionament
Av. Diagonal, 647. Pl. 2
08028 Barcelona

Copyright © Eduard Bullich-Massagué, 2018

Primera impressió, Juliol 2018

**Acta de qualificació de tesi doctoral****Curs acadèmic: 2018-2019**

Nom i cognoms

Eduard Bullich Massagué

Programa de doctorat

Doctorat en Enginyeria Elèctrica

Unitat estructural responsable del programa

Resolució del Tribunal

Reunit el Tribunal designat a l'efecte, el doctorand / la doctoranda exposa el tema de la seva tesi doctoral titulada

Acabada la lectura i després de donar resposta a les qüestions formulades pels membres titulars del tribunal, aquest atorga la qualificació:

 NO APTE APROVAT NOTABLE EXCEL·LENT

(Nom, cognoms i signatura)	(Nom, cognoms i signatura)	
President/a	Secretariària	
(Nom, cognoms i signatura)	(Nom, cognoms i signatura)	(Nom, cognoms i signatura)
Vocal	Vocal	Vocal

_____, ____ d'/de _____ de _____

El resultat de l'escrutini dels vots emesos pels membres titulars del tribunal, efectuat per la Comissió Permanent de l'Escola de Doctorat, atorga la MENCÍÓ CUM LAUDE:

 Sí NO

(Nom, cognoms i signatura)	(Nom, cognoms i signatura)
President/a de la Comissió Permanent de l'Escola de Doctorat	Secretariària de la Comissió Permanent de l'Escola de Doctorat

Barcelona, _____ d'/de _____ de _____

Menció Internacional en el títol de doctor o doctora

- Com a secretariària del tribunal faig constar que part de la tesi doctoral, com a mínim el resum i les conclusions, s'ha redactat i presentat en una de les llengües habituals per a la comunicació científica en el seu camp de coneixement i diferent de les que són oficials a Espanya. Aquesta norma no s'aplica si l'estada, els informes i els experts provenen d'un país de parla hispana.

(Nom, cognoms i signatura)

Secretariària del Tribunal

A la meva mare

Acknowledgements

En primer lloc voldria agrair als directors d'aquesta tesi Andreas Sumper i Mònica Aragüés. Considero que el vostre suport, consells i, en general, la col·laboració en tot moment han resultat molt valuosos. També voldria donar les gràcies a l'Anna Cabrera, que m'ha permés col·laborar amb les seves investigacions, cosa que ha resultat molt útil per a la realització de la tesi.

En segon lloc voldria agrair a tots els companys i companyes del CITCEA-UPC. Tots. Perquè directament o indirectament, tots heu col·laborat durant el transcurs d'aquesta tesi. Dit això, voldria donar les gràcies a l'Oriol Gomis, que ha confiat en mi i m'ha donat la oportunitat per col·laborar en el desenvolupament de projectes reals en instal·lacions fotovoltaïques i microxarxes, així com a en Ricard Ferrer per la gran ajuda amb el PSS/E i el control de les plantes fotovoltaïques. Als companys d'energia: Pol, Pau, Íngrid, Francesc, Mònica, Miguel i Marc Galceran, us vull reconeixer l'ajuda que m'heu prestat durant aquests anys així com tot el que he après de vosaltres i les bones estones que hem compartit. També a l'Edu Prieto i al Paco per a la seva ajuda desinteressada. Als altres companys, amb qui he compartit projectes (o amb qui espero fer-ho en un futur): Andreu, Enric, Marc Cheah, Joan, Gabri, Cristian, Macià, Tomàs, Carlos Miguel, Carlos Collados, Dani Heredero, Marc Pagès, Pablo, Jose i Sergi. Tot això ha estat possible gràcies a que l'equip directiu ha confiat en mi i m'ha donat la oportunitat de formar part d'aquest gran equip, gracies Toni, Dani, Sam, Roberto, Oriol i Andreas. No puc oblidar l'equip de gestió, que sempre estan disposats a donar un cop de mà, a l'Anna, la Maria, l'Adrià i al Jordi.

Je souhaiterais remercier le Dr. Raphael Caire, pour m'avoir ouvert les portes du G2Elab de Grenoble, pour l'intérêt qu'il a porté sur ma thèse, ses conseils et ses commentaires qui m'ont été très utiles pour avancer sur la dernière ligne droite de ce travail. A Bhargav Prassanna Swaminathan qui m'a donné son aide désintéressée et aux collègues Nikolaos, Stéphane, Felix, Karla, Kevin y Laurène.

A GreenPowerMonitor, i especialment al Carlos i al Lluis, els quals han permès la implementació dels controladors desenvolupants en plantes de generació fotovoltaica reals. Ha estat una gran experiència treballar amb vosaltres i per vosaltres.

A la meva família, Mariona, Ramir, Ignasi, Clara, Aina, Bruna i el/la que està per venir, que heu estat sempre al meu costat. També a la Rosa, al

Lluis i la Piedi i tota la colla de cosins i tiets. Voldria expressar especialment la meva gratitud a la meva mare, Mariona, qui em va motivar per iniciar-me en aquesta aventura i que, desafortunadament, no la veurà acabar. No obstant sempre ha estat molt present en els meus pensaments. Gràcies per tot Mariona!

A la meva segona família, els amics: els de 'La Rampa', els de 'La Casesita' (Raul i Solene), a 'Los Pepos', a la Júlia i a tots els que m'heu acompanyat desde ja fa molts anys.

Abstract

This thesis deals with the integration of photovoltaic energy into the electrical grid. For this purpose, two main approaches can be identified: the interconnection of large scale photovoltaic power plants with the transmission network (high voltage), and the interconnection of small and medium-scale photovoltaic installations with the distribution network (medium and low voltage).

The first part of the thesis is focussed on the interconnection of large scale photovoltaic power plants. Due to the increase of photovoltaic generation in the electrical energy share, large scale photovoltaic power plants are required to provide different ancillary services to the electrical networks. For this purpose, it is necessary to control the active and reactive power injected by photovoltaic power plants at the point of interconnection, i.e. to control the power flow through the main feeder. In this direction, it is developed a central controller capable of coordinating the different devices of the photovoltaic power plants as photovoltaic inverters, FACTS, capacitor banks and storage.

The second part is focused on the distributed generation, consisting on small and medium-scale generation facilities connected to the distribution system. In this context, distribution grids, traditionally operated as passive systems, become active operated systems. In this part, the microgrid concept is analysed, which is one of the most promising solutions to manage, in a coordinated manner, the different distributed energy resources. Taking into account the possible transformation of the current distribution system to a multi-microgrid based system, the different architectures enabling microgrids interconnections are analysed. For the multi-microgrid operation, it could result interesting that a portion of their networks operate so that the power exchange is maintained constant, i.e. controlling the power flow at the main feeder. In this thesis, an optimal power flow problem formulation for managing the distributed generation of these feeder flow controlled microgrids is proposed.

Resum

La present tesi tracta de la integració d'energia fotovoltaica en xarxes elèctriques. Per a tal finalitat, es poden identificar dues grans tendències en l'actualitat: la interconnexió de grans plantes de generació en la xarxa de transport (alta tensió), i la interconnexió de petites i mitjanes instal·lacions en la xarxa de distribució (mitja i baixa tensió).

La primera part s'enfoca a la interconnexió de grans plantes de generació fotovoltaica. Degut als canvis dels darrers anys en el mix de generació elèctrica, les grans plantes de generació fotovoltaica es veuen obligades a donar diversos serveis de suport a les xarxes elèctriques. Per a aquesta finalitat, resulta necessari controlar la potència activa i reactiva que la planta injecta en el punt de connexió, és a dir, controlar la potència en la línia d'alimentació principal, *feeder*. En aquest sentit, es desenvolupa un controlador central capaç de coordinar els diferents elements de les plantes fotovoltaiques com els inversors fotovoltaics, FACTS, bancs de condensadors i bateries d'emmagatzematge.

La segona part s'enfoca a l'anomenada generació distribuïda, de la que formen part les petites instal·lacions generadores connectades a la xarxa de distribució. En aquest context, aquestes xarxes passen de ser operades de forma passiva a forma activa. En aquesta part s'analitza el concepte de microxarxa, una de les solucions més prometedores per gestionar els diferents recursos distribuïts. Donat que es pot esperar una transformació del sistema de distribució actual a un sistema basat en multi-microxarxes, s'analitzen les diferents arquitectures amb les quals aquestes es poden interconnectar. Per la operació de multi-microxarxes pot resultar interessant que algunes microxarxes operin de forma que la potència intercanviada amb la xarxa externa sigui constant, és a dir, controlant el flux de potència de la línia d'alimentació principal. En aquesta tesi es realitza la formulació d'un problema d'optimització de fluxos de potència per gestionar la generació distribuïda d'aquestes microxarxes.

Contents

List of Figures	xiii
List of Tables	xvii
Thesis outline	xix
Nomenclature	xxi
1 Introduction	1
1.1 Context	1
1.2 Objectives and scope	2
1.2.1 Part I	2
1.2.2 Part II	3
I Feeder flow control in large scale photovoltaic power plants	7
2 Introduction to large scale photovoltaic power plants	9
2.1 Introduction	9
2.2 General description of PV power plants	11
2.2.1 Classification	11
2.2.2 Main components	11
2.2.3 Collection grid architectures	16
2.2.4 Other equipment of PV power plants	19
2.3 Grid code requirements	19
2.3.1 Fault ride through	20
2.3.2 Frequency limits	20
2.3.3 Reactive power control and voltage regulation	20
2.3.4 Active power control and frequency regulation	23
2.4 Conclusions	24
3 Power plant control in large scale photovoltaic power plants	25
3.1 Introduction	25

Contents

3.2	Power plant control design	26
3.2.1	LS-PVPP description	26
3.2.2	Active power control design	28
3.2.3	Reactive power control design	30
3.3	Results	34
3.3.1	Case study	34
3.3.2	Simulation results	34
3.3.3	Test site results	40
3.4	Conclusions	44
4	Active Power Control in a Hybrid PV-Storage Power Plant for Frequency Support	45
4.1	Introduction	45
4.2	Power plant control design	47
4.2.1	Hybrid PV-Storage power plant description	47
4.2.2	Controller architecture	47
4.2.3	Reference computation	48
4.2.4	Summary	55
4.3	Results	57
4.3.1	Case study	57
4.3.2	Simulation results	57
4.4	Conclusions	65
II	Multi-microgrids and optimal feeder flow operation of microgrids	67
5	Introduction to microgrids	69
5.1	Introduction	69
5.2	The microgrid concept	70
5.2.1	Definition	70
5.2.2	Microgrid connected to an external distribution grid .	71
5.2.3	Point to point connection between microgrids	72
5.3	Multi-microgrids	74
5.4	Control of microgrids	76
5.4.1	Hierarchical control architecture of microgrids	76
5.4.2	Control strategies for DG in microgrids	76
5.5	Conclusions	78

6 Multi-microgrid architectures	79
6.1 Introduction	79
6.2 Architectures for clustering microgrids	80
6.2.1 Layout	80
6.2.2 Line technology	82
6.2.3 Interconnection technology	83
6.3 Qualitative comparison of architectures	83
6.3.1 Cost	83
6.3.2 Scalability	86
6.3.3 Protection	89
6.3.4 Reliability	94
6.3.5 Stability	99
6.3.6 Communications	104
6.3.7 Business models	110
6.3.8 Summary	113
6.4 Conclusion	113
7 Optimal feeder flow control for grid connected microgrids	117
7.1 Introduction	117
7.2 Formulation of the optimal feeder flow problem	118
7.2.1 Notation	119
7.2.2 Stochastic formulation	119
7.2.3 Power flow equations	119
7.2.4 UPC and FFC constraints	123
7.2.5 Objective function	125
7.2.6 Optimal feeder flow problem	127
7.3 Case study	130
7.4 Results	130
7.4.1 Convergence	131
7.4.2 Feeder flow control performance	133
7.5 Conclusion	138
8 Conclusions	139
8.1 Contributions	139
8.2 Future work	141
Bibliography	143
9 Publications	163
9.1 Related journal articles	163

Contents

9.2	Related conference papers	163
9.3	Other Publications	164
9.3.1	Other journal articles	164
9.3.2	Other conference papers	165
A	Simulation model of Vanju-Mare PV power plant	167
A.1	Electrical data	168
B	Working principle of the measurement filter for improving the ramp rate performance	171
C	Simplified simulation model of Vanju-Mare PV power plant	173
D	IEEE 33-Bus distribution system data	177

List of Figures

2.1	Global annual solar PV installed capacity	10
2.2	European share in installed capacity in 2005 and 2017	10
2.3	PV module interconnections	13
2.4	Characteristic curves of the PV array	14
2.5	PV inverter topologies	15
2.6	Simplified scheme of a PV inverter and its control architecture	17
2.7	Typical LS-PVPP configuration	17
2.8	PV power plant collection grid topologies	18
2.9	LVRT and HVRT requirements	21
2.10	Minimum reactive power capability in LS-PVPPs	23
3.1	PV plant control design and implementation process	27
3.2	General scheme of a LS-PVPP and its central controller (ring configuration)	28
3.3	Active power control scheme	28
3.4	Droop curves for frequency regulation	30
3.5	Reactive power control scheme	31
3.6	Droop curve for voltage regulation	32
3.7	Capacitor bank connection/disconnection criterion	33
3.8	Vanju-Mare PV plant	35
3.9	Control response of: active power, reactive power and power factor setpoints (simulation 1)	36
3.10	Frequency droop response (simulation 2)	37
3.11	Control droop modes response (simulations 2 and 3)	38
3.12	Filter response performance (simulation 4)	39
3.13	PPC implementation scheme	41
3.14	Active and reactive power response in Vanju-Mare PV plant .	43
3.15	Power Factor response in Vanju-Mare PV plant	44
4.1	General scheme of a hybrid PV-battery power plant	47
4.2	Power plant controller architecture	48

List of Figures

4.3	Modes of the reference computation block. MPP: PCC set-point = rated power and the plant operates at the MPP. Droop 1: frequency deviation during MPP mode. Curtailment: TSO sets a PCC setpoint different than the rated power. Also applied for the transition from Droop 1 to MPP mode. Droop 2: frequency deviation during curtailment mode	49
4.4	Reference computation block - MPP mode concept. This basic scheme is just to help understanding how it works	49
4.5	Reference computation block - MPP mode. Proposed control scheme	51
4.6	Example of ramp rate performance without and with filter. $T_w = 2$ s. Total communication delay + battery response time = 50 ms (2.5% of T_w). Total communication delay + PV plant response (PV controller + inverter dynamics) ≈ 1 s (50% of T_w)	52
4.7	Droop application under MPP mode	54
4.8	Droop application under curtailment mode	55
4.9	Flow diagram of the control solution	56
4.10	Simulation of a complete day under MPP mode. Top plot: PCC (blue), PV (red), and battery (green) active power. Bottom plot: SOC (blue) and 0.4-0.6 p.u. range (dashed)	58
4.11	Comparison of SOC control strategies (MPP mode). Top plot: PV power profile. Bottom plot: SOC for both strategies, $SOC^* = 0.5$ in blue and $SOC^* = \text{eq. (4.5)}$ in red.	59
4.12	Ramp rate performance during 43 days for different scenarios: i) without battery, ii) with battery 1 MW and iii) with battery 7 MW	61
4.13	PV, battery and PCC active power response after curtailment. Curtailment is set at 2 MW between 29800 s and 32000 s (blue dashed line).	62
4.14	Frequency droop response during curtailment. PCC, PV and battery active power and SOC control analysis. Up frequency event. Enough PV power is available and no battery support is required.	63
4.15	Frequency droop response during curtailment. PCC, PV and battery active power and SOC control analysis. Down frequency event. Lack of PV power available and battery provides support to comply the setpoint.	64

4.16 Frequency droop response during MPP operation mode. PCC, PV and battery active power analysis. In this case, there is enough PV power. So, no battery support is required.	64
5.1 Scheme of a microgrid	71
5.2 Microgrid as a single entity viewpoint. Interconnection to an external distribution grid	72
5.3 Interactions between interconnected microgrids	74
5.4 Hierarchical control architecture for microgrids	77
5.5 Power control mode of a DG	78
6.1 Layout architectures	81
6.2 Power Router architecture	83
6.3 Example of a cluster of 4 microgrids under GSIM and PCM layout architectures for cost comparison	84
6.4 Protections schemes in function of the layout	92
6.5 Communication architectures for PCM layout	105
6.6 Communication architectures for GSIM layout	106
6.7 2-level communication architecture for MPSC layout	107
7.1 Scheme of the DistFlow model	121
7.2 Scheme of IEEE 33-Bus distribution system	130
7.3 Scenarios used for the optimization problem	131
7.4 Convergence process of the proposed algorithm	132
7.5 Algorithm evolution. Analysis of the relaxation gap and the objective function	133
7.6 Active power generation (generator 2) and active power feeder flow for 25 random scenarios	134
7.7 Voltages for 25 random scenarios	136
A.1 Scheme of Vanju-Mare PV plant simulation model in PSS/E®. Red = 100 kV, black = 20 kV, blue = 0.315 kV, grey = 0.27 kV	167
B.1 Ramp rate response after a 1 MW PV power step at second 200. Conventional method without the filter	172
B.2 Ramp rate response after a 1 MW PV power step at second 200. Proposed method: filter applied	172
C.1 Simplified PV generator model	173
C.2 Simplified Battery model	174

List of Figures

C.3 Simplified model of the hybrid PV-storage power plant	175
D.1 Scheme of IEEE 33-Bus distribution system	177

List of Tables

2.1	Details of some operational LS-PVPPs	16
2.2	Frequency limits and disconnection times	22
3.1	PV power installed capacity controlled by the PPC	42
4.1	Time [min] during which the SOC is out of the standby condition (43 days of simulation)	60
4.2	Total energy flow through the battery [kWh] (43 days of simulation)	60
5.1	Possible microgrid ancillary services	73
6.1	Layout architecture vs. cost	85
6.2	Line technology vs. cost	86
6.3	Interconnection technology vs. cost	87
6.4	Layout architecture vs. scaling capacity	88
6.5	Line technology vs. scaling capacity	89
6.6	Interconnection technology vs. scaling capacity	90
6.7	Layout architecture vs. protections requirements	92
6.8	Line technology vs. protections	94
6.9	Interconnection technology vs. protections	95
6.10	Layout architecture vs. Reliability	97
6.11	Line technology vs. Reliability	98
6.12	Interconnection technology vs. Reliability	99
6.13	Layout architecture vs. stability	101
6.14	Line technology vs. stability	102
6.15	Interconnection technology vs. stability	103
6.16	Layout vs. communications and operation	107
6.17	Line technology vs. communications and operation	109
6.18	Interconnection technology vs. communications and operation	110
6.19	Overall comparisson between the presented microgrid clustering architectures	113

List of Tables

7.1	Sets definition	119
7.2	Variables definition	120
7.3	Parameters definition	121
7.4	Optimal setpoints. $(FFP_n^*, FFQ_n^*) = (1350 \text{ kW}, 900 \text{ kvar})$.	135
7.5	Optimal setpoints. $(FFP_n^*, FFQ_n^*) = (2500 \text{ kW}, 1500 \text{ kvar})$.	137
A.1	Grid nodes	168
A.2	Equivalent grid data	169
A.3	Line data	169
A.4	3 winding transformer data	169
A.5	2 winding transformer data	170
C.1	Parameters used in the simulation	175
D.1	Bus data	178
D.2	Line data	179
D.3	Additional parameters	179

Thesis outline

This PhD presents the studies developed on the feeder flow control and operation in large scale photovoltaic power plants and microgrids. The context, the objectives and the scope are explained in **Chapter 1**. Then, this thesis is organized into two parts.

Part I is focused on the control of large scale photovoltaic power plants and is divided into three chapters. The energetic scenario is explained in **Chapter 2**, where the current situation of photovoltaic installations, large scale photovoltaic power plants devices and topologies and the grid code requirements are described. Then, the control of active and reactive power in large scale photovoltaic power plants with absence of storage is described in **Chapter 3**. To improve the frequency and active power support functions, a battery energy storage is included in **Chapter 4**, where the coordinated operation of the photovoltaic inverters together with the battery energy storage is developed.

Part II is focused on microgrids and multi-microgrids and is divided into three chapters. **Chapter 5** provides the context of the microgrid concept. Then, the multi-microgrids are analysed in **Chapter 6**. Research on multi-microgrids has only been focused on the control and operation. In contrast, this chapter defines and analyses the multi-microgrid interconnection architectures and a qualitative comparison is performed. In a multi-microgrid system, some microgrids might be operated so as to maintain a constant power exchange with the external networks. In this direction, **Chapter 7** explains a novel formulation of an optimal power flow problem for those microgrids that operate in a way that the power exchange with external grid is controlled, i.e. for feeder flow controlled microgrids. In addition, an algorithm for solving the optimal power flow problem is proposed.

Finally, **Chapter 8** summarizes the conclusions of the thesis.

Nomenclature

AC	Alternating Current
DC	Direct Current
DER	Distributed Energy Resource
DG	Distributed Generation
EMS	Energy Management System
EPS	Electrical Protection System
ESS	Energy Storage System
FACTS	Flexible AC Transmission System
FFC	Feeder Flow Control
FRT	Fault Ride Through
GSIM	Grid Series Interconnected Microgrids
H2020	Horizon 2020
H2030	Horizon 2030
HV	High Voltage
HVRT	High Voltage Ride Through
IEA	International Energy Agency
IEEE	Institute of Electrical and Electronics Engineers
LS-PVPP	Large-Scale PV Power Plant
LV	Low Voltage
LVRT	Low Voltage Ride Through
MISOCP	Mixed Integer Second Order Cone Programming
MPP	Maximum Power Point
MPPT	Maximum Power Point Tracker
MPSC	Mixed Parallel-Series Connection
MV	Medium Voltage
NREL	National Renewable Energy Laboratory
OFFP	Optimal Feeder Flow Problem
PF	Power Factor
PI	Proportional Integral
PLL	Phase Locked Loop

List of Tables

PCC	Point of Common Coupling
PCM	Parallel Connected Microgrids
PPC	Power Plant Controller
PPT	Power Point Tracker
PV	Photovoltaic
SCADA	Supervisory Control And Data Acquisition
SOC	State Of Charge
SOCP	Second Order Cone Programming
STATCOM	STATIC synchronous COMPensator
TSO	Transmission System Operator
UPC	Unit output Power Control

Chapter 1

Introduction

1.1 Context

As global warming and the consequent climate change are one of the major problems for the present and the future of the Globe, different policies and initiatives have been established to slow down and push back their effects. For example, the European Union established an ambitious long term goal of reducing the greenhouse emissions by at least 80% with respect to the emissions in 1990. To achieve this goal, partial objectives for the horizon years 2020 and 2030 have been defined. Particularly, the Horizon 2020 (H2020) defines that the energetic scenario in 2020 must ensure that 20% of the energy consumption comes from renewable sources, a CO₂ emission reduction of 20% and the improvement of the energy efficiency by 20% compared to 1990 levels. On the other hand, the H2030 targets increase the cut in CO₂ emissions and the share of renewable energy consumption up to 40% and 27%, respectively, as well as imposes a 27% of energy savings [1, 2]. These objectives encourage the bulk integration of renewable energy sources, which has been mainly dominated by wind and photovoltaic (PV) technologies [3]. Two main approaches are being considered for the integration of renewable energy into the electric power system. The first is through large wind and PV installations from few MW to hundreds of MW, which are commonly connected to the electric transmission system. On the other hand, the second approach is through smaller scale installations connected to the distribution networks [4].

The displacement of the conventional generation power plants to wind and PV technologies is leading to several technical challenges at transmission and distribution levels. At transmission level, the term wind or PV power plants is displacing the concept of wind or PV farms because they are required not only to generate electrical power but also to provide grid support functions as conventional generation plants do [3]. Despite these power plants are composed by many interconnected generation units, from the transmission

grid viewpoint they are seen as a single generation unit. Accordingly, most of the required grid support functions are defined at the interconnection point between the power plant and the network, being necessary the development of controllers capable to manage the power flow at the interconnection feeder.

Similarly, the installation of renewable generation at distribution level is changing the way these low voltage (LV) and medium voltage (MV) grids are being operated. In this direction, the concepts of smart grid and microgrid have emerged. Microgrids are smart distribution networks that integrate distributed energy resources (DERs) and can be operated as a single entity from both, the grid and the market perspective [5,6]. The presence of intermittent power generation such as wind and PV together with time-varying loads in microgrids can compromise the grid stability causing, for example, voltage variations [7]. Accordingly, in a near future, when many microgrids will be interconnected forming multi-microgrid systems, the control of the power exchange between the microgrids and the external grid will be required, i.e. the control of the feeder flow at the point of interconnection [7,8].

1.2 Objectives and scope

The main objective of this thesis is to develop useful and efficient methods for controlling the feeder flow at large scale PV power plants (LS-PVPPs) as well as at grid connected microgrids. For this purpose, this thesis is divided into two main parts with differentiated objectives:

1.2.1 Part I

The first part, entitled *Feeder flow control in large scale photovoltaic power plants*, has the main objective of developing a power plant controller (PPC) for LS-PVPPs. This PPC will be in charge of controlling the active and reactive power flow at the main feeder providing grid support functions and complying with the grid code requirements at the connection point. For this purpose, this part is divided into three chapters with the following specific objectives:

- **Analyse the current status of LS-PVPPs**

An overview of the current situation of the renewable power installations is provided. Then the elements of the LS-PVPPs and their configuration are reviewed. Finally, the grid support functions demanded by different countries are analysed, concluding that central controllers are necessary to comply with these requirements.

- Design a PPC that coordinates all the PV inverters within a LS-PVPP together with the reactive power support devices such as flexible alternating current transmission systems (FACTS) and capacitor banks.

A PPC design is proposed in order to comply with grid support function requirements for those LS-PVPPs that do not include any energy storage device. The proposed PPC combines a hysteresis based dispatch system for deciding the connection of capacitor banks with a low pass filter for the voltage measurement at the feeder. This way, reactive power response oscillations are avoided when the voltage droop support is required. The controller also includes the possibility of installing FACTS devices. In addition, a basic active power controller is also implemented. Transmission System Operators (TSOs) have permitted the interconnection of the power plants. Accordingly, the PPC has been implemented in several LS-PVPPs that are currently operative, validating the proposed control scheme.

- Design a PPC that coordinates all the PV inverters within a LS-PVPP together with energy storage devices for providing grid frequency support functions.

The proposed PPC has been enhanced adding the possibility to include energy storage devices for providing active power ramp rate and frequency support requirements. The controller mitigates the power fluctuations caused by clouds passing over the LS-PVPPs by requiring the energy storage to inject or consume the required active power. In addition, the state of charge (SOC) is also controlled so that the energy storage device is charged when down ramps of active power can be expected and being discharged when up active power ramps are more probable. On the other hand, it is identified that the response, which is not instantaneous, can cause problems on the ramp rate limitation. Accordingly, a solution has been proposed. The storage system does not operate at the maximum active power in order to be able to provide down frequency support when required. The PPC has been validated by means of simulations.

1.2.2 Part II

The second part, entitled *Multi-microgrids and optimal feeder flow operation of microgrids*, has the main objective of analysing the possible future distribution grid architectures and to propose an energy management system

(EMS) for optimizing the operation of microgrids. Their local controllers are in charge of controlling the power exchange at the interconnection feeder. For this purpose, this part is divided into three chapters with the following objectives:

- **Define and analyse the microgrid and multi-microgrid concepts and their control architectures.**

A review of the microgrid concept and its development status is performed. In addition, the multi-microgrid concept is presented. The control architecture is also reviewed as well as the distributed generation (DG) local control. The feeder flow control (FFC) method is identified as a promising solution for providing grid support functions for multi-microgrids.

- **Define how the future distribution system based on multi-microgrids could be designed and evaluate, qualitatively, the possible performance characteristics of each possibility.**

The way microgrids can be interconnected forming multi-microgrids can affect their performance. Accordingly, an analysis about the possible multi-microgrid architectures is performed. For this purpose, the basic architectures are defined according to the layout, the line technology and the interconnection technology. Then a qualitative analysis regarding the strong points and the weaknesses of each architecture is performed. This permits to give an insight on how the future networks should be built depending on the necessities of the region, and to define the most interesting cases to be studied.

- **Propose a novel optimization problem for an EMS of feeder flow controlled microgrids considering the uncertainty and the power flow constraints.**

Multi-microgrid systems are expected to require grid support functions from microgrids. One of these functions is to control a constant power exchange at the interconnection feeder, the so-called FFC. In this thesis an optimization problem for feeder flow controlled microgrids is proposed. To obtain the optimum active and reactive power setpoints of the DGs, the PV and load forecasting uncertainty is considered by means of stochastic formulation. This permits to obtain better setpoints than just considering the forecasted scenario, improving the objective function and the grid performance. The optimization problem formulation considers the power flow equations in its relaxed form, leading to a mixed integer second order cone problem (MISOCP)

1.2 Objectives and scope

formulation. This permits to find a global optimum despite being a non-linear problem. As the objective function does not meet the conditions to ensure the relaxation holds, an alternative reformulation is proposed. Particularly, the objective function is penalised by the currents and an algorithm to find the minimum penalty weight to ensure the relaxation holds is proposed. The algorithm is applied to the IEEE 33-bus distribution system. The convergence of the algorithm is shown, also proving the global optimum is found. In addition the stochastic formulation is compared to a non-stochastic one, showing the advantages of the proposed method.

Part I

Feeder flow control in large scale photovoltaic power plants

Chapter 2

Introduction to large scale photovoltaic power plants

2.1 Introduction

The energy demand has commonly been supplied by fossil fuels. Due to the adverse effects of these energy sources, the human-induced climate change has became one of the major global challenges worldwide. In this direction, international agreements to reduce the greenhouse gas emissions have been signed, i.e. the Kyoto protocol and its amendment [9]. On the other hand, the last update from the International Energy Agency (IEA) indicates that electricity, heat and transport sectors represent 2 thirds of the global CO₂ emissions [10]. Accordingly, the electrical generation from renewable energy sources is one of the key issues for mitigating the global warming.

Due to the rising awareness around clean energy, the variability of electricity price and the reduction of fossil fuel reserves, countries and organizations consider renewable energy as a solution to satisfy the future energy demand. Among the different renewable energy resources, wind and PV power technologies are by far the most representative in the electric sector. Particularly, the PV market has grown significantly during the last decade, mainly dominated by China. As it can be observed in Figure 2.1, while around 20 GW of PV power was installed in 2010, this value raised up to 76 GW in 2016. In the case of PV facilities, rooftop PV installations were dominant until the early 2000. But during last years, motivated by the uncapped incentive schemes, utility-scale or LS-PVPPs have become dominant, reaching in 2016 a total of 72 % of the total new PV facilities [4]. On the other hand, according to Wind Europe [11], the annual renewable power capacity installed in Europe has represented over 60 % of the total new power installations during the last decade and around 80 % since 2014. As a result, the electric power generation capacity has experienced a significant change as shown in Figure 2.2, where it can be observed that the PV and wind power share

raised from 6.3% in 2005 to 29.5 % in 2017.

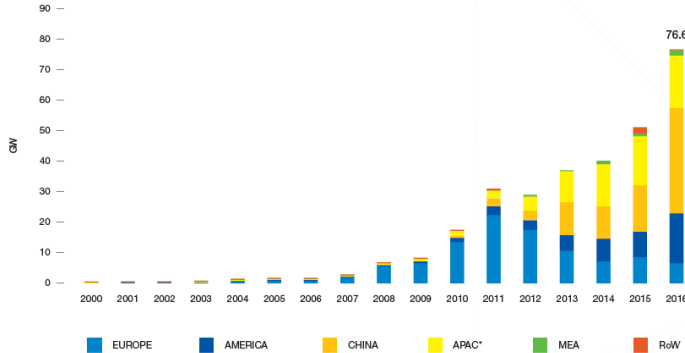


Figure 2.1: Global annual solar PV installed capacity. *Apac excluding China [4]

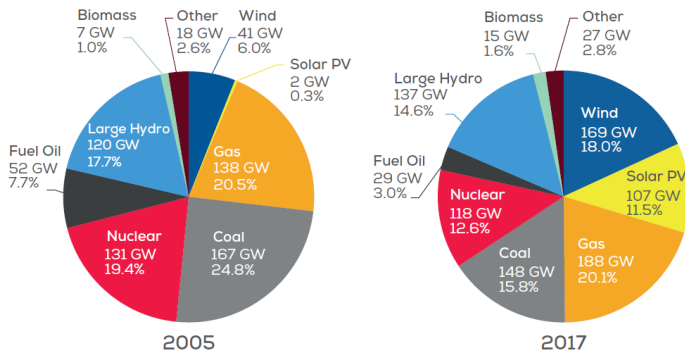


Figure 2.2: European share in installed capacity in 2005 and 2017 [11]

The electric grid has traditionally been controlled by synchronous generators. To ensure the grid stability in the new scenario with large portion of PV and wind power penetration, renewable power plants should also participate in the grid support functions. Accordingly, standards and grid codes have been (and are currently being) updated. One of the main changes is the inclusion of more restrictive grid support requirements. Due to the intermittent and non-dispatchable nature of wind and PV resources, the control of renewable power plants to fulfil these new requirements has become challenging. In the case of PV technology, its lack of inertia (stored kinetic energy)

2.2 General description of PV power plants

leads to additional difficulties for the management of the active power. As a solution, hybrid systems including PV and storage are being considered for improving its integration into the electrical grid.

2.2 General description of PV power plants

2.2.1 Classification

There are two main approaches for the grid integration of PV power: i) the interconnection of PV power facilities into the distribution system, i.e. the MV or LV grid and ii) the interconnection of PV power plants into the transmission system, i.e. the high voltage (HV) grid. In the first case, the power plants have capacities from 1 kW to few MW and are typically installed in the rooftops of customer residences, government sites or directly connected to distribution feeders [12]. On the other hand, LS-PVPPs (also known as utility-scale) are commonly connected to the transmission system. Note that distribution networks have technical constraints for the integration of large amount of generation, hence LS-PVPPs are rarely connected to these networks [13]. Despite there is not a clear definition about what is considered a LS-PVPPs, it is well accepted that they are power plants from several MW to GW scale [14]. For example, the National Renewable Energy Laboratory (NREL) sets the threshold at 5 MW [15].

2.2.2 Main components

PV modules, strings and arrays

The basic generation units of PV power plants are the PV cells, whose mission is the conversion of the solar energy into electricity. Solar cells can be classified according to the materials they are composed. Crystalline and thin film technologies dominate the market. Crystalline (c-Si) solar cells are based on mono or poly crystalline silicon. Due to the one single crystal in mono crystalline solar cells, electron's movement is less obstructed obtaining greater efficiencies, which are around 22 %. On the other hand, poly crystalline technology presents little lower efficiencies, but its lower manufacturing cost makes this material attractive. In contrast, thin film based solar cells present much lower costs than crystalline technology due to its reduced amount of semiconductor material required. Thin film solar cells can use different materials as amorphous silicon (a-Si), Cadmium-Telluride (CdTe), Copper-Indium-Selenide (CIS) among others. One of the main dis-

advantage of these technologies is the efficiency that can vary from 4 % to 15 % [16].

The voltage produced by a solar cell at its maximum power point (MPP) is around 0.5 V, which is not practical for real applications. To produce useful voltages, tens of solar cells are interconnected in series and encapsulated obtaining the basic commercial unit, known as the PV module [17]. The power output of a PV module is relatively small, in the order of several tens or hundreds W. In addition, the output of the PV panels is direct current (DC) while the electrical grid is alternating current (AC), 50 Hz or 60 Hz. Hence, for grid connected PV systems, a PV inverter must be installed. Accordingly, the DC characteristics of the PV output must be coherent with the DC characteristics of the PV inverter, i.e. the maximum current, the nominal and minimum voltage and the maximum power point tracking (MPPT) range. To obtain the desired characteristics and higher power output, PV modules can be interconnected in series or parallel [17]. Commonly, PV modules are first interconnected in series, obtaining a PV string, whose output voltage is proportional to the number of modules in series. Once this voltage is adequate, different strings can be connected in parallel, using a junction box, obtaining higher output current and power [18]. These interconnections can be observed in Figures 2.3(a), 2.3(b) and 2.3(c), respectively.

The current generated by PV modules depends on the voltage at their terminals, on the irradiation they receive and on the ambient temperature as shown in Figure 2.4, obtained after simulating a PV array of 118 parallel strings formed by 16 series connected modules *Artesa A-265M GS* using the model developed in [19]. As it can be observed, the active power generation is proportional to the irradiation received by PV modules, strings or arrays and decreases with the increase of the temperature. In addition, the DC voltage also has a great influence on the power generation. In fact, as the ambient conditions are not controllable, the power generation will be controlled varying the DC voltage thanks to a power converter.

PV converters

Power converters are power electronic devices used as interface elements between two electrical systems with different voltage nature. In the case of PV converters, they serve as interface between the DC side of the PV module, PV string or PV array with the external grid, which is usually AC. In addition, they have the task of controlling the DC voltage so that the solar panels operate at the desired point, which can be the MPP or below

2.2 General description of PV power plants

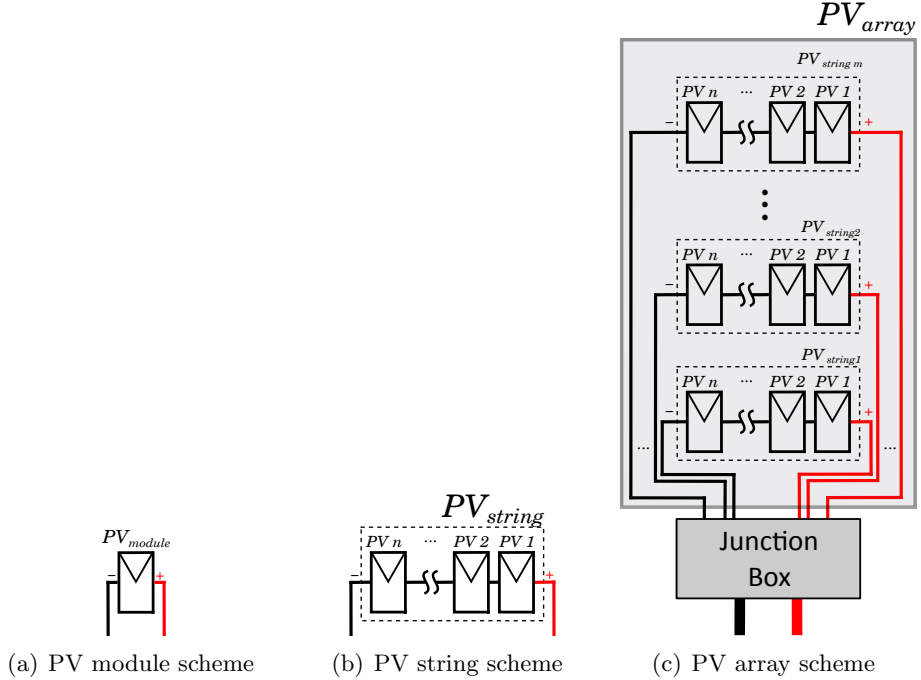


Figure 2.3: PV module interconnections

it, i.e. to a specific power point, and to control the reactive power at the AC side.

Considering an AC external grid, PV converters can have one or two conversion stages. The first consists of a single DC-AC inverter, while two stage converters add an additional DC-DC converter. On the other hand, as depicted in Figure 2.5, different topologies of PV inverters have been considered. Central inverters integrate a PV array using a single converter. In the multi-string topology, different PV strings are interconnected to a DC line through DC-DC converters and a central AC-DC converter is in charge of interconnecting the AC and the DC sides. In contrast, in the string topology, each PV string is directly connected to the AC side through a DC-AC inverter. Finally, each PV module is connected to a DC-AC inverter in the module integrated inverter architecture [20–22].

The configuration identified as single stage central DC-AC_{3-phase} converter has high mismatch losses between PV panels, poor centralised MPPT efficiency and lower reliability than other configurations. Nevertheless, it is the most used architecture in LS-PVPPs because of the simplicity and the lower investment and maintenance costs [18, 22]. Their power rating is

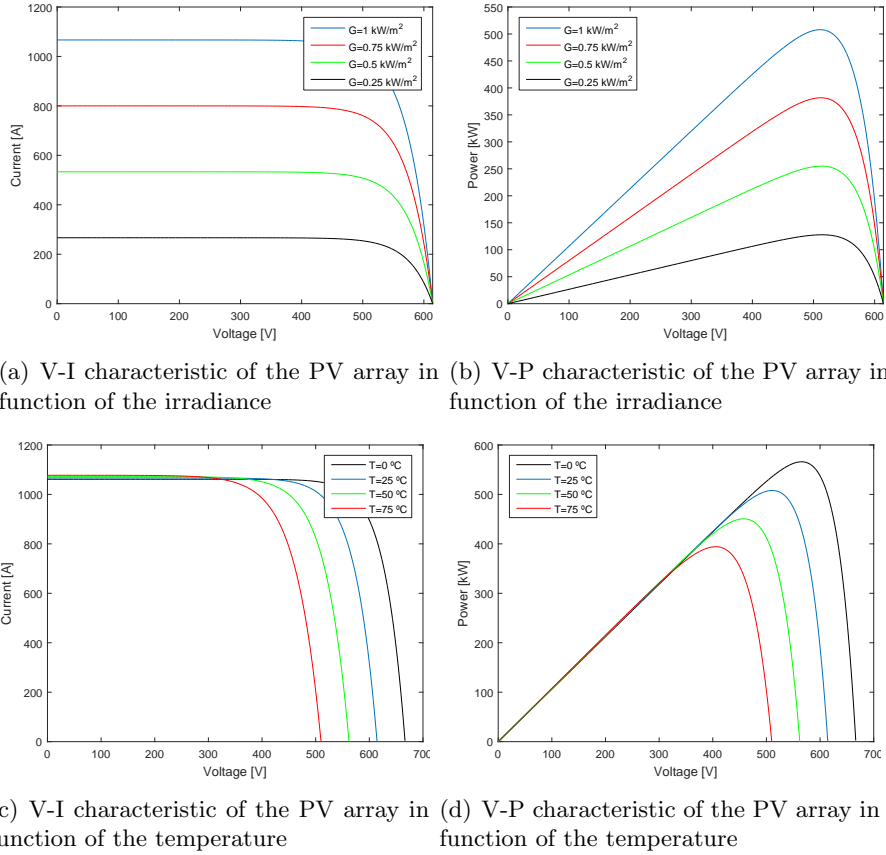


Figure 2.4: Characteristic curves of the PV array

from 100 kW to 1500 kW with a MPPT DC voltage that oscillates between 400 and 1000 V, being the output voltage between 270 and 400 V_{3-phase}. Table 2.1 shows the inverter topologies for some LS-PVPPs among other characteristics, showing that effectively, central inverters are dominant.

Central converters have two important control tasks: the active power control and the reactive power control. The control scheme and tuning of a voltage source converter for renewable energy generation systems is explained in detail in [23], and specific controllers for PV inverters are discussed in [24]. The first control stage is the synchronisation with the external grid, which is done by a phase locked loop (PLL). As it has been shown previously, the active power generated by the PV units depends on the DC voltage. Accordingly, a first control layer named power point tracker (PPT)

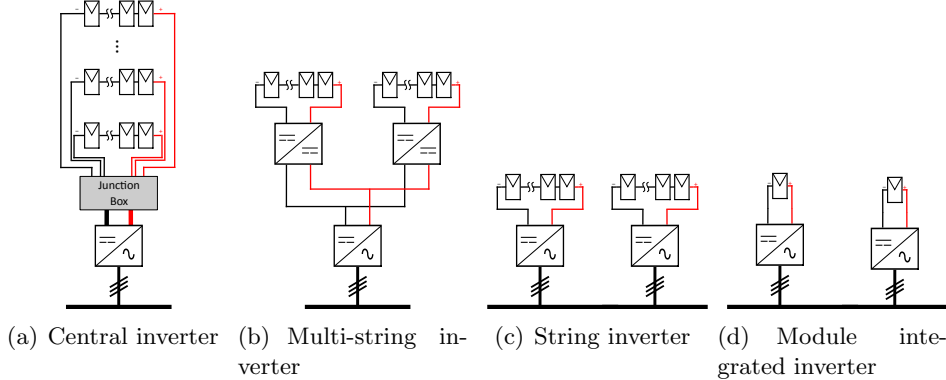


Figure 2.5: PV inverter topologies

is responsible to set the DC voltage setpoint in order to achieve the desired active power generation, which can be the maximum available active power or a fixed value. The controller of the DC voltage and the reactive power, which can be based on a proportional-integral (PI) controller, determines the current references in the synchronous reference frame. Then, an inner control loop is in charge of implementing these currents finding the AC voltages to be applied by the PV converter. Finally, the switching to reach the desired voltages are set by the voltage modulation block. A simplified scheme is shown in Figure 2.6. In addition, the controllers provide fault support functionalities and islanding detection for disconnecting in case of detecting islanding operation.

Power transformers

As stated before, LS-PVPPs are commonly connected to HV transmission lines. Usually, the output of the PV inverters is below 1000 V. The interconnection of the PV inverters to the utility grid is done through two transformation stages as shown in Figure 2.7. Some examples of this configuration can be found in [25–27]. First, the LV output of the PV inverters is stepped up to few kV according to the PV plant collection grid voltage rating, which is usually within the MV range. This transformation can be done using two or three winding transformers, being the later the most used topology. Then, a two winding transformer elevates the collection grid voltage to perform the connection of the PV plant to the external grid at the point of common coupling (PCC) providing, at the same time, galvanic isolation to the PV plant.

Table 2.1: Details of some operational LS-PVPPs [18]

PV power plant	Power (MW)	Area (km ²)	Panels (x10 ³)	Panel type	Inverters	Inverter topology
Korat I	6.0	0.13	29	m-Si	540	M
Narbonne	7.0	0.23	95	Thin film	19	C
Rapale	7.7	0.49	100	Thin film	900	M
Airport, Athens	8.1	0.16	29	m-Si	12	C
Saint Amadou	8.5	0.24	113	Thin film	16	C
Volkswagen Chattanooga	9.5	0.13	33	m-Si	10	C
Masdar	10	0.22	87	m-Si, Thin film	16	C
Adelanto	10.4	0.16	46	m-Si	13	C
Taean	14	0.30	70	m-Si	28	C
Jacksonville	15	0.4	200	Thin film	20	C
San Antonio	16	0.45	214	Thin film	22	C
Cotton Center	18	0.58	93	m-Si	36	C
Almaraz	22.1	1.2	126	m-Si	6697	M
Veprek	35.1	0.83	185	c-Si	3069	M
Long Island	37	0.8	164	m-Si	50	C
Reckahn	37.8	0.98	487	Thin film	43	C
Ban Pa-In	44	0.8	160	m-Si	61	C
Lieberose	71	2.2	900	Thin film	38	C
Kalkbult	75	1.05	312	m-Si	84	C
Eggebek	80	1.29	76	m-Si	3200	M
Montalto di Castro	85	2.83	280	c-Si	124	C
Templin	128	2.14	1500	Thin film	114	C
California Valley Ranch	250	6.01	749	c-Si	500	C
Agua Caliente	290	9.71	5200	Thin film	400	C

*C refers to central inverter

*M refers to multi-string inverter

2.2.3 Collection grid architectures

The collection grid is in charge of transmitting the power generated by PV the arrays to the external utility grid and the performance of the PV power plant can vary depending on its configuration. The architectures of the PV power plant collection grid have not been extensively analysed, but similar approaches as wind power plants can be adopted. These architectures can be classified in i) radial configuration, ii) ring configuration and iii) star configuration [18,28]. In the radial configuration, as shown in Figure 2.8(a), several main feeders collect the PV power generated, being the PV generation units distributed along these feeders. When a fault occurs along the feeder, switches or circuit breakers will isolate it, losing the power generation

2.2 General description of PV power plants

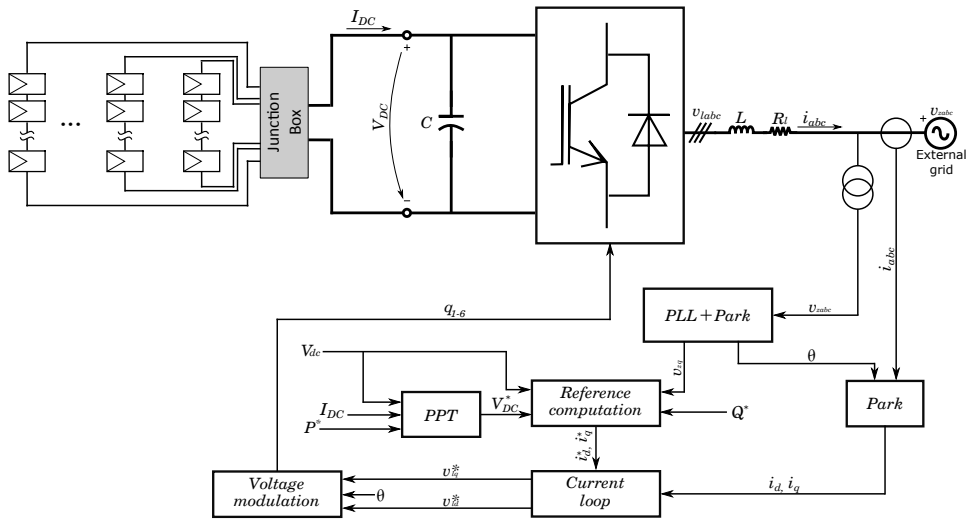


Figure 2.6: Simplified scheme of a PV inverter and its control architecture

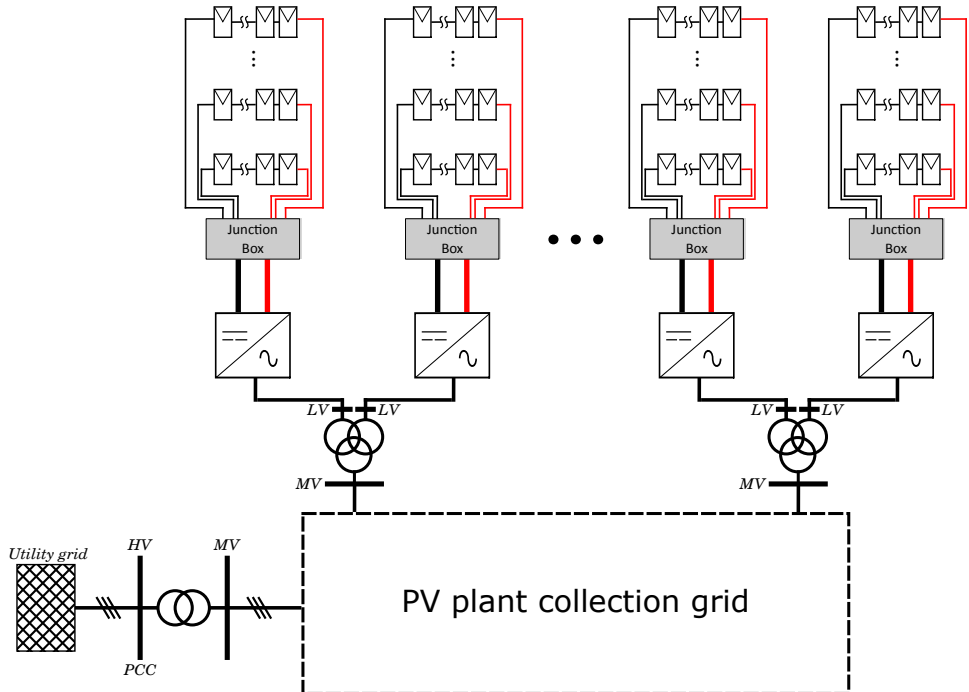


Figure 2.7: Typical LS-PVPP configuration

downstream the fault. On the other hand, power cables require to be sized in accordance with the power installed in the feeder. To avoid the power loss due to a fault along the feeder, two feeders can be interconnected at the end point forming a ring as shown in Figure 2.8(b). This PV power plant architecture can be operated in ring or in radial configuration, but faults can be isolated and the system can be reconfigured to avoid the loss of PV generators. In this case, the power cables should be oversized to transport the power generated by both feeders which will carry an additional cost. Finally, the star architecture consists in installing one feeder per generation unit, which will be tripped in case of fault without affecting the rest of the power plant. Due to the amount of feeders and the increased quantity of cable, the cost will increase. The most used architectures are the ring and radial ones, where an example of them can be found in [29] and [26] respectively.

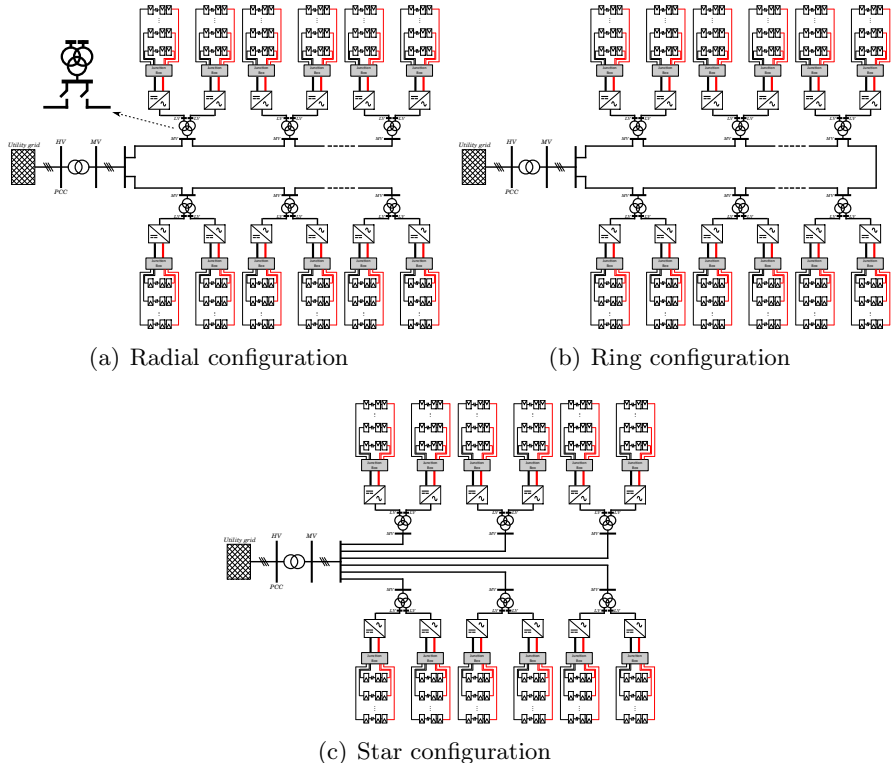


Figure 2.8: PV power plant collection grid topologies

2.2.4 Other equipment of PV power plants

The intermittent nature of the power generation of LS-PVPPs may lead to some issues that can be mitigated by energy storage devices. Some of these issues are reported in [30], i) it is not easy for conventional generators to track the rapid changes in PV generation in systems with high PV power penetration; ii) the area control error might exceed its limits when large and rapid PV power changes occur; iii) uncontrolled PV penetration may change the dispatch of regulating units; and iv) the operation cost may be increased. The power output fluctuation mitigation in LS-PVPPs can be done by the use of energy storage devices [31–35]. The energy storage in PV applications should have a proper energy and power capacities to mitigate the power fluctuations, a significant cycling capacity and a quick response time [36], which makes the Li-Ion technology one of the most promising ones.

On the other hand, LS-PVPPs also provide reactive power services. Accordingly, reactive power support devices such as capacitor banks and FACTS such as static synchronous compensator (STATCOM) can be found in these power plants.

2.3 Grid code requirements

First standards for regulating small PV power plants connected to the distribution level as the IEEE 1547 appeared for safety purposes, preventing these small systems from providing ancillary service support [37]. But as commented earlier in the introduction, the large amount of intermittent renewable power generation installed during the last decade and the future predictions of new wind and PV intermittent generation power plants could cause problems to the conventional grid. Accordingly, grid codes for the connection of LS-PVPPs to the transmission grid have been developed, obligating the provision of ancillary services as fault ride through (FRT), voltage and frequency support as well as reactive power control.

Germany included specific requirements for the connection of PVPPs to the transmission system in its grid code in 2007 [38]. After that, other countries included similar requirements in their own grid codes, as Romania [39], South Africa [40] or China [41]. On the other hand, in the United States there is the Standard Large Generator Interconnection Agreement, but TSOs have their own requirements [42]. In the case of Puerto Rico, its grid code [43] is specially strict, probably due to its geographical situation. This section summarizes the grid code review [42].

2.3.1 Fault ride through

The FRT requirements regulate the behaviour of the PV power plant under fault conditions. Basically, these requirements specify the minimum time the PVPP must remain connected after a fault occurs and the reactive current injection requirements for large voltage deviations.

The low voltage ride through (LVRT) establishes the minimum time the PVPP must remain connected in front of the voltage depth of the voltage sag. This requirement can be drawn as a general curve as shown in Figure 2.9(a), while specific requirements in some countries are depicted in Figure 2.9(b). In regions A and B, the PVPPs must remain connected, while in region C it can be disconnected. It can be observed that Puerto Rico's LVRT is the most restrictive as it has to withstand 100 % voltage sags during, at least, 600 ms and must operate indefinitely if the voltage is higher than 0.85 p.u. In addition to the LVRT, some countries as South Africa and Puerto Rico also establish high voltage ride through (HVRT) constraints, which are depicted in Figure 2.9(c). Again, Puerto Rico imposes more restrictive constraints preventing its disconnection for over voltages up to 1.15 p.u. indefinitely or over voltages up to 1.4 p.u. during several milliseconds.

In addition, reactive power support must be provided during voltage sags. This requirement defines the reactive current injection in function of the voltage, which is shown in Figure 2.9(d). The response time of this requirement is in the order of ms. For example in Puerto Rico, it must be applied in less than 100 ms. The supply of reactive power has first priority in area B (Figure 2.9(a)), while the supply of active power has a second priority [40].

2.3.2 Frequency limits

LS-PVPPs have also to withstand frequency deviations. The disconnection of LS-PVPPs is allowed after exceeding a specified frequency deviation during a predefined time. Table 2.2 shows the frequency limits and disconnection times for several countries.

2.3.3 Reactive power control and voltage regulation

LS-PVPPs must be able to generate or consume reactive power in order to provide voltage support to the grid. Accordingly, grid codes define the minimum reactive power capability that LS-PVPPs must be able to generate or consume, as shown in Figure 2.10. PV inverters were initially designed without considering this capability requirement, but now several companies are considering it. The reactive power capability in PV inverters has recently

2.3 Grid code requirements

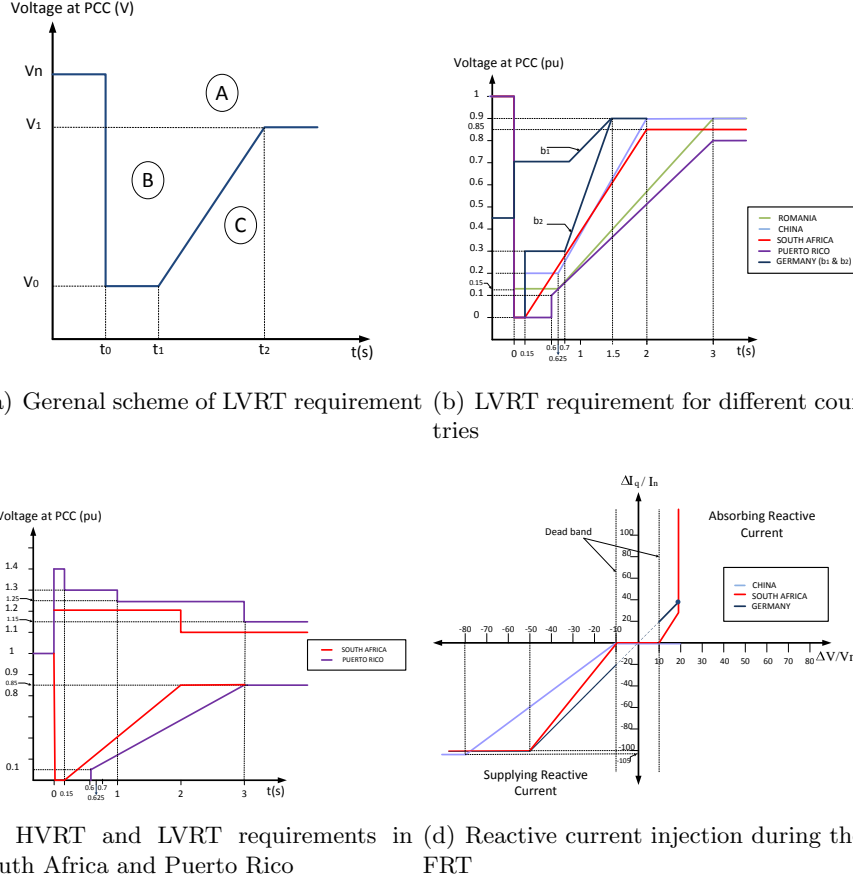


Figure 2.9: LVRT and HVRT requirements [42]

been studied in [44]. This capability varies in function of the irradiation and temperature and has different limits for the inductive or capacitive operational conditions. Between the PV inverters and the PCC there are power transformers and cables that usually have inductive behaviour. Because of the fact that the reactive power capability requirements is at the PCC, the capability of the inverters may not be sufficient. Additional devices such as capacitor banks or STATCOMs may help the fulfilling of this requirement.

Regarding the reactive power control and voltage regulation, there are three main actions that LS-PVPPs should be able to perform. These actions are i) reactive power control, ii) power factor (PF) control and iii) voltage droop or V-Q control. The reactive power and PF control consist in applying, at the PCC, the reactive power setpoint or the PF setpoint received from the

Table 2.2: Frequency limits and disconnection times [42]

Grid code	Frequency [Hz]	Limits [Hz]	Maximum duration
Germany	50	$f > 51.5$	Instantaneous trip
		$47.5 < f < 51.5$	Continuous
		$f < 47.5$	Instantaneous trip
Romania	50	$f > 52$	Instantaneous trip
		$47.5 < f < 52$	Continuous
		$f < 47.5$	Instantaneous trip
US (Puerto Rico)	60	$f > 62.5$	Instantaneous trip
		$61.5 < f < 62.5$	30 s
		$57.5 < f < 61.5$	Continuous
		$56.5 < f < 57.5$	10 s
		$f < 56.5$	Instantaneous trip
		$f > 61.7$	Instantaneous trip
		$61.6 < f < 61.7$	30 s
		$60.6 < f < 61.6$	3 min
US (FERC LGIA)	60	$59.4 < f < 60.6$	Continuous
		$58.4 < f < 59.4$	30 min
		$57.8 < f < 58.4$	30 s
		$57.3 < f < 57.8$	7.5 s
		$57 < f < 57.3$	0.75 s
		$f < 57$	Instantaneous trip
		$f > 50.2$	2 min
		$49.5 < f < 50.2$	Continuous
China	50	$48 < f < 49.5$	10 min
		$f < 48$	PV inverters characteristics
		$f > 52$	4 s
		$51 < f < 52$	60 s
South Africa	50	$49 < f < 51$	Continuous
		$48 < f < 49$	60 s
		$47 < f < 48$	10 s
		$f < 47$	0.2 s

TSO. In some countries as in Germany, the PF setpoint may be defined by the TSO or by a predefined curve P-PF. On the other hand, according to the Q-V control, LS-PVPPs must modify the reactive power setpoint in function of the voltage measured at the PCC. The curve defining the V-Q control is predefined by the TSO. Not all countries apply all these requirements. For example Puerto Rico and China only apply the V-Q control mode, while South Africa, Germany or Romania apply all of them. The reactive power setpoint and PF setpoint control modes can not be applied simultaneously. In contrast the V-Q control mode can be applied together with the reactive power setpoint or with the PF setpoint control modes. The required response time varies depending on the country. The fastest response requirement

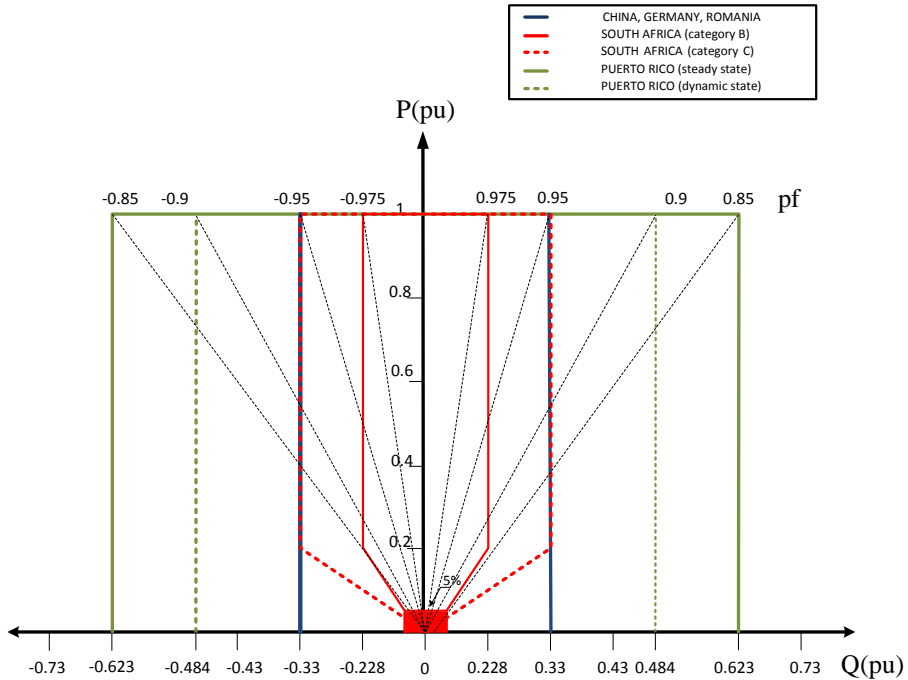


Figure 2.10: Minimum reactive power capability in LS-PVPPs [42]

appears in the Puerto Rico's grid, where it is required to reach the 95 % of the reactive power setpoint in less than 1 s. This value increases to 30 s in South Africa or 1 min in Germany. On the other hand, during the realisation of this thesis, Romanian TSO also required a reactive power ramp rate limitation of 10 %/min respect the rated reactive power.

2.3.4 Active power control and frequency regulation

LS-PVPPs also have to comply with different active power generation requirements. In South Africa they are defined as i) absolute production constraint or power curtailment, ii) delta production constraint and iii) power gradient or ramp rate constraint. The absolute production constraint limits the active power generated at the PCC to a certain value. The delta production refers to a power reserve, i.e. to apply an active power limitation which is a % of the available active power. This constraint is not required in other countries as Germany, Romania, US or China. In addition, according to the author's experience, despite appearing in the South African grid code,

in reality this constraint is not applied, probably due to the difficulty on estimating the available active power, specially when clouds pass over the PV plant. The ramp rate consists in limiting the active power variations at the PCC, typically to a 10 %/min respect to the rated active power of the power plant when the active power setpoint changes, but does not apply when the LS-PVPP operates under the MPPT mode. Only in Puerto Rico and in Hawaii this limitation must be fulfilled at any time. The ramp rate limitation can be evaluated between to endpoints of any 60-second interval or considering instantaneous power fluctuations as in Hawaii which limits the output power to 1 MW/2-s each 2 second scan [45]. And similar conditions have been considered in Puerto Rico [46, 47].

On the other hand, frequency regulation establishes a frequency droop or f-P control mode, in which the active power setpoint is modified in function of the measured frequency. This requirement can be applied together with the power curtailment but not with the ramp rate, as fast response is needed, e.g. Puerto Rico establishes a response time of 1 s.

2.4 Conclusions

During the last decade, a large amount of wind and PV power plants have been built and connected to the electrical grid. As a result, the share in wind and PV installed capacity has been significantly increased. For example, the European share of these renewable power plants has been increased from 6.3 % in 2005 to 29.5 % in 2017. Due to the significant penetration of PV power into the electrical grid, grid codes of different countries have been updated so that they require LS-PVPPs to provide ancillary services to the electrical grid. These services consist in controlling the power exchange at the feeder of the power plants, i.e. at the PCC to contribute to the grid support functions. LS-PVPPs include a significant number of PV inverters that are controlled locally in an independent way. In addition, other support devices as capacitor banks, STATCOMs or storage systems can also be installed to help these power plants to achieve the desired behaviour. Hence, for controlling the active and reactive power at the PV power plant feeder, there is the necessity to coordinate all these devices. This coordination is possible thanks to a central PPC, which will be developed in the next chapters.

Chapter 3

Power plant control in large scale photovoltaic power plants

This chapter describes the design of a new LS-PVPP PPC for coordinating PV inverters, STATCOM and capacitor banks so that the grid codes are met.

3.1 Introduction

Power management applied to PV plants has encountered many technical challenges. For instance, the integration of storage systems to deal with the variability of the renewable sources and the appropriate coordination with the PPC, which has been addressed in [32,48–55]. The authors from [48] propose a control method for a battery energy storage system to be integrated in renewable plants so that the intermittent resource can be dispatched on an hourly basis. In [49], a PPC for a PV plant is proposed to accomplish grid code requirements, comparing the operation when the PV plant includes storage support and when it does not. Focusing on the ramp rate control, a model to simulate effective dispatch of energy storage units so as to ensure this requirement is shown in [50]. A different approach for PV inverter ramp rate control, also using an integrated energy storage device, is suggested in [32]. It is proposed as a more accurate solution than the traditional moving average method, for allowing to limit the ramp rate within a desired level. The utilization of PV solar farm inverters as STATCOMs for improving power transfer limits is addressed in [56]. The LVRT requirement is examined in [57], proposing a control strategy to improve voltage profiles in steady state and when facing load variations at grid buses [52]. The authors from [54] propose a control coordination for capacitor banks and an on-load tap changer in a wind power plant to accomplish the grid code requirements. This proposal is based on the knowledge of the capacitor’s state by the central controller, thus bidirectional communications

are required. On the other hand, in [55] an algorithm for the coordinated control of automated devices and PV generators is presented, based on an optimization approach for minimizing circuit losses and motion of utility controls while solving voltage rise problems. However, the analysis does not take into account the controls needed and their dynamics.

The before cited studies analyse specific devices and/or strategies that can enhance the grid integration of PV plants by affecting the power management. A global approach on the active and reactive power controls needed to fulfil the grid codes requirements and their interaction is addressed in this thesis, which extends the basic concepts presented in [53]. The control proposed does not need to know the power production state of each converter and the communication system needed is unidirectional. In addition, the coordination of the PV inverters with other devices such as capacitor banks and STATCOMs is addressed in this chapter.

Figure 3.1 shows the sequence followed to manage the PV plant project development in different countries as Romania, South Africa or the U.S.A. Grid code requirements have implications in PV plant design and control. Most of the plants to be controlled have already been constructed, so the focus is to design a control and, if needed, to redesign the PV plant adding, for instance, FACTS devices. After addressing the control algorithms, TSOs require simulation models of the PV plants including their control. So, the corresponding models are made in PSS/E® and DIgSILENT Power Factory® software, as it is indicated in most grid codes [39, 40, 43]. After performing some simulations and validating the grid code compliance, the implementation is permitted and own tests are made before the TSO performs the validation tests to consider the PV plant able to be operative.

3.2 Power plant control design

3.2.1 LS-PVPP description

As described in Chapter 2, there are different topologies of PV power plants. In this chapter the ring configuration is used as it is the configuration of one of the LS-PVPPs operating under the controller developed here. For the purpose of designing the PPC for any LS-PVPP, capacitor banks and a STATCOM is added to the LS-PVPP simulation model as shown in Figure 3.2.

Despite having local controls, it is necessary to coordinate PV inverters together to achieve the desired setpoints at the PCC. Hence, a PPC must act as a master to drive all PV plant devices. In this way, the PPC will read the

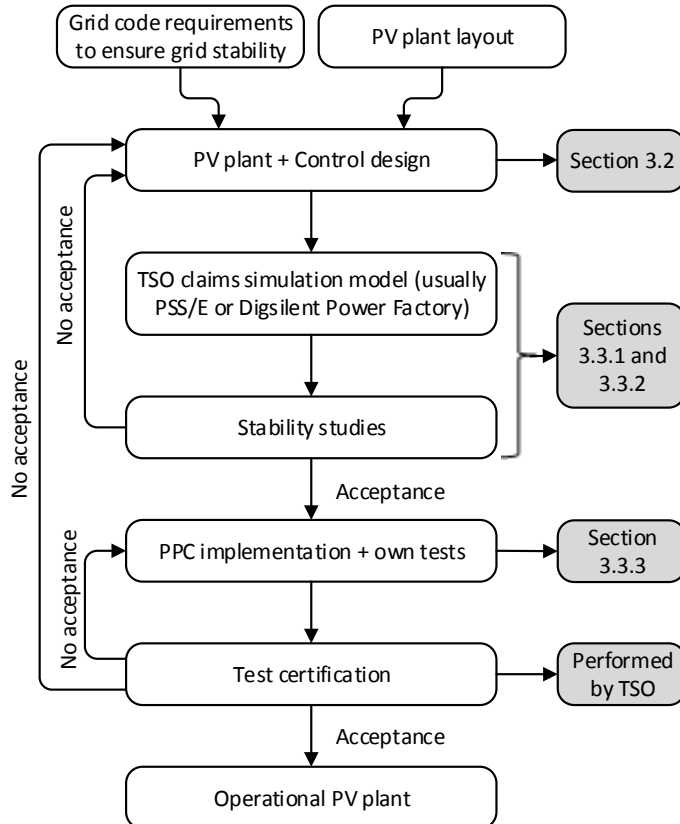


Figure 3.1: PV plant control design and implementation process

measurements from the PCC and will send orders (active and reactive power setpoints) to all inverters or FACTS, as well as connection/disconnection orders to capacitor banks if they are installed in the PV plant. Then, the inverters will perform their own controls to follow their master (PPC) orders. Only in the case of FRT, inverters and FACTS will omit the PPC orders. This is due to the fact that grid codes require a rapid response during fault events where a communication delay and the additional control loop of the PPC would result in the PV plant being non-compliant to the FRT requirement.

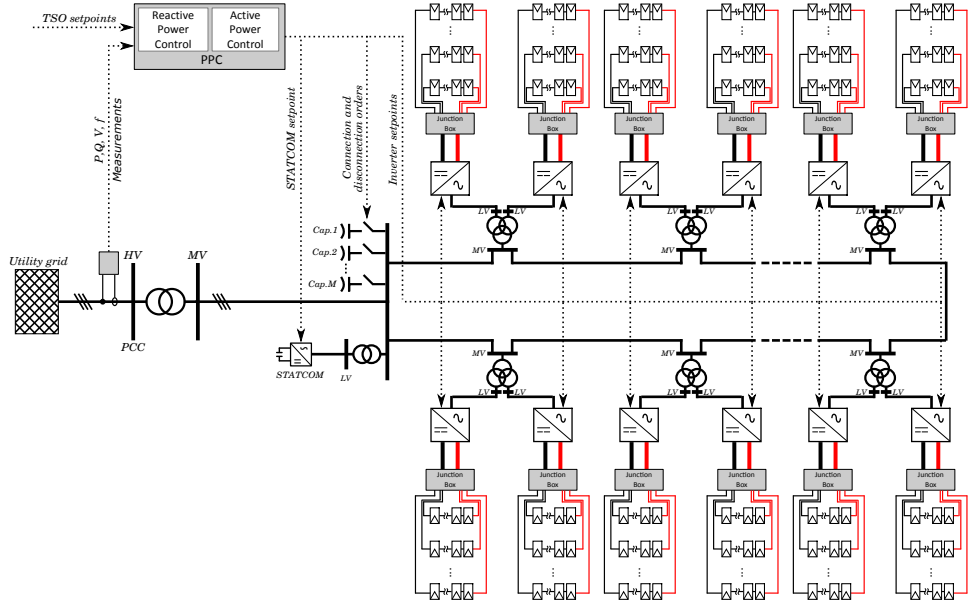


Figure 3.2: General scheme of a LS-PVPP and its central controller (ring configuration)

3.2.2 Active power control design

The active power control scheme is shown in Figure 3.3. The control is divided in the reference computation block, the controller and the dispatch system.

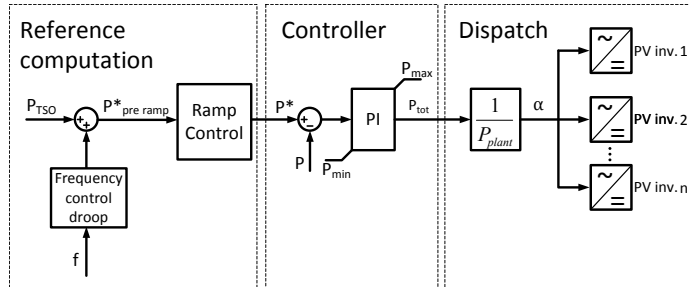


Figure 3.3: Active power control scheme

The reference computation block calculates the active power setpoint that must be injected at the PCC. Despite the TSO may send a curtailment setpoint, P_{TSO} , a frequency droop is applied continuously so that it modifies

3.2 Power plant control design

the desired setpoint at the PCC, $P_{pre-ramp}^*$. Furthermore, there is a ramp rate limitation provided by the grid code. So, $P_{pre-ramp}^*$ is limited by a ramp rate controller which computes the desired active power at the PCC, P^* .

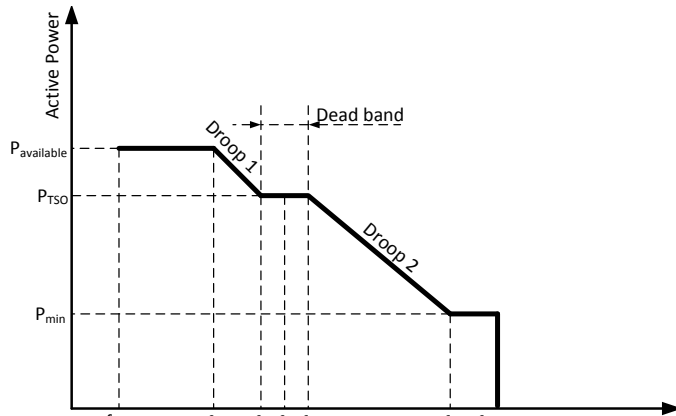
If there is not a curtailment event, P_{TSO} is set to the nominal PV plant power, P_{plant} . The frequency droop curve is set in the most generic shape [40] and shown in Figure 3.4(a), where $P_{available}$ is the maximum available active power, P_{TSO} is the TSO curtailment setpoint, P_{min} is the active power that the PV plant has to deliver when a maximum overfrequency deviation, f_{max} , occurs (for frequencies over f_{max} it is permitted to disconnect), f_4 establishes when the overfrequency droop finishes and P_{min} must be delivered, f_n is the nominal frequency (the TSO can modify it slightly according to its necessities), f_2 and f_3 determine a deadband zone where the frequency droop is not applied, f_1 establishes when the underfrequency droop finishes and f_{min} is the maximum underfrequency deviation where the PV plant must remain connected. The definition of the frequency droop curve is done according to [40], where TSOs specify the *dead band*, f_{min} , P_{min} , f_{max} , *Droop 1* and *Droop 2*. As mentioned before, agreements with TSOs are made to implement the frequency droop curve in absence of power reserves. In the case of the PV plant operating at the MPP (no curtailment required), $P = P_{available} \leq P_{TSO} = P_{plant}$. Under this condition, P_{TSO} is greater than $P_{available}$ and the TSOs have agreed to implement the curve depicted in Figure 3.4(b). In this situation, once the frequency exceeds the threshold, f_3 , P_{TSO} is fixed at the current active power value and the over frequency droop operation is performed. During curtailment events, $P_{TSO} < P_{available}$ and the curve of Figure 3.4(a) is implemented.

Once P^* is obtained, the controller computes the aggregated power, P_{tot} , that must be generated by all PV inverters. The controller is based on a typical PI controller which ensures the error between P^* and the measured power at PCC, P , to be 0 in a steady state.

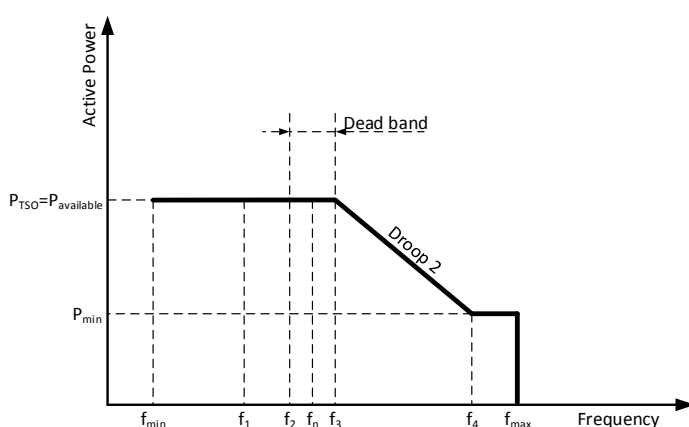
The dispatch system is applied using p.u. signals as in [58]. However, the present approach does not need any information of the available power.

The dispatch system takes the P_{tot} and distributes it among all PV inverters. It is dispatched in a per unit system so that there is only 1 signal to be sent despite different PV inverter power ratings. In this way, P_{tot} is divided by the nominal PV plant power, P_{plant} , to obtain α that is sent to all inverters. Each inverter i receives the α signal and computes its local active power setpoint according to the expression (3.1).

$$P_{inv,i}^* = \alpha \cdot P_{nom,i} \quad (3.1)$$



(a) Generic frequency droop curve



(b) Frequency droop curve in absence of curtailment event

Figure 3.4: Droop curves for frequency regulation

Where $P_{nom,i}$ and $P_{inv,i}^*$ are the nominal active power and the local active power setpoint of the inverter i respectively.

3.2.3 Reactive power control design

The reactive power control is performed similarly to the active power control. Figure 3.5 depicts its corresponding scheme. In addition to PV inverters, FACTS devices or capacitor banks are commonly found in a PV plant. So, the control is designed for a generic PV plant which can contain all these

3.2 Power plant control design

elements. To do so, a priority criteria has been established. First, capacitor banks are managed to deliver the major part of reactive power (only when capacitive power is required). These banks have two states i) ON, where full reactive power is delivered and ii) OFF, where 0 reactive power is delivered. So, the fine regulation is performed by FACTS and PV inverters. FACTS have priority over PV inverters as they are installed for this particular application. However, when a FACTS device reaches a specified level of reactive power (not necessarily its nominal power) the remaining amount of reactive power is delivered by both (FACTS and PV inverters).

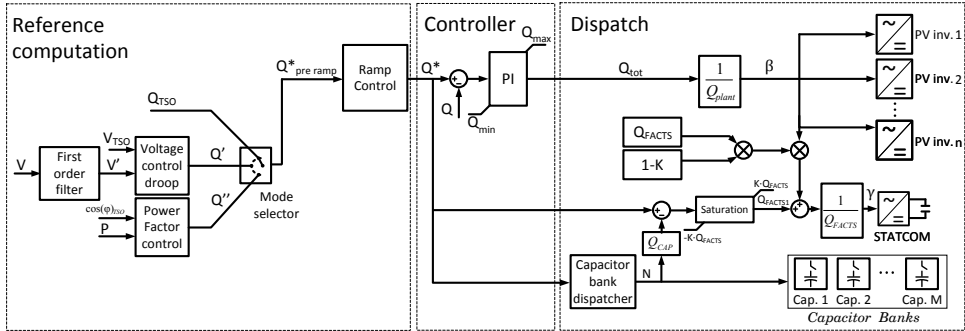


Figure 3.5: Reactive power control scheme

Contrary to the frequency regulation actions, the voltage regulation actions do not require simultaneous operations as for example reactive power setpoint plus voltage droop. So, a mode selector is implemented to determine the way to calculate the desired reactive power setpoint, $Q^*_{pre-ramp}$. If the TSO sends a reactive power setpoint, Q_{TSO} , then $Q^*_{pre-ramp} = Q_{TSO}$. When PF setpoint is set, the corresponding desired reactive power is calculated as (3.2). When a voltage droop mode is set, the $Q^*_{pre-ramp}$ is calculated according to a curve depicted in Figure 3.6. In this case, due to the system response, it is needed to filter the voltage measurement, V , to obtain the droop input, V' . This filtering is to avoid multiple connections/disconnections of the capacitor banks (a connection of a capacitor bank provokes a voltage increase and so, a decrease of Q' and the corresponding capacitor disconnection). With this filter and an hysteresis applied to capacitor bank dispatcher, the multiple connections/disconnections are avoided. When there are not capacitor banks, the time constant of the filter is set to 0.

$$Q^*_{pre-ramp} = P \cdot \frac{\sin(\varphi)_{TSO}}{\cos(\varphi)_{TSO}} \quad (3.2)$$

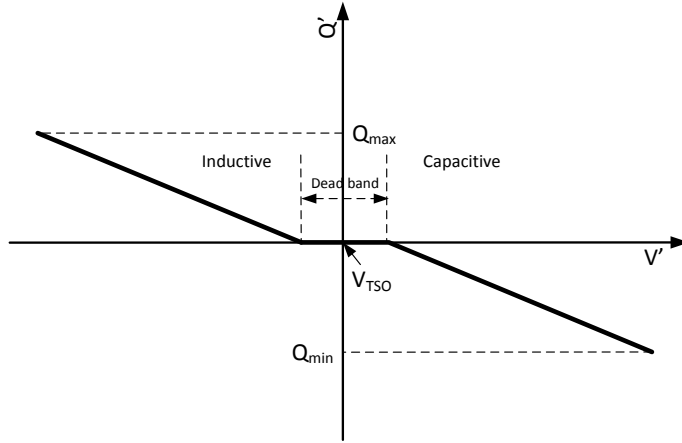


Figure 3.6: Droop curve for voltage regulation

Where P is the measured active power at PCC and $\cos(\varphi)_{TSO}$ is the PF setpoint.

Once $Q_{pre-ramp}^*$ is obtained, it can be limited by a ramp rate limiter obtaining the desired reactive power at PCC, Q^* . At this point, if Q^* is capacitive, capacitor banks (if they are available) generate the major part of Q^* . This is performed calculating the number of capacitors to be connected in the capacitor bank dispatcher. The connection orders of capacitor banks are set according to the following criterion (3.3) and (3.4) and are represented in Figure 3.7.

Connection/disconnection orders for the i -th capacitor bank:

$$\text{SET}_{CAP_i} = Q^* > (i - 0.4) \cdot Q_{CAP} \quad (3.3)$$

$$\text{RESET}_{CAP_i} = Q^* < (i - 0.6) \cdot Q_{CAP} \quad (3.4)$$

Where Q_{CAP} is the reactive power supplied by a capacitor bank at nominal voltage.

Then, the finer control is performed first by FACTS and with PV inverters afterwards. A factor $K \in [0, 1]$ determines the amount of reactive power that is supplied only by FACTS devices. In a first stage, Q_{FACTS1} is calculated according to (3.5) with a maximum absolute value of $K \cdot Q_{FACTS}$, where Q_{FACTS} is the nominal reactive power of the FACTS device.

$$Q_{FACTS1} = Q^* - N \cdot Q_{CAP} \quad (3.5)$$

3.2 Power plant control design

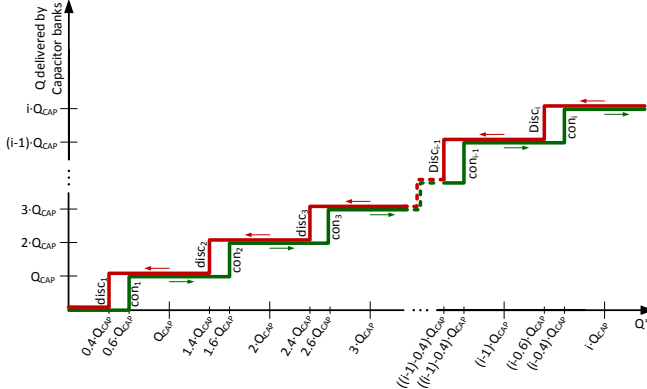


Figure 3.7: Capacitor bank connection/disconnection criterion

Where N is the number of capacitor banks connected.

Then, the controller computes the rest of the reactive power that FACTS plus PV inverters have to supply, Q_{tot} . It is performed by a PI controller as shown in Figure 3.2, and the corresponding p.u. value β is calculated by dividing Q_{tot} by Q_{plant} , where Q_{plant} is the nominal reactive power of the PV plant. At this point, as the available reactive power remaining in the FACTS device is $(1 - K) \cdot Q_{FACTS}$, the additional part of FACTS contribution is calculated as $\beta \cdot (1 - K) \cdot Q_{FACTS}$. The total reactive power setpoint to the FACTS device in a per unit system is calculated as (3.6).

$$\gamma = \frac{Q_{FACTS1} + Q_{FACTS} \cdot \beta \cdot (1 - K)}{Q_{FACTS}} \quad (3.6)$$

Each PV inverter i receives the β signal and computes its local reactive power setpoint according to the expression (3.7).

$$Q_{inv,i}^* = \beta \cdot Q_{nom,i} \quad (3.7)$$

Where $Q_{nom,i}$ and $Q_{inv,i}^*$ are the nominal reactive power and the local reactive power setpoint of the inverter i respectively.

The FACTS device receives the γ signal and computes its local setpoint according to (3.8).

$$Q_{FACTS}^* = \gamma \cdot Q_{FACTS} \quad (3.8)$$

Where Q_{FACTS} and Q_{FACTS}^* are the nominal reactive power and the local reactive power setpoint of the FACTS device.

3.3 Results

3.3.1 Case study

The PV plant model corresponds to the Vanju-Mare PV plant (Figure 3.8). The PV plant is located in Romania close to the village of Bucara covering a total area of 23.4 ha ($234 \cdot 10^3$ m²) [59]. It consists of 15 PV inverters with a total peak power of 9.4 MW [60]. The PV inverters are connected to a 20 kV PV collection grid in ring configuration and then, to a 110 kV transmission grid through a MV/HV transformer. The PV inverters are the SMA Sunny Central HE series (SMA500HE and SMA630HE). These inverters are voltage source inverters (VSI) and are classified as high-frequency, pulse-width modulated current-regulated inverters. A STATCOM (GPCOM model) of 2 MVar is added at node 91. When capacitor banks are used, they are connected at bus 100. The electrical model of the PV plant is described in Appendix A.

The PPC including all controls explained above has been programmed in FORTRAN for PSS/E® simulations and in DSL for DiGSILENT Power Factory® simulations. The PPC model can be treated as a black box where the user (TSO) can connect the required measurements and the outputs (α, β, γ and capacitor banks orders) to the required devices. Most of the parameters are configurable: droop curves, PI controller parameters K_P , K_i and K_w (antiwindup constant), ramp rate limits, sample times, communication delays, etc.

3.3.2 Simulation results

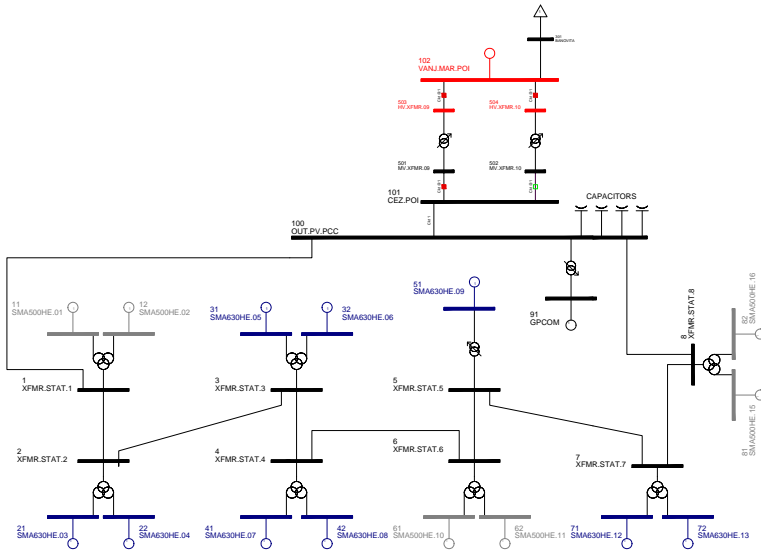
Active power curtailment, reactive power setpoint and power factor setpoint

Figure 3.9 shows the response at PCC after setting active and reactive power setpoints and a PF setpoint (simulation 1). This is performed in a PV plant only equipped with inverters. Figure 3.9(a) shows the active and reactive power response, the corresponding setpoints and the ramp limitation. Figure 3.9(b) shows the PF response as well as the PF control flag (the activation signal of power the factor control mode). It can be observed a power curtailment at the beginning and how the ramp limiter, as well as the active power at the PCC, respond properly. At second 80 of the simulation, the reactive power setpoint is changed. The results show again a good response and in addition, the capacity to perform independent active and reactive power controls. At second 250, the PF flag is set and the corresponding

3.3 Results



(a) Vanju-Mare PV plant image [61]



(b) Scheme of Vanju-Mare PV plant simulation model in PSS/E[®]. Red = 100 kV, black = 20 kV, blue = 0.315 kV, grey = 0.27 kV

Figure 3.8: Vanju-Mare PV plant

setpoint is stepped-down to 0.90. As a result, in the upper plot it can be observed that the reactive power setpoint is recalculated to obtain the desired PF. At second 350, a power curtailment is set and, as the PF control remains active, the reactive power setpoint recalculation to maintain the PF at 0.90 is observed. These results can be concluded as appropriate for curtailment and reactive setpoint events as well as for the PF control mode.

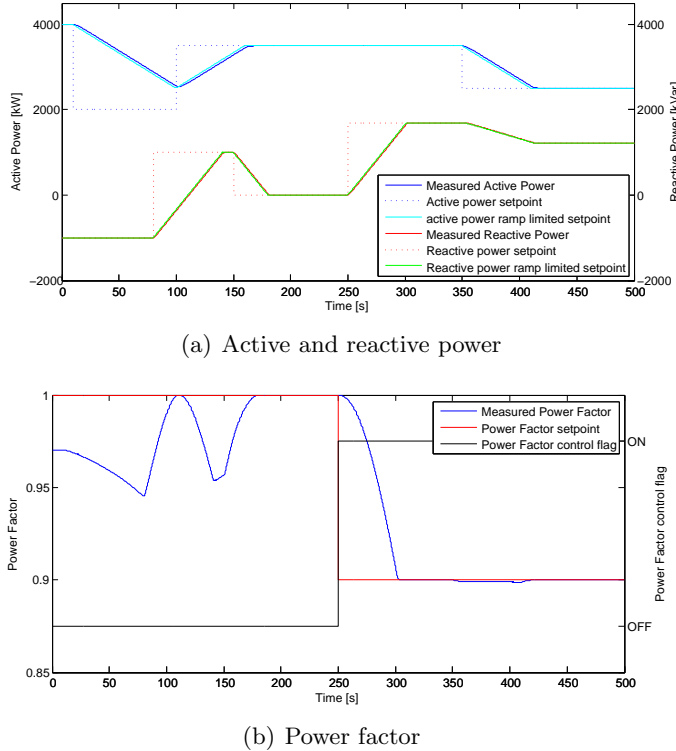


Figure 3.9: Control response of: active power, reactive power and power factor setpoints (simulation 1)

Frequency droop

In Figure 3.10, the frequency droop operation can be observed (simulation 2). In this case, the simulation begins with an active power setpoint with ramp limitation. The frequency droop control flag is set at second 200 of the simulation. In this case, the droop curve is defined by: $P_{TSO} = P_{available} = 4$ MW, $f_n = 50$ Hz, $f_3 = 50.5$ Hz, $f_4 = 52$ Hz, $f_{max} = 53$ Hz, $P_{max} = 4$ MW and $P_{min} = 1$ MW. Furthermore, the active power contribution from droop control is not limited by a ramp rate. To perform the simulation, the frequency is not measured but set manually to test the different droop curve zones. First, it can be observed that when the frequency is in the deadband range, the active power setpoint does not change. Once it is over the deadband (51 and 52.0 Hz), the active power setpoints changes according to the droop curve and the real power achieves these new levels. Between f_4 and f_{max} the active power setpoint remains constant at P_{min} as it can be

3.3 Results

seen in the last frequency step. The result shows an appropriate behaviour of the frequency droop control.

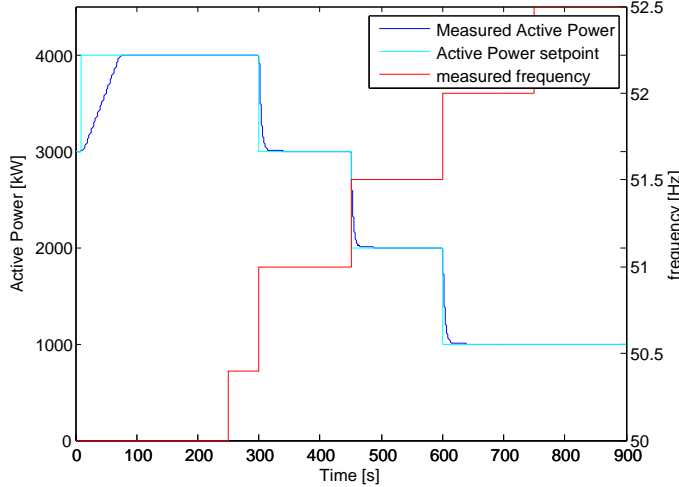
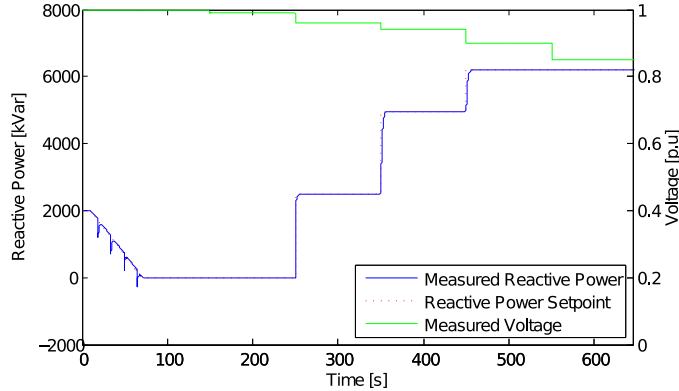


Figure 3.10: Frequency droop response (simulation 2)

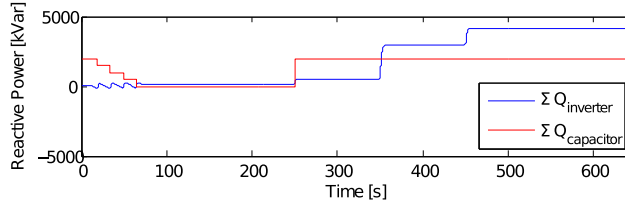
Voltage droop

Figures 3.11(a) and 3.11(b) show the voltage droop control mode response (simulation 3). In the simulation case, 4 capacitor banks of 500 kVar have been added. Figure 3.11(a) shows the reactive power setpoint, Q^* in red, the measured reactive power in blue and the measured voltage in green. The ramp rate limiter is deactivated when the voltage droop operation is set (as usually required by TSO). At the beginning the reactive power setpoint is changed from 2MVar to 0 MVar and the ramp limiter is active. It can be observed how the capacitor banks disconnect when Q^* decreases enough, followed by the corresponding correction by PV inverters (Figure 3.11(b)). Then, at second 100, the voltage droop control mode is set. The droop curve is defined by a deadband between 0.98 and 1.02 p.u, $Q_{max} = 6.2$ MVar, $Q_{min} = -4.2$ MVar and $K_{droop} = 5\%$ where K_{droop} is the slope of the droop curve. It can be observed the first voltage step (0.99 p.u) is inside the deadband and so, the reactive power setpoint is not modified. Then, the voltage decreases by steps (0.96, 0.94, 0.9, 0.85 and 0.75 p.u respectively). The corresponding reactive power setpoint according to the droop curve can be observed. When the grid voltage changes to 0.96 p.u, the reactive power setpoint is 2.48 MVar. So, all capacitor banks are connected and the remaining reactive power is delivered by the inverters (bottom plot). Then,

as the voltage decreases, inverters deliver the additional required reactive power as all capacitors are connected.



(a) Voltage droop response (simulation 3)



(b) Inverter and capacitor banks reactive power injection during voltage droop operation (simulation 3)

Figure 3.11: Control droop modes response (simulations 2 and 3)

Finally, the filter response performance is shown in Figure 3.12 (simulation 4). In this case 6 capacitor banks and a STATCOM of 2 MVar have been added. The operation mode is the voltage droop and at second 2, the grid voltage steps down. Therefore, reactive power needs to be injected. Figure 3.12(a) shows the reactive power injected at PCC in 3 scenarios: without filter (green line), with a filter time constant of 0.15 s (red line) and with filter time constant of 0.5 s (blue line). Figure 3.12(b) depicts the voltage measured at PCC (solid lines) and the corresponding filter outputs (dashed lines) and finally, the capacitor banks connections are shown in Figure 3.12(c). As it can be observed, when there isn't any filter, the connection of a capacitor bank provokes an increase of voltage. As a result, the reactive power required steps down and the capacitor bank disconnects. It happens successively provoking multiple connections and disconnections. To avoid

3.3 Results

this phenomenon, a filter is set at the voltage measurement, avoiding fast changes. It can be observed that the slower the filter, the more stable is the response. In this case, a filter with time constant of 0.5 s was enough to obtain a stable operation.

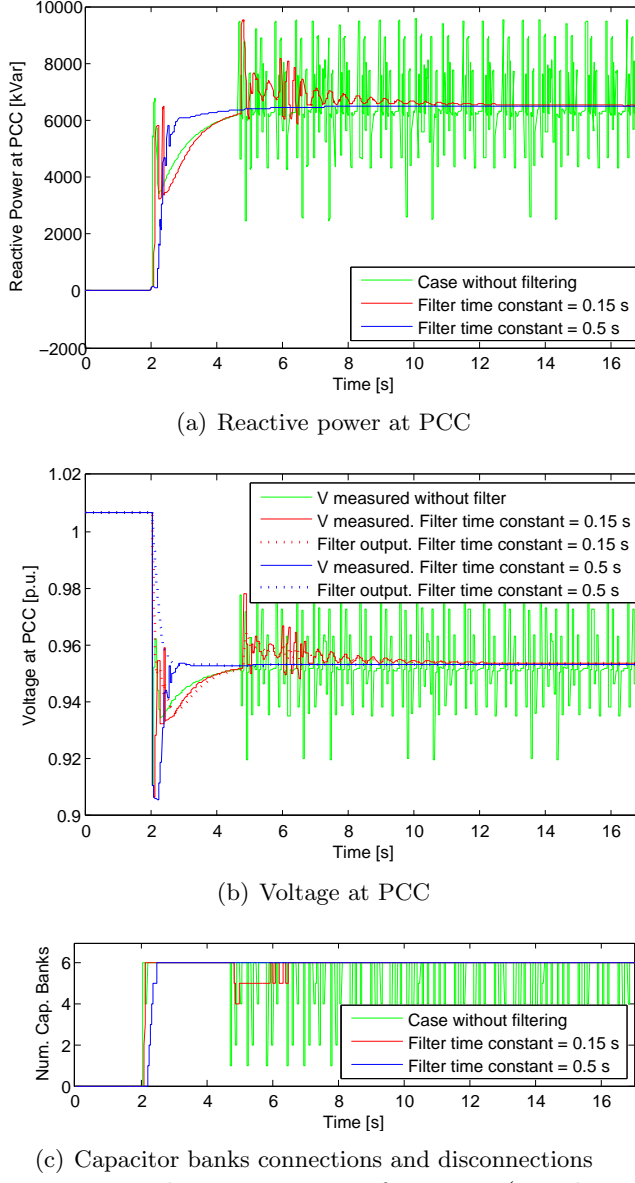


Figure 3.12: Filter response performance (simulation 4)

3.3.3 Test site results

Implementation

The PPC has been implemented as shown in Figure 3.13. The main elements of the whole PPC system are the PV supervisory control and data acquisition (SCADA) system, the PPC controller, the smart bridge and the communication system.

Each remote terminal unit (RTU) system is associated with a set of inverters, FACTS devices, batteries, capacitor banks or to the point of interconnection (POI) meter. RTUs allow the sending/receiving of data to/from any PV inverter or other elements. The PV SCADA will collect and display on a screen all PV plant information in real time. It will also allow the user to set the control mode and the local setpoints ($P_{pre-ramp}^*$, $Q_{pre-ramp}^*$, etc.). As the PV SCADA system is thought only to display and interact with the PV power plant, another system is still required to implement the PPC and hence, the PV SCADA needs to send the control mode and setpoints to this system. The Smart Bridge receives data from PV SCADA and from the TSO, interacts with the PPC controller and sends the PPC orders to all inverters, capacitor banks or other elements. The PPC receives the setpoints coming from the PV SCADA or from the TSO through the Smart Bridge. It also receives measurements directly from PCC (in order to avoid delays through the Smart Bridge) and executes the control algorithm explained previously. The algorithm outputs are sent from the PPC controller to all inverters or any other element through the Smart Bridge system.

Results

The following results correspond to a 9.4 MW PV power plant in Romania (Vanju-Mare PV plant). After the PPC implementation, a set of tests were carried out to verify that the PV plant behaviour was correct. The tests were performed from 10h 45min until 13h 11min on a cloudy day and the data results were obtained every 500ms. Due to the fact that capacitor banks were not installed in the PV plant, the PPC actions regarding these elements could not be tested in a real application.

Figure 3.14(a) depicts the active power measured and the corresponding setpoint at PCC. It can be observed that 3 curtailments have been tested. In this PV plant, PV inverters responses are extremely slow (time constant of about 10 seconds). So, in the first curtailment attempt the sampling time has been set to 10 seconds; time enough to achieve the P^* setpoint before sending a new setpoint. This way, some steps in the ramp response can be observed. At the end of the first curtailment, the available active power

3.3 Results

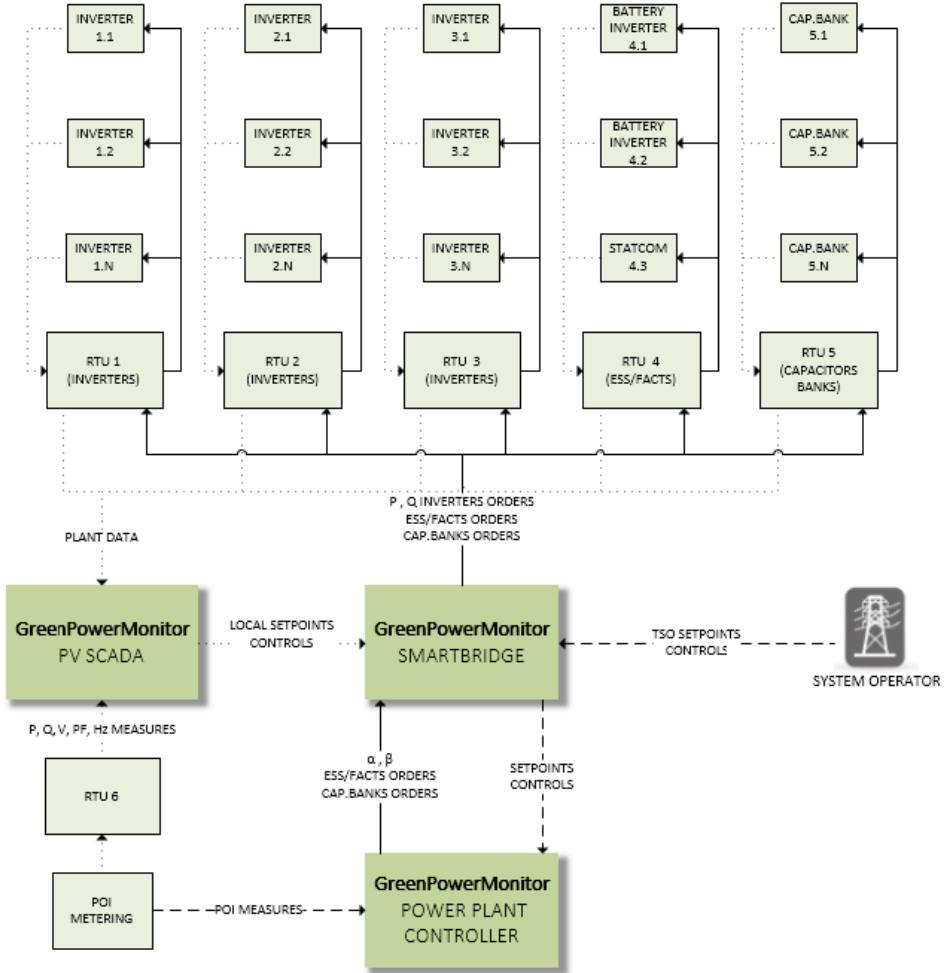


Figure 3.13: PPC implementation scheme [26]

decreased, so the following ramp up response could not be observed. In the second curtailment, an attempt to reduce the stepping during the ramp event has been done. The sampling time has been set faster than the PV inverter dynamics (1 second). This way, a ramp event improvement could be observed. Furthermore, after the second curtailment, the ramp up event is performed perfectly as the available active power was high enough. The third curtailment confirms the appropriate control response.

Reactive power response has also been studied. Figure 3.14(b) depicts the reactive power measurement and its corresponding setpoint at PCC during

the tests. At the beginning β and γ are set directly to 0. So, the reactive power measured is the one generated by transformers and cables. After the first reactive power setpoint these values become controlled (the variations around second 3000 and after second 8000 are due PF control tests). Analysing the reactive power setpoints and the response behaviour (in this case, a reactive ramp rate limiter was requested by the TSO) it can be concluded that the reactive power control fulfils the grid code.

PF control response is shown in the upper plot of Figure 3.15(a). Until the second 8147, the PF control is disabled but reactive power setpoint is set to 0. Then, a 0.97 setpoint is applied. In Figure 3.15(b), it can be observed how the reactive power setpoint is changed automatically according to (3.2). Due to the low active power variability at the beginning, the reactive power setpoint is nearly constant. Then, a power curtailment is performed 3.15(c) and the reactive power setpoint reacts to it to maintain the PF.

In general, the real results presented show a good performance of the PV plant with the explained PPC. Other control results, such as voltage or frequency droop, are based on calculating the necessary active or reactive power setpoints (it has been proven they work under simulation tests) and none of them has presented any grid code breach since its start up (more than 2 years of operation).

Overall implementation results

The PPC presented in this chapter has been implemented in more than 30 LS-PVPPs worldwide. Table 3.1 shows the amount of PV power capacity controlled by the proposed PPC. This data has been provided by GreenPowerMonitor.

Table 3.1: PV power installed capacity controlled by the PPC

Region	Controlled PV power
US/Canada	1 GW
Uruguay	95 MW
Mid Asia	260 MW
South Africa	66 MW
Rumania	16 MW
Thailand	60 MW
Honduras	226 MW
UK	12 MW
Total	1.735 GW

3.3 Results

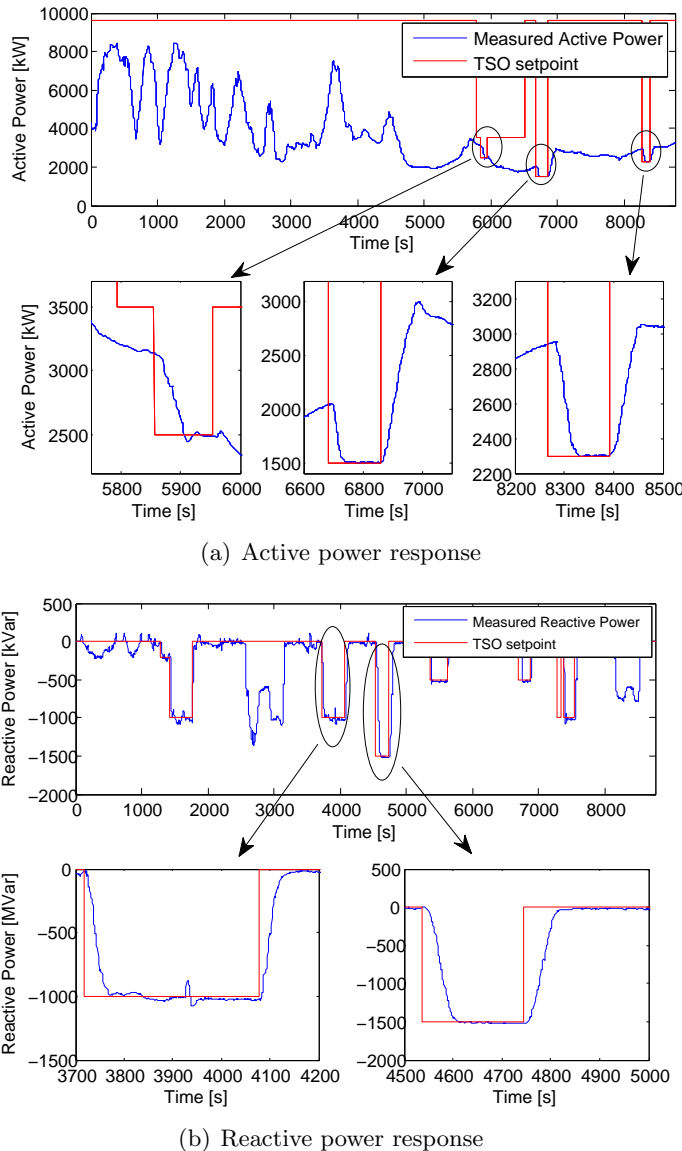


Figure 3.14: Active and reactive power response in Vanju-Mare PV plant

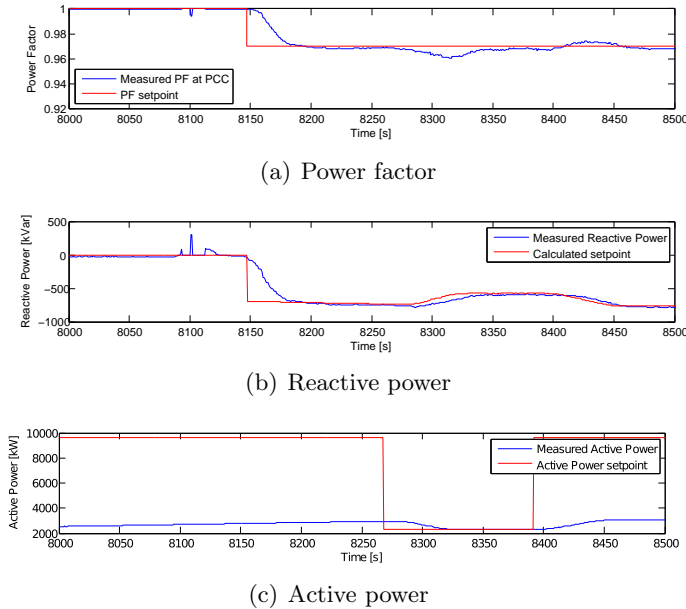


Figure 3.15: Power Factor response in Vanju-Mare PV plant

3.4 Conclusions

In this chapter, the different stages for designing and implementing a PPC for LS-PVPPs have been presented. The control algorithm has been designed for a generic PV power plant, where its robustness has permitted it to be implemented in several PV plants (with different devices installed) and to accomplish different grid codes.

The proposed PPC includes the management of PV inverters, capacitor banks and FACTS devices. Taking into consideration the typical ancillary devices for voltage support actions, a new dispatching system based on priorities has been implemented satisfactorily. This dispatching system is designed to be flexible in order to be adapted to any PV power plant provided with FACTS, capacitor banks, both ancillary devices or none of them. The voltage droop operation can present problems when capacitor banks are installed. Accordingly, a solution based on a combination of hysteresis for the capacitor bank connection/disconnection with a voltage measurement filter is proposed. This way, reactive power injection oscillations produced by multiple capacitor bank connections and disconnections are avoided.

Finally, after monitoring a 9.4 MW Romanian PV plant, real results have been presented showing the fulfilment of the grid codes.

Chapter 4

Active Power Control in a Hybrid PV-Storage Power Plant for Frequency Support

In Chapter 3 a PPC for the grid code compliance in LS-PVPPs has been presented, showing its implementation in real cases around the world. However, the sites where it was implemented had 'soft' active power requirements, allowing ramp rates deviations and under frequency droop violation when the plants operate at the MPP. As it has been explained in Chapter 2, some grid codes require ramp rate constraints as well as under frequency droop response even if the power plant operates at its MPP. As PV systems do not store energy in the form of kinetic energy in rotating machines, additional energy storage devices is commonly used for mitigating PV power fluctuations. This chapter proposes an active power control of an hybrid PV-storage power plant for providing frequency support and ramp rate limitation.

4.1 Introduction

Several strategies for mitigating the PV power fluctuations has been studied in [31–35]. These studies are based on integrating ESS in the PV power plant. In [31], two ramp rate control strategies are developed depending on the cycle-life of storage technology. For low cycle-life technologies, it is intended to maintain the SOC between 40-60 %, where the storage device operates on stand-by condition. In contrast, for long cycle-life technologies, the SOC follows the PV plant relative output. The study performed in [32] proposes a method to limit the power fluctuations of a PV inverter. The strategy is developed for ramping and post-ramping event to recover the SOC. In this case, the storage device is connected to the DC link of the PV inverter. However, this topology is not reasonable for a power plant with

more than 1 inverter as it is well-known that PV power fluctuations reduce as the plant size increases [62]. So, a centralized energy storage seems to be more reasonable. In [33], a ramp rate control strategy based on irradiance forecasting is presented. Thanks to the irradiance prediction, the controller anticipates the ramp events and the battery nominal power is reduced. This strategy does not consider the SOC of the storage device. In the work presented in [34], a ramp rate control for PV installation in microgrids is proposed. Furthermore, it explains the limitations of the traditional moving average control strategy. This traditional strategy does not provide direct ramp rate control and the storage system operates continuously even if the ramp rate is between the up-down limits. In contrast, the energy flow through the battery is much lower with a direct ramp rate control due to the fact that the battery does not operate if it is not strictly necessary. In [35], it is said that *delay in power measurement and transmission may cause significant error which may not only generate a less smooth output but also may act in reverse direction and add even more fluctuation to the aggregate output.* However, the effect of the delays are not studied in [35].

The studies performed in [31–34] do not explain how to control the PV plant during curtailments and frequency droop events. In general, when the ramp rate is controlled directly, these studies do not consider communication delays nor plant dynamics. The utilization of ESS during curtailments or frequency droop events can help to improve the performance (e.g. during a power curtailment, a SOC control can be performed or the battery can help to reach the setpoint in case of a lack of available PV power). There are no previous studies suggesting how to coordinate the utilization of the storage systems with the PV inverters during curtailment or frequency droop events.

In this Chapter, a practical method to fulfil the grid code requirements including the ramp rate limitation, the power curtailment and the frequency droop considering a hybrid PV-ESS power plant is proposed. For the ramp rate limitation, the direct ramp rate control strategy, explained later, is used. The results are validated by simulations, where communication delays and a simplified model of plant dynamics are taken into account. The effect of the delays and plant dynamics are mitigated thanks to the proposed controller. Highest resolution PV forecasts are usually made for periods of 5-15 min, while as explained in Chapter 2, some grid codes require ramp rate constraints in a time-scale of seconds. Hence, forecasting is not considered in this work.

4.2 Power plant control design

4.2.1 Hybrid PV-Storage power plant description

Figure 4.1 depicts a general scheme of PV power plant including a centralised EES. The reason for using centralized storage is that as the PV plant size increases, the relative power fluctuations diminish [63]. So, when it is desired to limit the fluctuations at the PCC, lower storage features are required than when considering a strategy based on limiting the power fluctuations at the PV inverters output. A central PPC coordinates all PV inverters together with the ancillary devices to achieve the desired setpoints at the PCC. This controller sends active and reactive power setpoints to PV inverters, storage and FACTS devices as well as connection/disconnection orders to capacitor banks as explained in Chapter 3. This chapter enhances the PPC performance considering energy storage devices.

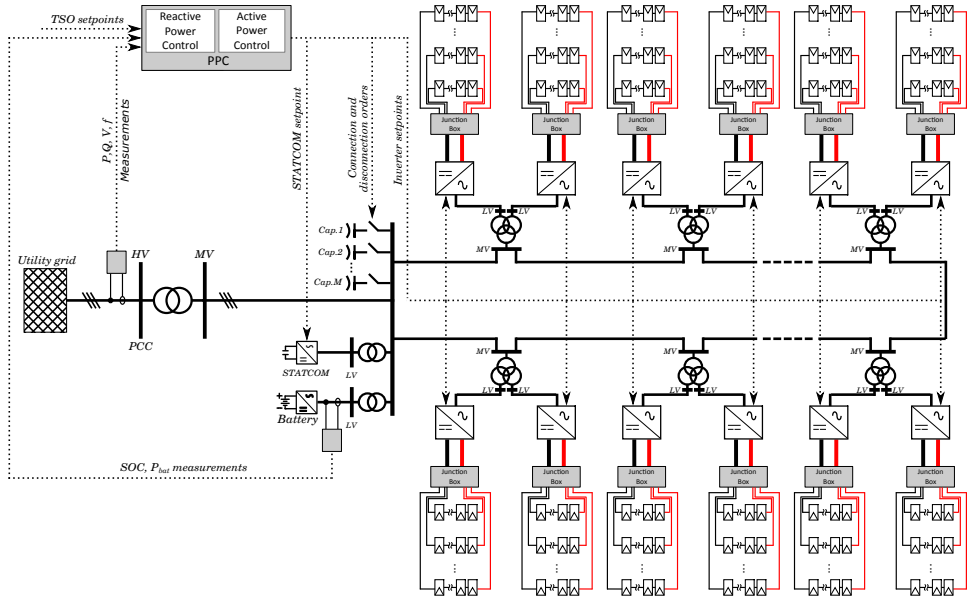


Figure 4.1: General scheme of a hybrid PV-battery power plant

4.2.2 Controller architecture

The controller can be divided, again, into three steps as shown in Figure 4.2: reference computation, PV controller and PV dispatch. The first step (reference computation) computes the battery and PV setpoints taking into

account the grid code requirements and the SOC of the battery. The battery setpoint is sent directly to the battery inverter and will be achieved thanks to the inverter local controller. On the other hand, the PV power setpoint is used as the active power reference value of the central active power controller, which output will be dispatched as in Chapter 3. The subscript *meas* in Figure 4.2 refers to the measured values.

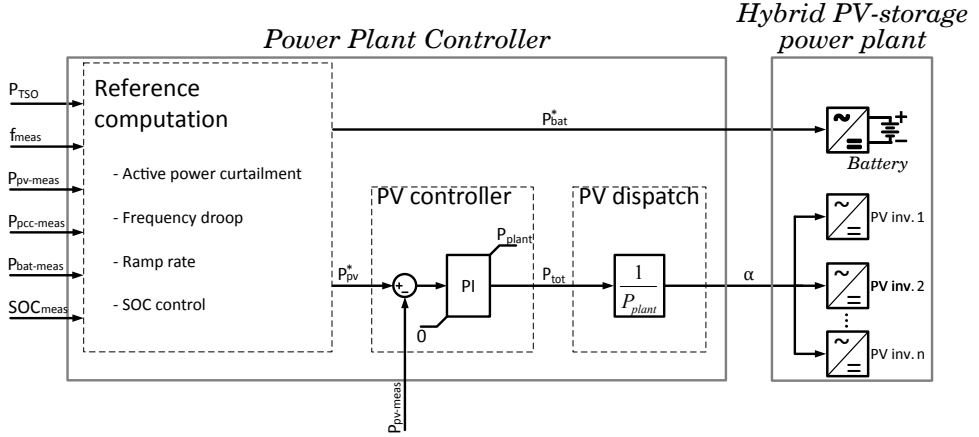


Figure 4.2: Power plant controller architecture

4.2.3 Reference computation

The reference computation block is divided into MPP mode, curtailment mode and two frequency droop modes. The conditions to change the mode are shown in Figure 4.3. The flow chart shown later in Figure 4.9 depicts when the mode selection is performed.

MPP mode

For the MPP mode, the basic concept for mitigating PV power fluctuations is shown in Figure 4.4. There are different strategies in the literature to mitigate the power fluctuations. However, the strategies consisting on filtering the PV power measurement (e.g. the typical medium average technique) are not adequate for the purpose of this thesis. This is due to the fact that grid codes require a ramp rate limitation while these strategies, despite being effective, do not have a direct control of the power ramp rate [34]. So, a direct ramp rate control strategy is chosen in this thesis. This controller is corrective as it reacts once a ramp fault is detected. It means that for short

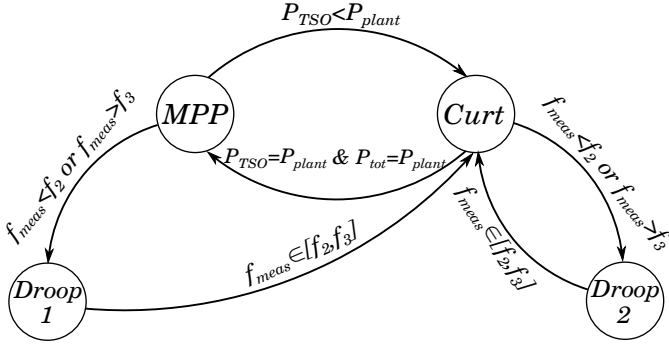


Figure 4.3: Modes of the reference computation block. MPP: PCC setpoint = rated power and the plant operates at the MPP. Droop 1: frequency deviation during MPP mode. Curtailment: TSO sets a PCC setpoint different than the rated power. Also applied for the transition from Droop 1 to MPP mode. Droop 2: frequency deviation during curtailment mode

periods ramp faults will occur, especially at the beginning of the event. The basic idea is that if the PV power at time t does not exceed the ramp rate limitation, the reference power at the PCC will be P_{plant} and the battery setpoint will be set to 0. On the other hand, if the ramp rate is exceeded, the battery setpoint is calculated to bring the ramp rate to its limit. It can be expressed mathematically as (4.1). Obviously, $P_{bat}^*(t)$ is constrained to its limits and if it is at the lower limit, the PV setpoint $P_{pv}^*(t)$ is modified (curtailed) to avoid exceeding the ramp rate, which is expressed as equation (4.2).

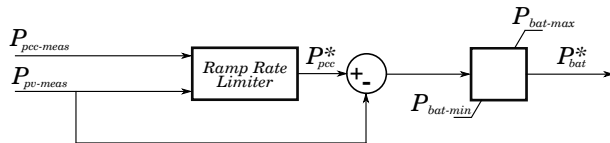


Figure 4.4: Reference computation block - MPP mode concept. This basic scheme is just to help understanding how it works

$$P_{bat}^*(t) = \begin{cases} P_{pcc-meas}(t - T_w) + \Delta P_{max} - P_{pv-meas}(t) & \text{if } P_{pv-meas}(t) - P_{pcc-meas}(t - T_w) > \Delta P_{max} \\ P_{pcc-meas}(t - T_w) + \Delta P_{min} - P_{pv-meas}(t) & \text{if } P_{pv-meas}(t) - P_{pcc-meas}(t - T_w) < \Delta P_{min} \\ 0 & \text{otherwise} \end{cases} \quad (4.1)$$

$$P_{pv}^*(t) = \begin{cases} P_{pcc-meas}(t - T_w) + \Delta P_{max} - P_{bat-meas}(t) & \text{if } P_{bat}^* = P_{bat-min} \\ P_{plant} & \text{otherwise} \end{cases} \quad (4.2)$$

Where $\Delta P_{max} = RR_{max} \cdot \frac{T_w}{60} \cdot \frac{P_{plant}}{100}$ and $\Delta P_{min} = RR_{min} \cdot \frac{T_w}{60} \cdot \frac{P_{plant}}{100}$, being RR_{max} and RR_{min} the maximum (>0) and the minimum (<0) active power ramp rate expressed in %/min, respectively. T_w refers to the time window in which the ramp rate is evaluated.

Over this basic ramp rate limiter structure, some modifications are performed to improve the performance. The MPP mode applies the control block shown in Figures 4.5(a) and 4.5(b). To better understand how the control is performed, a flow diagram is included at section 5.3 (Figure 4.9). First of all, taking into account that the setpoints are not applied instantaneously due to the communication delays and the PV and battery time response, the response of the system (specially if T_w is small) presents power oscillations during ramp events, where the main frequency is $\frac{1}{T_w}$. More details are provided in Appendix B. Therefore, a filter to the measurement at the PCC is included. This filter adds a delay T_d on the measurement that has to be taken into account. The maximum and minimum allowed active power variations ΔP_{max} and ΔP_{min} are calculated considering the filter delay as (4.3) and (4.4). Figure 4.6 shows an example of the performance with and without the filter. The filter proofs beneficial as it eliminates the ripple of the power generated when the battery is limiting the ramp rate. The other modification is the SOC control. With the scheme of Figure 4.5(a) [64], an offset to the battery setpoint is applied depending on the $SOC^*(t)$ and $SOC_{meas}(t)$. The setpoint $SOC^*(t)$ is computed following the $P_{pv-meas}(t)$, which means that the higher is the PV power measured, the higher will be the SOC setpoint. If the PV power is at high level, ramp-down events are more probable. So, in order to discharge the battery when the ramp-down event occurs, it is desired to maintain the SOC at high level. On the other

hand, if the PV power is low, ramp-up events will be expected. So, the desired SOC will be at low levels to be able to charge the battery when the ramp-up event occurs. The SOC ref calculation block computes the $SOC^*(t)$ as (4.5). Note that the $SOC^*(t)$ is between 0.4 and 0.6. It is due to the fact that batteries have low cycle-life. So it is desired to operate it within the stand-by condition [31]. Once the $SOC^*(t)$ is obtained, $P_{bat}^*(t)$ is calculated as (4.6). The PV power setpoint $P_{pv}^*(t)$ is calculated as (4.7) taking into account that $P_{bat}^*(t)$ has been previously limited to between P_{bat_max} and P_{bat_min} .

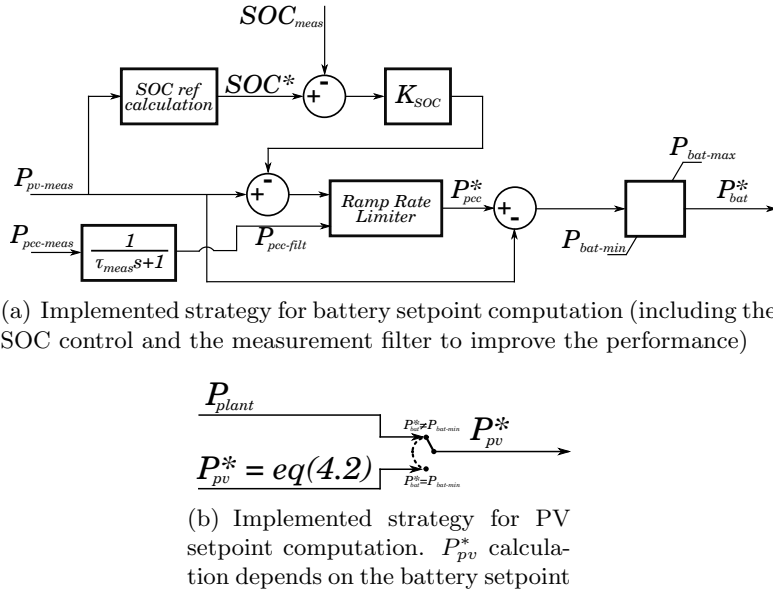
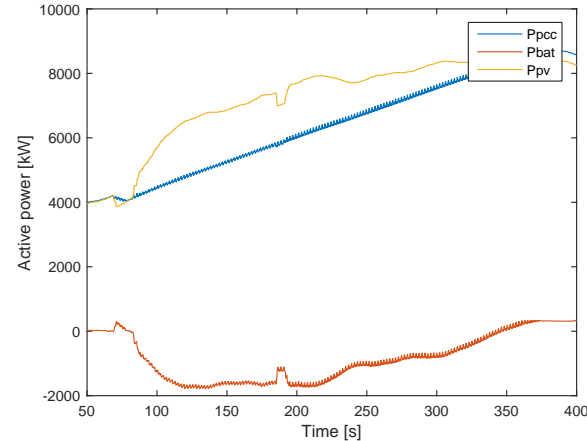


Figure 4.5: Reference computation block - MPP mode. Proposed control scheme

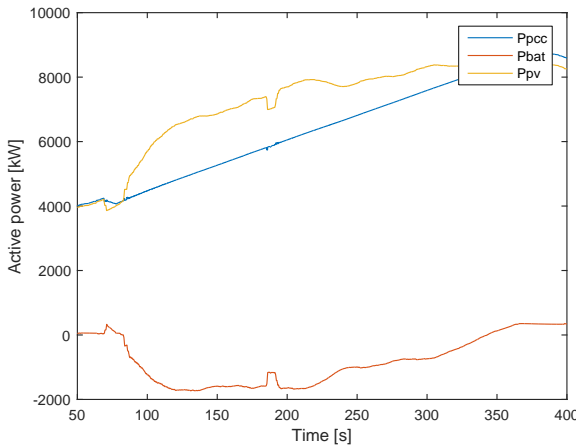
$$\Delta P_{max} = RR_{max} \cdot \frac{T_w + T_d}{60} \cdot \frac{P_{plant}}{100} \quad (4.3)$$

$$\Delta P_{min} = RR_{min} \cdot \frac{T_w + T_d}{60} \cdot \frac{P_{plant}}{100} \quad (4.4)$$

$$SOC^*(t) = 0.4 + \frac{0.6 - 0.4}{P_{plant}} \cdot P_{pv-meas}(t) \quad (4.5)$$



(a) Ramp limiter without filtering



(b) Ramp limiter with filter

Figure 4.6: Example of ramp rate performance without and with filter. $T_w = 2$ s. Total communication delay + battery response time = 50 ms (2.5% of T_w). Total communication delay + PV plant response (PV controller + inverter dynamics) ≈ 1 s (50% of T_w)

$$P_{bat}^*(t) = \begin{cases} P_{pcc-filt}(t - T_w) + \Delta P_{max} - P_{pv-meas}(t) & \text{if } P_{pv-meas}(t) - e(t) - P_{pcc-meas}(t - T_w) > \Delta P_{max} \\ P_{pcc-filt}(t - T_w) + \Delta P_{min} - P_{pv-meas}(t) & \text{if } P_{pv-meas}(t) - e(t) - P_{pcc-meas}(t - T_w) < \Delta P_{min} \\ -e(t) & \text{otherwise} \end{cases} \quad (4.6)$$

$$P_{pv}^*(t) = \begin{cases} P_{pcc-filt}(t - T_w) + \Delta P_{max} - P_{bat-meas}(t) & \text{if } P_{bat}^*(t) = P_{bat-min} \\ P_{plant} & \text{otherwise} \end{cases} \quad (4.7)$$

Where $e(t) = K_{SOC} \cdot (SOC^*(t) - SOC_{meas}(t))$

Curtailment Mode

Considering the PPC is operating in MPP mode, once the TSO sets an active power setpoint ($P_{TSO}(t) < P_{plant}$) the curtailment mode begins. $P_{pv-r}^*(t)$ (the TSO setpoint after applying the ramp limitation) is updated at the first iteration of the PPC according to (4.8). Then, at each PPC execution $P_{pv-r}^*(t)$ is updated following a ramp rate limitation according to (4.9). A saturation is applied as (4.10) in the case of ramp-up or as (4.11) in the case of ramp-down. Finally, $P_{pv}^*(t)$ and $P_{bat}^*(t)$ are calculated as (4.12) and (4.13) respectively. In this way, the battery ensures that the active power at the PCC is the required by the ramp rate limitation. Adding an offset to the PV setpoint (see equation (4.12)) ensures the SOC control of the battery. The corresponding flow chart can be observed in Figure 4.9.

$$P_{pv-r}^*(t) = P_{pcc-meas}(t) \quad (4.8)$$

$$P_{pv-r}^*(t) = \begin{cases} P_{pv-r}^*(t - T_s) + \frac{RR_{min}}{100} \cdot \frac{P_{plant}}{60} \cdot T_s & \text{if } P_{TSO} < P_{pv-r}^*(t - T_s) \\ P_{pv-r}^*(t - T_s) + \frac{RR_{max}}{100} \cdot \frac{P_{plant}}{60} \cdot T_s & \text{if } P_{TSO} \geq P_{pv-r}^*(t - T_s) \end{cases} \quad (4.9)$$

Where T_s is the sampling time of the PPC.

$$P_{pv-r}^*(t) = \begin{cases} P_{pv-r}^*(t) & \text{if } P_{TSO} \geq P_{pv-r}^*(t) \\ P_{TSO} & \text{if } P_{TSO} < P_{pv-r}^*(t) \end{cases} \quad (4.10)$$

$$P_{pv-r}^*(t) = \begin{cases} P_{pv-r}^*(t) & \text{if } P_{TSO} \leq P_{pv-r}^*(t) \\ P_{TSO} & \text{if } P_{TSO} > P_{pv-r}^*(t) \end{cases} \quad (4.11)$$

$$P_{pv}^*(t) = P_{pv-r}^*(t) + (SOC^*(t) - SOC_{meas}(t)) \cdot K_{SOC} \quad (4.12)$$

$$P_{bat}^*(t) = P_{pv-r}^*(t) - P_{pv-meas}(t) \quad (4.13)$$

Droop 1 mode

During the MPP mode ($P_{TSO} = P_{plant}$), a frequency deviation can occur. In this case the so-called Droop 1 mode is applied. This mode is represented in Figure 4.7. P_D is set to the active power measurement at the PCC as soon as a frequency deviation exceeds the dead band $f_2 - f_3$ (4.14). This setpoint P_D remains constant until the frequency goes back to the dead band. The grid code specifies that $P_{pv_av} \geq 1.03 \cdot P_D$. Due to the fact that forecast is not considered, the energy storage must reserve a minimum power of $0.03 \cdot P_{pcc_meas}$ when the PV plant operates under MPP mode. The droop contribution ΔP is calculated at each computation loop of the PPC according to the droop curve. Then, the PV and battery setpoints are calculated as (4.15) and (4.16) respectively.

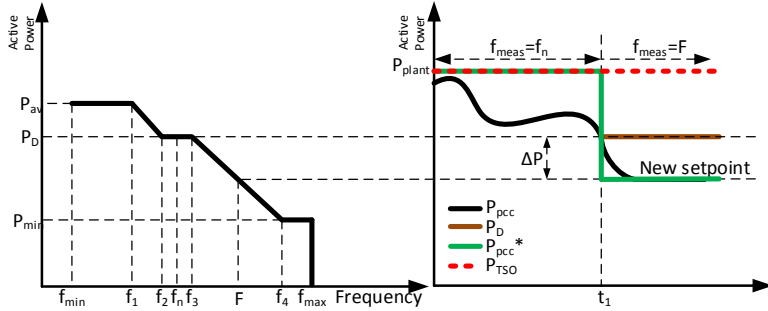


Figure 4.7: Droop application under MPP mode

$$P_D = P_{pcc-meas} \quad (4.14)$$

$$P_{pv}^*(t) = P_D + \Delta P + (SOC^*(t) - SOC_{meas}(t)) \cdot K_{SOC} \quad (4.15)$$

$$P_{bat}^*(t) = P_{pv}^*(t) - P_{pv-meas}(t) \quad (4.16)$$

Once the frequency recover the normal values ($f_{meas}(t) \in [f_2, f_3]$), it is desired to return to the MPP mode. Fast power changes can be avoided setting the curtailment mode despite $P_{TSO} = P_{plant}$, which will perform the ramp up event until the PV plant reaches the MPP and then the operation mode will change to MPP mode (see the transition conditions from Droop 1 to MPP modes in Figure 4.3).

Droop 2 mode

If a frequency deviation occurs during a curtailment the reference computation block computes the Droop 2 mode. In this case P_D is updated at each PPC execution as (4.17), where $P_{pv-r}^*(t)$ is obtained by the same way than in the curtailment mode ($P_{pv-r}^*(t)$ is the TSO setpoint after applying a ramp limitation). The PV and battery setpoints are calculated again considering the droop curve, the updated P_D and equations (4.15) and (4.16). An example of how this mode works is depicted in figure 4.8. When the droop mode ends, $P_{pv-r}^*(t)$ is updated to $P_{pcc-meas}(t)$ and curtailment mode is applied again to go from mode Droop 2 to mode curtailment with ramp transition avoiding fast changes.

$$P_D(t) = P_{pv-r}^*(t) \quad (4.17)$$

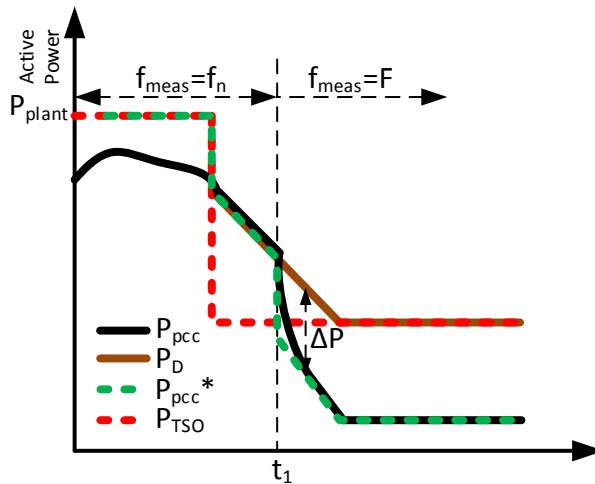


Figure 4.8: Droop application under curtailment mode

4.2.4 Summary

A flow diagram of the control solution is summarized in Figure 4.9

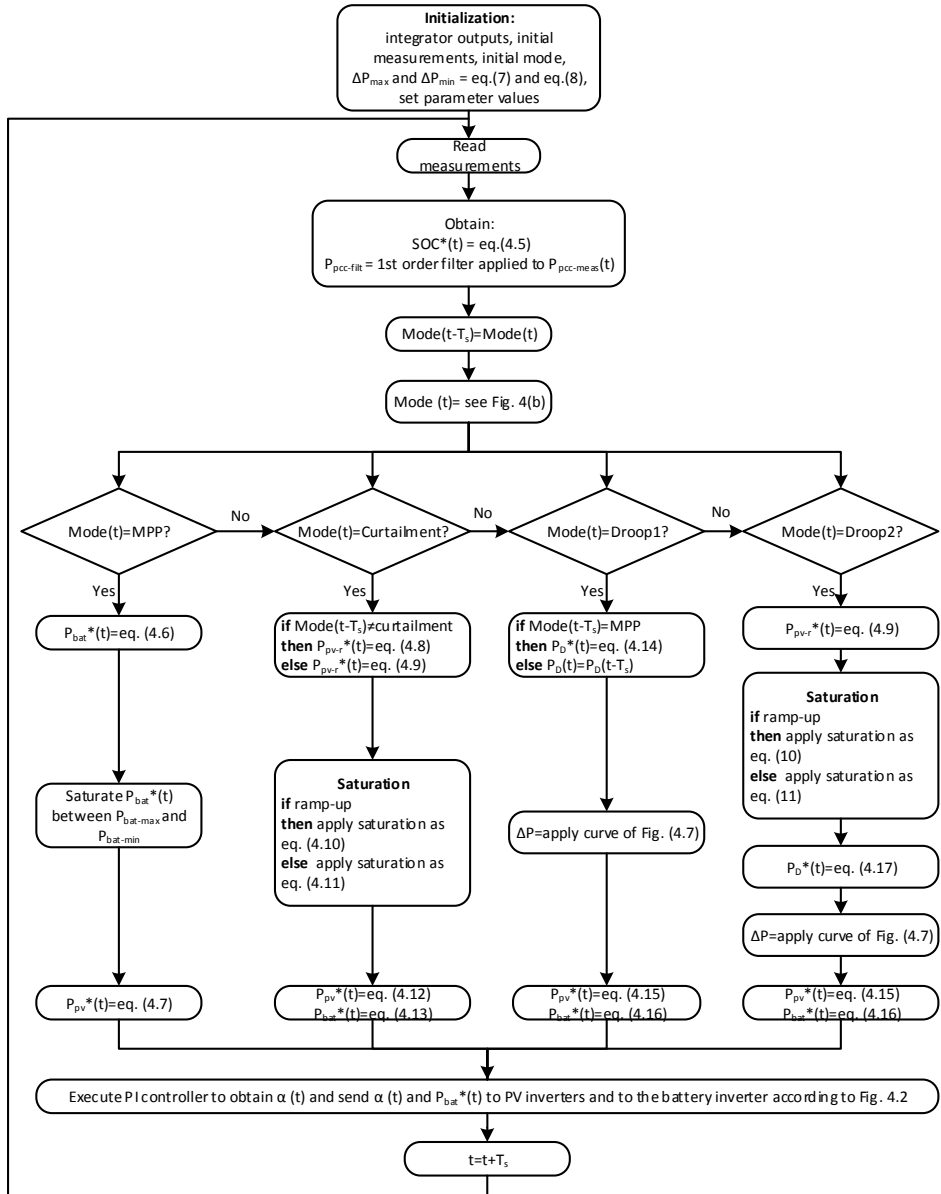


Figure 4.9: Flow diagram of the control solution

4.3 Results

4.3.1 Case study

The case study corresponds to the vanju-Mare PV power plant. In this chapter, long simulations will be required. Accordingly a simplified model will be considered. To obtain real available PV power data, P_{pv_av} , the NREL irradiance database has been used [65]. First, second by second irradiance data (from 1 Apr. of 2011 to 13 May of 2011 in Oahu, Hawaii) has been obtained and then, based on the model of [62], the available PV power has been calculated. According to [62], the PV power output can be obtained applying a first order filter to the irradiance data and scaling the result by a gain of $\frac{P_{plant}}{1000}$. The filter time constant is $\frac{\sqrt{S}}{2\pi \cdot 0.02}$, where S is the area of the PV plant in ha. The model assumptions are described in the Appendix C.

4.3.2 Simulation results

MPP mode

Figure 4.10 shows a complete day operating under MPP mode. It can be observed that the battery is only used during periods of high solar energy variability. The rest of the time, the battery is only used for the control of the SOC. The zoomed area shows the PV power and the PCC power. It can be observed that the ramp rate limitation is fulfilled. As explained previously, the SOC setpoint is computed depending on the PV power generated. It is shown on the bottom plot of Figure 4.10, where during sunny hours the SOC tends to increase.

In [46], it is suggested to evaluate ramp rate compliance by taking a sample of the ramp rate each two seconds and calculating the % of ramp rate excursions out of the limits (for 10 % ramp rate limit, a breach is considered to be at 11 %). The time window for calculating the ramp rate is 2 seconds. By the methodology presented in this chapter, the ramp rate compliance is 98 %, while without battery compliance drops to 91 % (calculations exclude night-time). It is worth noting that the battery sizing is out of the scope of this thesis. Larger battery of 7 MW and 900 kWh has also been simulated. In this case the ramp rate compliance increases up to 99.3 % higher than the 98.5 % required according to [46]. Reaching the 100 % of the ramp rate compliance will rarely occur as the controller is corrective (first detects the ramp fault and then reacts).

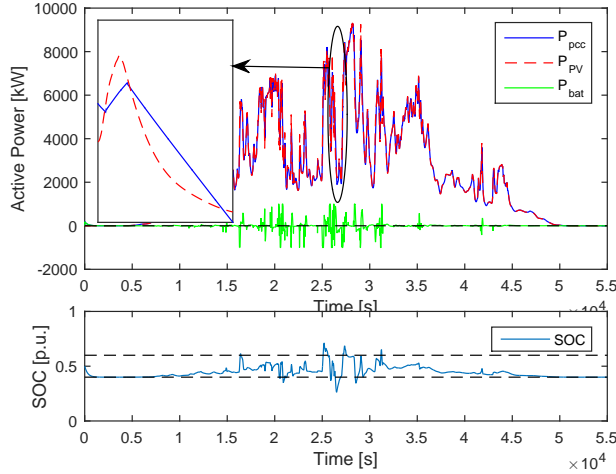


Figure 4.10: Simulation of a complete day under MPP mode. Top plot: PCC (blue), PV (red), and battery (green) active power. Bottom plot: SOC (blue) and 0.4-0.6 p.u. range (dashed)

SOC control

The SOC control strategy is evaluated by means of how the battery operation could affect its lifetime. It is known that the desirable SOC level is between 0.4 and 0.6 p.u, defined as standby condition [31]. In addition, the amount of power flowing through the battery indicates its usage and hence, it also affects the battery lifetime. These two parameters are compared here for each SOC control strategy.

Figure 4.11 compares the SOC control strategies: in blue considering constant SOC setpoint and in red the proposed strategy according to equation (4.5). Forty three consecutive days have been simulated. Figure 4.11 shows the first 7 days where the night time has been reduced due to the limitation of computational time. To compare these strategies, MPP mode is applied. The PV power is shown in the top plot, while the SOC is shown in the bottom plot. As it can be observed, the time of 'out of the standby operation' reduces compared to a constant SOC setpoint. In addition, the range of utilization of the SOC for the presented strategy is lower than the range used by the constant SOC setpoint strategy. Thus, the proposed strategy will require lower battery energy capacity for complying with the ramp rate limitation.

The results for 43 consecutive days are summarized in Tables 4.1 and

4.3 Results

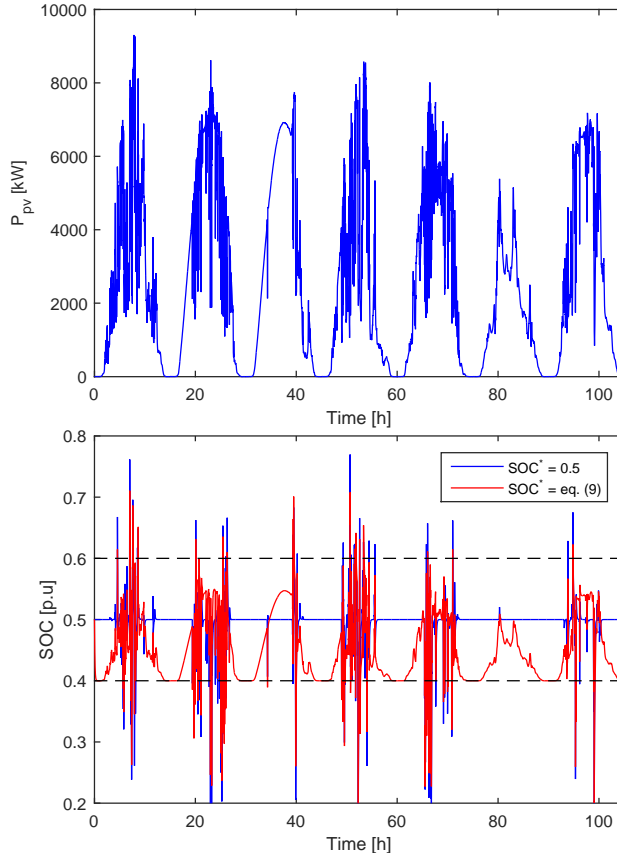


Figure 4.11: Comparison of SOC control strategies (MPP mode). Top plot: PV power profile. Bottom plot: SOC for both strategies, $SOC^* = 0.5$ in blue and $SOC^* = \text{eq. (4.5)}$ in red.

4.2. Table 4.1 shows the amount of time during which the SOC exceeds the desired 0.4-0.6 p.u. range. Generally, this time is reduced by applying the proposed strategy. In addition, it can be observed that the higher the deviation from the standby condition, the higher is the time reduction. So, it can be concluded that the the desired SOC operation range is better fulfilled by the proposed strategy.

Table 4.2 shows the total energy flow through the battery during the 43 simulated days. It can be observed that for high variability days, the total energy flow is reduced, on average, by 2.8 % when the proposed strategy is used. In contrast, during the medium and low variability days, the total

Table 4.1: Time [min] during which the SOC is out of the standby condition (43 days of simulation)

	$SOC \in [0, 0.4) \cup (0.6, 1]$	$SOC \in [0, 0.3) \cup (0.7, 1]$	$SOC \in [0, 0.2) \cup (0.8, 1]$	$SOC \in [0, 0.1) \cup (0.9, 1]$
$SOC^* = 0.5$	1316	315	40	3
$SOC^* = \text{eq. (4.5)}$	1290	235	18	0
% of reduction	2.0	25.3	54.6	100

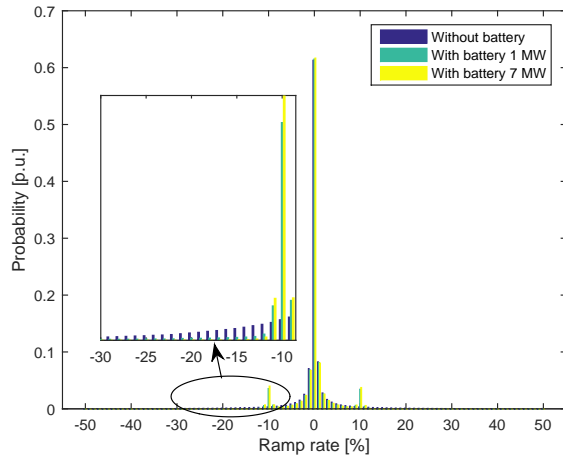
energy flowing through the battery with the proposed strategy is greater than considering a constant SOC setpoint. The high difference during low variability days is due to the fact that, while the proposed SOC control strategy performs one small cycle, the constant SOC strategy does not use the battery.

Table 4.2: Total energy flow through the battery [kWh] (43 days of simulation)

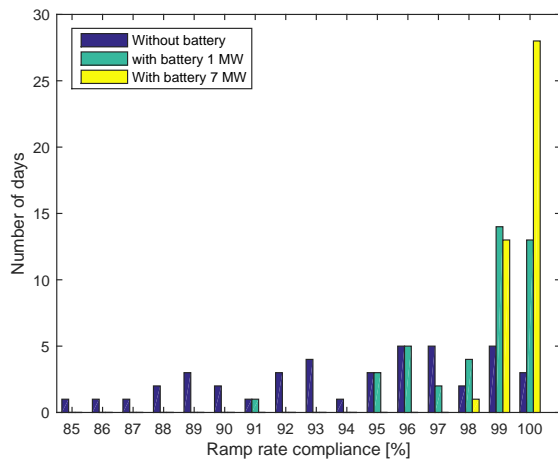
	High variability (14 days)	Medium variability (14 days)	Low variability (15 days)
$SOC=0.5$	24202	10100	2772.1
$SOC=\text{eq. (9)}$	23525	10199	3532.9
% of reduction	2.8	-1.0	-27.4

The ramp rate compliance has been analysed for the 43 simulated days (Figure 4.12). Considering the whole simulation period, the ramp rate compliance in absence of the energy storage reaches 88.9 %, while with the battery it reaches up to 97 % (night time is excluded). The remaining 3 % is due to the fact that the response is not instantaneous and because of the limitations of the battery power rating. The proposed control with a larger battery would have the potential to comply during 99 % of the time. For this latter calculation, a battery of 7 MW and 900 kWh is used . The corresponding ramp rate distribution is shown in Figure 4.12(a) where it can be observed that most of the ramp rate faults without battery are moved to the 10 % ramp rate limit when the battery is installed. Figure 4.12(b) shows the ramp rate compliance histogram for three different scenarios: i) without battery ii) with the simulated 1 MW battery and iii) with 7 MW battery. It is shown that with a properly sized battery the ramp rate specified by the grid code is accomplished.

4.3 Results



(a) Normalized distribution of the ramp rate



(b) Histogram of the ramp rate compliance per days for different scenarios

Figure 4.12: Ramp rate performance during 43 days for different scenarios:
i) without battery, ii) with battery 1 MW and iii) with battery 7 MW

Power curtailment

The power curtailment performance is shown in Figure 4.13. The PV power follows a ramp until reaching the setpoint. The battery just performs its SOC control. During the short period when there is not enough available PV power, the battery helps to achieve the setpoint. Once the available PV power is again greater than the TSO setpoint, a small transient that is due to the PV PI controller can be observed. This controller saturates its output at the nominal PV plant power (see the black dotted line). So, once the available power is greater than the setpoint, the output of the controller starts to decrease. However, at the beginning this reduction has no effect because the available active power is still smaller than the PI output. Nevertheless, the battery also contributes following the TSO setpoint during this transient. When the power curtailment ends, a ramp-up limitation is performed until the available power reaches its MPP. We know the MPP is reached because the PI controller output is saturated at the MPP.

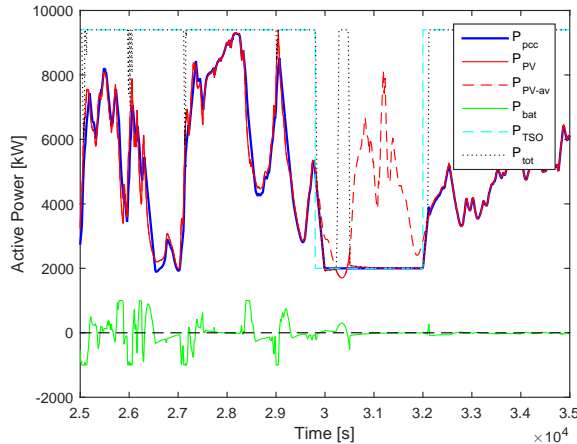


Figure 4.13: PV, battery and PCC active power response after curtailment. Curtailment is set at 2 MW between 29800 s and 32000 s (blue dashed line).

Frequency droop

Figures 4.14 and 4.15 show the previous scenario, but during the curtailment, a droop event occurs for over and under frequency deviation. In Figure 4.14, it is observed how once the frequency increases, the output power automatically reduces adding an offset ΔP to the TSO ramp limited setpoint. At

4.3 Results

the same time that the droop and curtailment operation is performed, the SOC control is applied. It can be observed in the bottom plot, where the SOC^* is calculated as (4.5). In Figure 4.15 the down frequency droop curve is shown. It is observed how the battery performs the SOC control and, when there is a lack of PV power, it supports the power plant by injecting additional active power.

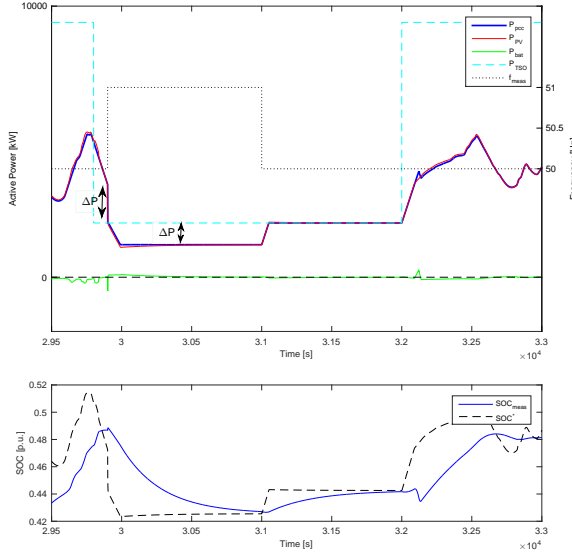


Figure 4.14: Frequency droop response during curtailment. PCC, PV and battery active power and SOC control analysis. Up frequency event. Enough PV power is available and no battery support is required.

Finally, Figure 4.16 depicts the good performance of droop operation when the PV plant is operating at the MPP mode. It is shown how the droop contribution is applied instantaneously and, when the frequency goes back to the dead band, the PV plant returns to the MPP in a smooth way, respecting the 10 % ramp rate limitation.

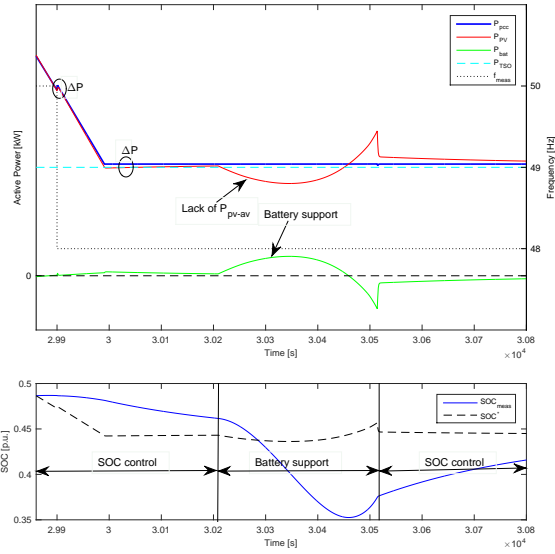


Figure 4.15: Frequency droop response during curtailment. PCC, PV and battery active power and SOC control analysis. Down frequency event. Lack of PV power available and battery provides support to comply the setpoint.

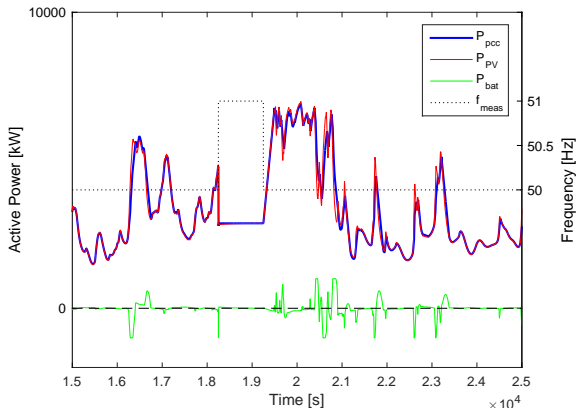


Figure 4.16: Frequency droop response during MPP operation mode. PCC, PV and battery active power analysis. In this case, there is enough PV power. So, no battery support is required.

4.4 Conclusions

In this chapter, a PPC to fulfil grid code requirements in hybrid PV-storage power plants has been presented. In particular, power curtailment, frequency droop and ramp rate limitation have been studied with satisfactory results.

When a direct ramp rate control is performed, some power oscillations can be observed at the point of common coupling. These undesired power oscillations appear because the setpoints are not applied instantaneously as explained in Appendix B. The solution to mitigate this effect is to filter the measurements at the PCC. The filter adds a delay that have to be considered because the control variable, i.e. the ramp rate, depends on the time.

The traditional SOC control for low cycle-life storage systems ($SOC^* = 0.5$) has been modified so that the SOC^* follows the PV power generated, where the result shows that it keeps the battery less stressed during days with high PV variability. On the other hand, the controller permits SOC control during curtailment and frequency droop events. In case of having a lack of available PV power to reach the frequency droop setpoints, the controller uses the battery to fulfil these requirements, which improves the performance in comparison with PV plants that are not equipped with storage systems.

It has been shown that the 2-second ramp rate compliance may be fulfilled by the proposed controller. For that purpose, a properly sized battery is required.

Part II

Multi-microgrids and optimal feeder flow operation of microgrids

Chapter 5

Introduction to microgrids

5.1 Introduction

As explained in Chapter 2, owing to the intermittent nature of wind and PV power and the distributed location of these resources, the integration of a large amount of renewable energy in the conventional power system is a challenging process. At the distribution level, grids have been traditionally operated as passive systems. But the integration of distributed resources is transforming these networks into active systems with distributed control and bidirectional power flows. So, new concepts are required for the expansion of active distribution networks, where one of the most promising network structure is based on microgrids [66].

The integration of DERs such as DG as wind and PV, combined heat and power (CHP) together with energy storage can potentially reduce the carbon emissions, improve the power quality, grid reliability and the energy efficiency. In addition, the integration of DER may mitigate the system expansion needs [5]. Due to the huge number of DERs, the new challenges focus on grid operation and control. These challenges can be addressed by microgrids [5, 6]. A microgrid is a group of interconnected loads and DERs that, operated in a coordinated way, behaves as a single producer or consumer from both the grid and the market perspective. Microgrids are basically LV (<1 kV) or MV (1-69 kV) grids that can operate in grid connected mode (interconnected to an external grid) or in an isolated or islanded mode (without the support of external grids).

The microgrid concept has been investigated since the early 2000. In [8, 67–83] the microgrid development status is summarized. The authors from [67] review the DG technology, the grid benefits from microgrids, the power electronics applications, the operation and control in microgrids, the protection, the communication systems and different economic aspects of microgrids. The concept of microgrid clusters is also included, showing they can benefit from lower costs and lower emissions. In addition, [67] high-

lights the need for further research studies in this field. In [68, 69], a review of the microgrid technology including DGs, storage and power electronics is performed. In [69], the potential benefits of microgrids, protection, control, economics and communication are also described. The works presented in [8, 70–73] are focused on the operation and control techniques of microgrids. These papers analyse the centralised, decentralised and hierarchical control of microgrids and issues related to the stability, power quality and the corresponding solutions. The work is mainly performed for radial¹ microgrids as meshed² topologies requires further development. The studies presented in [74, 75] review the particular case of hybrid AC/DC microgrids and are focused on the classification of the topologies and control strategies. A general overview of the microgrid status can be found in [76], which also includes real cases of microgrids (as in [77]) and standardization. In [78], a review of the microgrid DG resources and the operation of the microgrid is performed. It also includes different developments in recent projects around the world. On the other hand, the architecture of microgrids is reviewed in [79–83].

5.2 The microgrid concept

5.2.1 Definition

A microgrid is *a group of interconnected loads and DERs within clearly defined electrical boundaries that acts as a single controllable entity with respect to the grid. A microgrid can connect and disconnect from the grid to enable it to operate in both grid-connected or island-mode* [84].

A general scheme of a microgrid is shown in Figure 5.1 where, according to the definition, distributed resources (storage and generation), loads and controllable loads can be observed. It clearly defines electrical boundaries which are identified as the points of common coupling (PCC 1 to PCC n). These points are the interconnections with other grids. The voltage nature of the microgrid and the external grids can be different. In this case, an interface element which is part of the microgrid must be installed to permit the interconnection. The control, which can be centralized or decentralized [8], permits the operation as a single controllable entity. In addition, meters and a communication infrastructure must be installed. Finally, the microgrid must have a switch per PCC to permit the operation in island-mode.

¹grid where only one electrical path between two different points exists

²grid where more than one electrical path between two different points exist

5.2 The microgrid concept

The microgrid can be operated in AC, DC or mixed AC/DC technology. Depending on these technologies, power electronics or transformers should be used to interconnect distributed resources and loads with the microgrid.

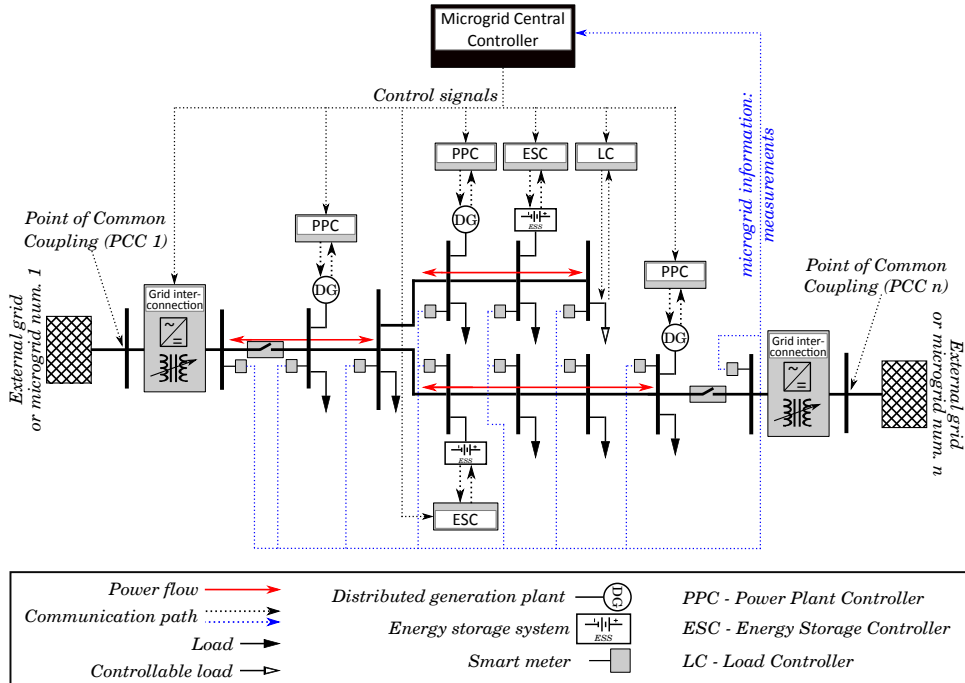


Figure 5.1: Scheme of a microgrid

One important aspect about this definition is that the microgrid acts as a single controllable entity. Regarding this concept, next sections are focused on how external agents of a microgrid can interact with it. Two differentiated cases can be identified. For the first one, when a microgrid is interconnected to a distribution grid, the external agent is the distribution grid operator. For the second one, in the case of having a point to point connection between microgrids, each microgrid can see the other one as an external agent.

5.2.2 Microgrid connected to an external distribution grid

From the external grid viewpoint, the microgrid can be observed as a single entity connected at the PCC that can generate or consume active power as shown in Figure 5.2. So, it can be seen as a controllable aggregated generator and load, where storage devices can be included in both sides. Thanks to

the smart nature of the microgrid, some ancillary services can be provided or required. These services are desirable due to the fact that, if the central generation is displaced by distributed resources without bringing additional support, the operation cost will increase. In addition, integrating ancillary services to the electricity market could contribute to the feasibility of projects on DG [85]. Table 5.1 describes ancillary services that a microgrid, as a single entity, can provide to the external grid [86].

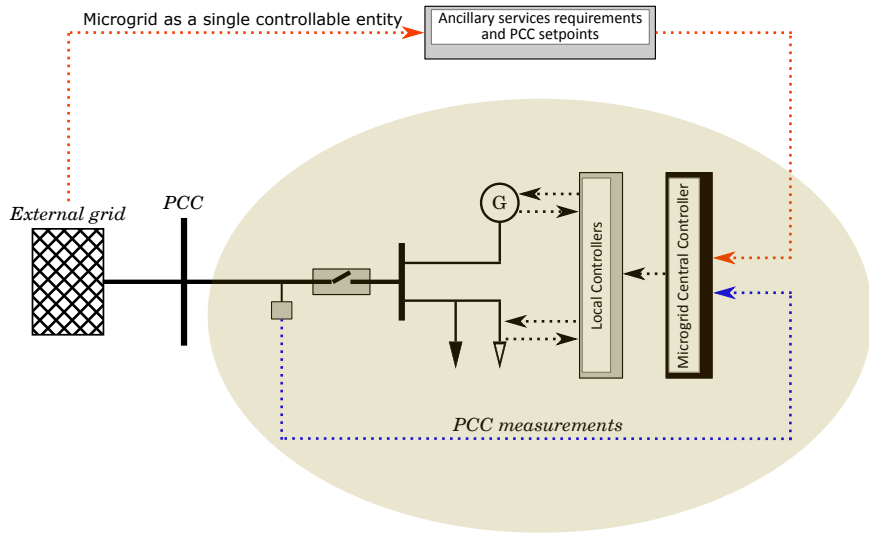


Figure 5.2: Microgrid as a single entity viewpoint. Interconnection to an external distribution grid

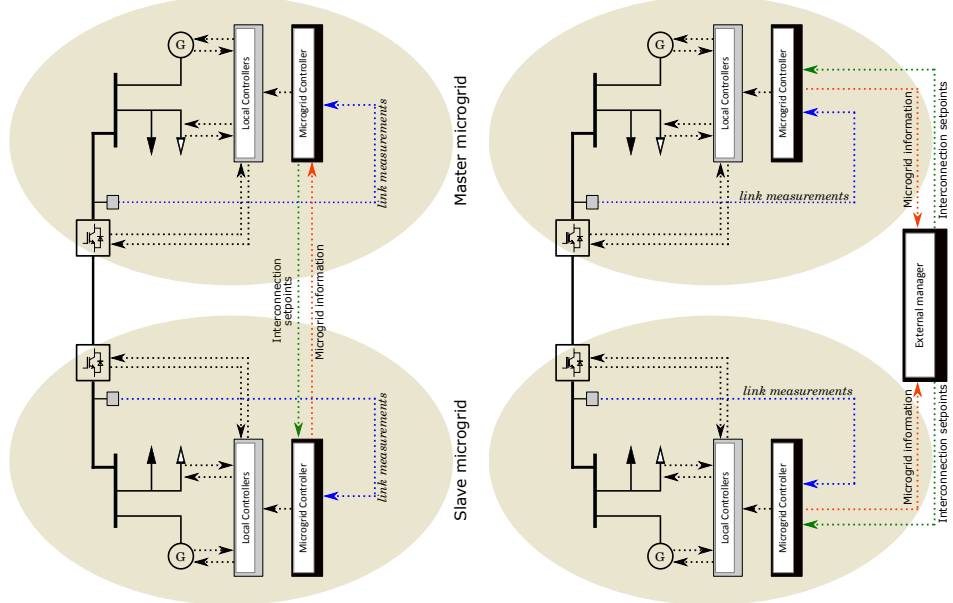
5.2.3 Point to point connection between microgrids

In the point to point connection between microgrids, each microgrid can also be seen as a controllable aggregated generator and load. In this case, the role of each microgrid can be different depending on the interaction rules between them. There are mainly two ways of interaction as shown in Figure 5.3. In the master-slave topology, the master microgrid is responsible for sending orders to the slave microgrid. So, the slave microgrid acts as a single controllable entity. On the other hand, in the central controlled topology there is an external agent who decides the actions that each microgrid has to perform. In this case, both microgrids act as controllable entities.

In addition to this example, other interconnections can be performed with external grids. So, a master microgrid can have more than one slave micro-

Service	Description
Reactive power and voltage control	<p>Microgrids can perform smooth voltage regulation supplying reactive power from microsources.</p> <p>It can avoid the traditional and abrupt voltage regulation (e.g. capacitor banks).</p> <p>It can help the utility generators to generate at their maximum capacity.</p>
Supply of reserves	<p>A microgrid can provide a frequency responsive spinning reserve due to the faster response of microsources in front of frequency deviations.</p> <p>Microgrids can provide supplemental reserve by making their generators obey the system operator's requests (e.g. peak shaving or FFC).</p> <p>Microgrids can provide backup supply by making arrangements with the system operator. By this, the system operator can manage the critical and non-critical loads during primary supply failures.</p>
Regulation and Load following	Plan the generation (load following) and adjust it minute by minute (regulation) according to the power demand in the microgrid. It avoids physical and economic transmission and distribution limitations in importing power.
Other	<p>Black start: microgrids can operate on islanded mode.</p> <p>When the main grid collapses, microgrids can export active power to the system black start.</p> <p>Network stability: microgrids can detect slow frequency oscillations and provide damping functions.</p>

Table 5.1: Possible microgrid ancillary services



(a) Microgrid as a single entity viewpoint. (b) Microgrid as a single entity viewpoint.
Point to point interconnection between mi- Point to point interconnection between mi-
crogrids and Master-slave topology crogrids and central controlled topology

Figure 5.3: Interactions between interconnected microgrids

grid and can be the slave of another microgrid or an external grid. The same happens with the central controlled microgrid. Several microgrids can be governed by a single central controller, which can respond to external grid requirements.

5.3 Multi-microgrids

Since the microgrid technology has been extensively studied, in the coming years a transformation of the current electric power system to a multi-microgrid power system can be expected. In this direction, the study of multi-microgrids is currently being explored.

Some studies have analysed the benefits of the multi-microgrids. The amount of DG that can be integrated in a single microgrid is limited, but the connection of multiple microgrids within the same network can mitigate this issue [87]. In addition, multi-microgrid systems can bring environmental

benefits, as analysed in [88]. The study, considers a typical distribution grid with 64 connected microgrids. The results show that the distribution grid losses and the pollutant emissions are reduced with the multi-microgrid system. The loss reduction in multi-microgrids is also studied in [89], where it is determined that coordinated multi-microgrids can improve the system efficiency. Furthermore, as stated in [90], microgrid interconnections can allow to combine the advantages of AC and DC microgrids. If they are properly planned, they also improve the reliability of the multi-microgrid system [90, 91]. The authors from [92] also identify benefits in microgrids clusters showing they can lead to mutual support among the interconnected microgrids during contingencies. Taking into account all these potential benefits, the research on microgrid clusters (or multi-microgrids) is one of the main drivers for the integration of microgrids into the power system.

Literature around this concept has been only focused on the system operation, control and management [87]. For the different analysis existing in the literature, either the type of interconnection between the microgrids is not addressed [93] or a particular microgrid cluster architecture is selected [87, 93–103]. Reference [93] reviews the control of DC multi-microgrid systems and their potential benefits without considering the possible architectures. This review is performed for the islanded mode (e.g. when the cluster operates without an external grid support). Among the benefits, the maximum utilization of energy sources and the improved reliability are identified. It is also introduced that the stress and ageing of the components can be diminished, reducing the maintenance costs. Additionally, the system stability can be improved in the case of clusters with large inertia, but degraded in the case of clusters with low inertia. On the other hand, examples of studies focusing on a specific microgrid clustering architecture are presented in [87, 94–103]. In [94–99], microgrids are interconnected through an external AC network using power transformers. In [100] the same architecture is studied, and also focusing on the case where microgrids are interconnected between them through point to point connections. The point to point interconnections between microgrids is also studied in [101, 102], where DC technology and power converters are used. On the other hand, mixed configurations can be found in [87, 103], where interconnections to the external grid are combined with point to point interconnections between microgrids. In this case, AC and DC technologies are used. A specific design for the hybrid AC/DC connection of multiple microgrids is proposed in [87] based on linking microgrids between each other through DC lines and on keeping the AC connection to the main grid.

5.4 Control of microgrids

5.4.1 Hierarchical control architecture of microgrids

Several approaches have been proposed for the control and operation of a microgrid. These approaches are named centralized, decentralized and distributed, respectively [8, 79]. In the centralized approach, the information of the DERs and loads are collected in a central aggregator. Then, this information is processed and setpoints are sent back to each DER through direct communication links. On the other hand, the decentralized architecture does not use direct communication links, they use the power lines to communicate by means of varying the voltage and frequency. Finally, in the distributed control, the coordination is done through direct communication links. But in this case, the communication is done between units [79]. Centralized approaches lead to high computational and communication needs while decentralized approaches do not offer a proper coordination level between the elements. Distributed control approach could offer a good solution to this problem. Nevertheless, a good performance can also be achieved by the combination of centralized and decentralized approaches, leading to a hierarchical control architecture, which is the most common solution [8].

The hierarchical control in microgrids is formed by primary, secondary and tertiary control layers, where each one has different objectives. The primary control, which is based on local measurements, is in charge of the power sharing and balance. This is done by the local controllers of the DERs using the P-f, Q-V droop methods. Then, the secondary control layer is performed in the central microgrid controller. This controller, also known as EMS, is in charge to perform the unit commitment and economic dispatch of the DERs with a specific optimization objective. In grid isolated operation, this controller also will restore the voltage and frequency deviations produced by power unbalances. The tertiary control layer is the upper control layer, which coordinates the main grid resources depending on its needs. The main grid can contain multiple microgrids as well as other controllable resources. For example, the tertiary controller determines the operational modes (voltage support, frequency support, etc.) and the power setpoints at the feeders or PCCs of microgrids and generators [8].

5.4.2 Control strategies for DG in microgrids

Two differentiated local control strategies have been proposed for the DGs within a microgrid, named Unit output Power Control (UPC) and Feeder Flow Control (FFC) [104].

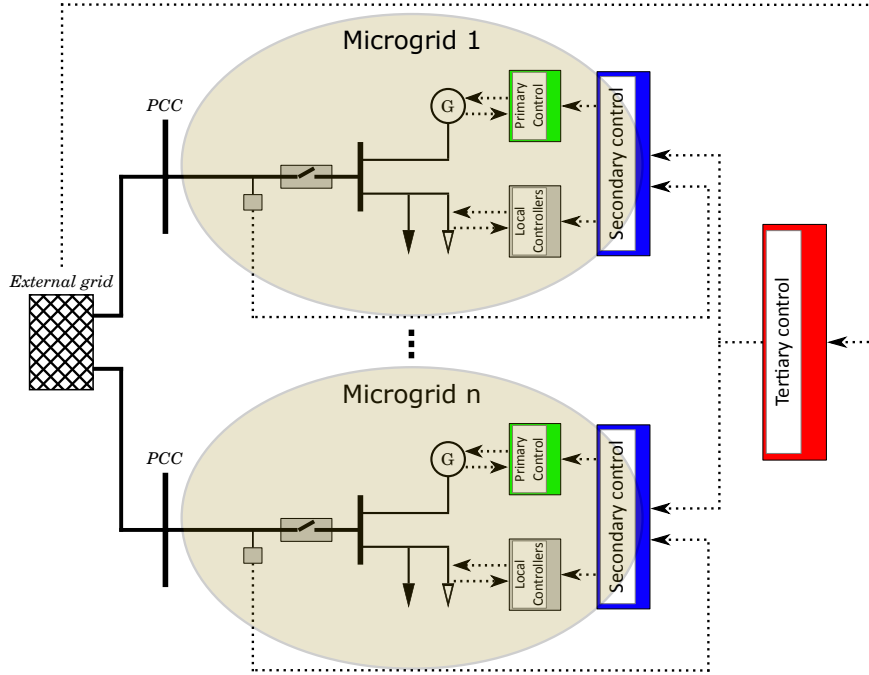


Figure 5.4: Hierarchical control architecture for microgrids

In the UPC mode, shown in Figure 5.5(a), the local control of the n -th DG is in charge of regulating the generation output to reach a constant setpoint P_{DGn}^* . It can be done using a conventional PI controller and comparing the power generation measurement with the power generation setpoint. This setpoint can be calculated by an EMS or by an external system operator to reach some objectives (usually minimum cost). In this case, any variation of either the demand or the non-dispatchable generation downstream the feeder flow controlled DG will be compensated by the external grid. In the FFC mode, shown in Figure 5.5(b), the local control of the n -th DG is in charge of regulating the power flow upstream the generator to reach a constant feeder flow setpoint FF_n^* . It can be done using a conventional PI controller and comparing the feeder flow measurement with the feeder flow setpoint. Again, this setpoint can be calculated by an EMS or by an external system operator. In this case, any load or non-dispatchable generation variation downstream the controlled feeder will be compensated by the dispatchable generators while the power exchange upstream the feeder flow controlled generator will be maintained constant.

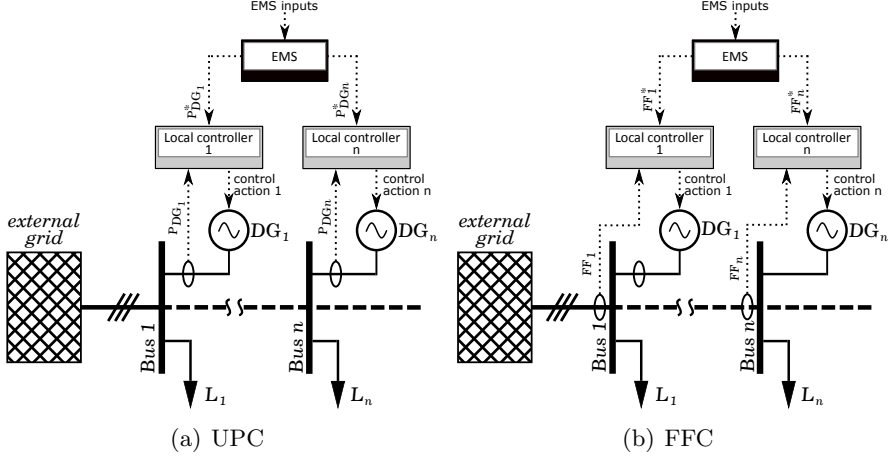


Figure 5.5: Power control mode of a DG

5.5 Conclusions

A large amount of the current centralised generation could be displaced to local generation within microgrids. At the same time, as the technology advances, an increase of the number of interconnected microgrids can be expected, transforming the current network to a multi-microgrid system. Under this scenario, and as happened with the integration of LS-PVPPs, multi-microgrid systems will require ancillary services from their microgrids. As commented before, the tertiary control layer of multi-microgrids sets the operational modes of microgrids as well as the setpoints at their feeders. The FFC approach turns microgrids as true dispatchable systems, which is adequate to comply with the tertiary control layer setpoints.

Further analysis regarding the multi-microgrid concept is still required. As commented earlier, this concept has only been studied in terms of operation, control and management. Studies regarding how these microgrids could be interconnected are still missing, i.e. the multi-microgrid architectures still require to be defined. On the other hand, the FFC of DGs within a microgrid for controlling the power exchange between the microgrid and an external grid has been presented in several studies as a solution to facilitate the management of multi-microgrids. The presented approaches mainly focus on the local controllers of the DGs, but very few research has analysed the outer control layer, i.e. the EMS for the feeder flow controlled microgrids. The following chapters will address these two main aspects.

Chapter 6

Multi-microgrid architectures

This chapter is focused on analysing how microgrids can be interconnected forming multi-microgrid networks. The concept of multi-microgrids is at the early stage of the state-of-the-art, hence more studies are required for accurately determining the potential of each architecture. Therefore, this chapter focuses on a qualitative and conceptual analysis rather than a numerical approach. This analysis can be used as a starting point for identifying the most promising topologies for designing multi-microgrids.

6.1 Introduction

Different studies related to multi-microgrids have been presented in Chapter 5 [87, 93–103]. These works analyse how the operation, control and/or management affects the performance of multi-microgrid systems, but none of these studies presents a comprehensive approach of microgrid clustering architectures. Currently, there is an important knowledge gap in the analysis of multi-microgrid architectures and their operational and economical characterization. The existing literature adopts particular architectures as use cases for their analysis, but does not study the wellness of these architectures against others. Accordingly, this chapter will identify, classify and analyse the multi-microgrid architectures. Three main concepts that can potentially affect the microgrid cluster performance are identified and classified into i) the layout, ii) the line technology and iii) the interconnection technology. Then, the possible architectures within these concepts are identified and defined. Finally, these architectures are compared evaluating the main parameters that defines the system behaviour, i.e. cost, scalability, protection, reliability, stability, communications and business models. As a result, a set of tables are created to show the value of each architecture, their strong points and their weaknesses. Finally, the results of this analysis can provide some guidance to grid planners and policy makers to take decision on how their future grids should be designed.

6.2 Architectures for clustering microgrids

Currently, the clustering of microgrids is being investigated taking into account that microgrids must be connected to an already existing external grid. So, very few architectures have been considered. For example, the control of multi-microgrids connected to the typical radial AC MV distribution network is studied in [94–99]. On the other hand, point to point interconnections between microgrids have been analysed in [100–102], while mixed configurations are considered in [87, 103].

In non electrified sites, there is the opportunity to build the whole grid in the most efficient way according to the present and future requirements. So, it is interesting to consider all possible architectures, which are identified in this chapter. Three main concepts that differentiate the interconnection architectures are defined:

- Layout: it defines the diagram of how microgrids are interconnected.
- Line technology: it defines how the electricity is transmitted.
- Interconnection technology: it defines the interconnection technology at the microgrid electrical boundaries. These technologies can be based on conventional power transformers or on power electronics devices.

Before describing these architectures, the concept *external grid* is clarified. An external grid is considered as a grid that contains conventional electrical equipment as loads or generators as well as microgrids and a system operator.

6.2.1 Layout

A microgrid cluster can be identified as one of the layouts depicted in Figure 6.1.

The Parallel Connected Microgrids with an external grid (PCM) layout, represented in Figure 6.1(a), refers to a structure in which all microgrids are connected to the same external grid, where each microgrid has only one PCC. So, it is considered as a parallel connection with the external grid, which implies that any electrical path from one microgrid to another microgrid must be performed through the external grid. Regarding this architecture and considering the grid connected mode, the microgrid can provide ancillary services to the external grid. So, the external grid operator has a controller or an EMS that can send orders to the microgrid. When a microgrid is operating in island mode, it must be self-sufficient as

6.2 Architectures for clustering microgrids

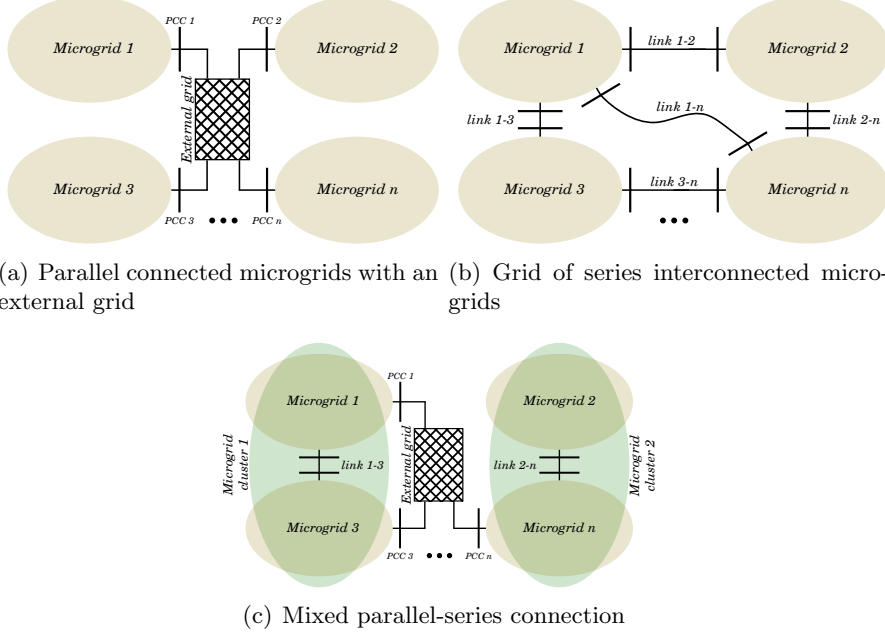


Figure 6.1: Layout architectures

it has not other external electrical connections to get support. Some references considering this architecture can be found in [96–99]. These references consider the already built MV distribution network. Other proposals, as the one performed in [105], also belong to this group.

The next layout architecture is the **Grid Series Interconnected Microgrids** (GSIM), which is shown in Figure 6.1(b). In this case, microgrids are interconnected between them forming a grid of microgrids, where the interconnections are based on the point to point structure. As it can be observed in Figure 6.1(b), microgrids can have more than one external connection. Due to the absence of an external grid, the interconnected system must generate the voltage and the frequency (in case of AC). Hence, the coordination of the cluster to match the power balance is essential. In contrast to the previous architecture, in case some disconnections occur, the system can be splitted forming smaller clusters of the same architecture. In this way, the microgrids within the sub-cluster do not lose completely the external support. So, this topology could have a better performance during off-grid operation mode. This architecture has not been extensively studied yet but due to its potential benefits, it makes worthy to evaluate its possible

performance. The point to point interconnections between these microgrids have been studied in [101, 102].

The third possibility is shown in Figure 6.1(c). It consists of a combination of the previous described architectures taking the advantage of each of them. So, it has been defined as **Mixed Parallel-Series Connection** (MPSC). In this architecture, microgrids can be connected directly to the external grid or can form clusters of series interconnected microgrids. Each of these clusters have, at least, one interconnection with the external grid. It allows microgrids to get support from other grids when they are disconnected or when the external network is overloaded. In addition, in grid connected mode, they can provide the ancillary services required by the main grid operator. In [106], there is an example of a MPSC layout, where two interconnected microgrids are connected to an external utility grid.

6.2.2 Line technology

For each layout architecture, the interconnection between microgrids can be performed using different natures of electricity transmission. The line technology can be DC or AC. It can affect the interconnection interface, the efficiency, the power transmission capacity, the voltage drops, the voltage stability, the power quality, the protection system and the overall cost [107–109].

The external grid (if the layout architecture contains it) can be both DC and AC or can be mixed AC-DC. When it is AC grid, the three phase system has better characteristics than single phase systems in terms of cost, efficiency and power capacity. So, for AC external grids, three-phase systems seem to be more adequate. Despite AC is the most mature technology for transmission and distribution, the interest in DC systems is growing due to the reduced losses because of the absence of reactive currents throughout. This advantage is being exploited in HVDC transmission grids for offshore wind parks [110]. One particular case of a DC external grid is the proposed in [105]. In this study, the power router concept for linking microgrids is introduced. The corresponding architecture is shown in Figure 6.2. The power router is a power electronic device that controls the power flow between different decoupled systems. As it can be observed, it consists of a parallel connected microgrids with an external grid topology. The external grid (power router) consists of power converters that are interconnected at a DC side. The other side of the converters can be DC, single-phase AC or three-phase AC depending on each microgrid technology.

The links between microgrids can be DC, single-phase AC or three-phase

6.3 Qualitative comparison of architectures

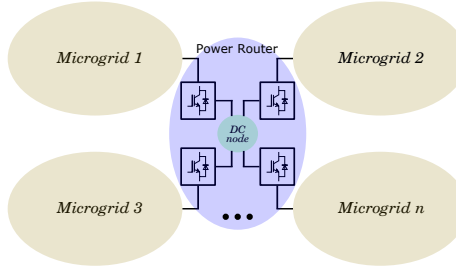


Figure 6.2: Power Router architecture

AC. In this case, the best choice will depend on the technology of the microgrids to be linked and on the requirements of the microgrid clusters in terms of cost, scalability, stability, etc.

6.2.3 Interconnection technology

The last architecture aspect is the interconnection technology. In this field, two technologies are considered: power transformers or power electronics converters.

Power transformers can be used when the line technology of the two sides of the interconnection is AC. Power transformers provide electric isolation and offer a robust and reliable interconnection interface at a reasonable cost, but its low level of controllability should be taken into account at the grid planning stage. On the other hand, power electronic converters offer a high level of controllability and can be used for both AC and DC technologies. The main drawback of this technology is the cost. Furthermore, power electronics do not provide electric isolation which can be solved with a combination of a power electronic converter and a power transformer.

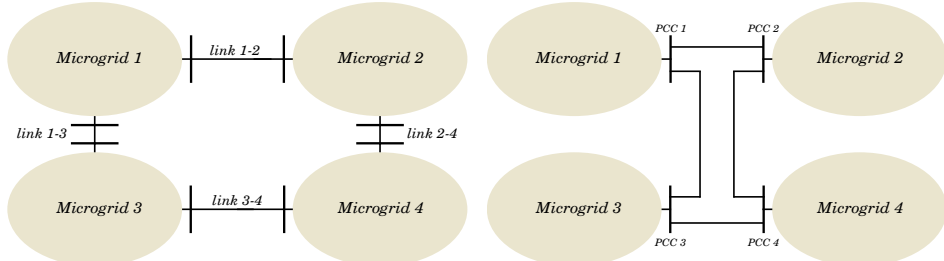
6.3 Qualitative comparison of architectures

6.3.1 Cost

The cost of clustering microgrids is determined by the infrastructure and operation costs. The infrastructure cost will depend on the amount of elements required to interconnect the microgrids, on the power rating of these elements and on the technology used. In addition, the operation cost will be affected by factors as the generation cost, the cost of providing ancillary services or the power losses.

Layout

The layout can greatly affect the infrastructure cost basically due to the interconnection devices (amount and rating). To show this, a simple example comparing the GSIM and PCM layouts is described. The example is shown in Figure 6.3. To compare both architectures, similar characteristics must be considered. Accordingly, both examples include 4 microgrids forming a ring. According to the N-1 criteria, in the case of failure of one element, the system should continue its operation. So, the power cables must be oversized considering the possibility of losing one path from the microgrid n to the microgrid m . Considering the example, this oversize will be the same for both layouts. But a difference can be observed after analysing the interface devices. Knowing that power cables must be oversized for the N-1 criteria, the interface elements of the layout GSIM must also be oversized (note that the power flowing through the cables is also flowing through the interface device). On the contrary, in the PCM layout, the interface elements only need to be sized according to the corresponding microgrid import/export requirements as the microgrids does not interfere any path. In addition, as it can be observed, the GSIM configuration requires more interface devices (8 in the example) than in the PCM (4 interface devices). So, due to the higher power rating required and the larger amount of interface devices, the infrastructure cost of the GSIM configuration will be greater than the cost of PCM. Due to its characteristics, the cost of a mixed configuration which combines both previous described layouts, e.g. a MPSC configuration, will be between the GSIM and the PCM configurations.



(a) GSIM layout example. 4 microgrids in with point to point interconnection forming a ring of microgrids
 (b) PCM layout example. 4 microgrids interconnected in ring configuration

Figure 6.3: Example of a cluster of 4 microgrids under GSIM and PCM layout architectures for cost comparison

6.3 Qualitative comparison of architectures

Due to the lack of experience in multi-microgrids deployment, the operation cost is not analysed in this study. Table 6.1 compares the cost (infrastructure costs) for the different layout architectures.

Layout Architecture	Infrastructure cost	Operation cost	Comments
PCM	L	N/A	Favourable: few interconnection devices, lower power rating of interconnection elements than for the rest of the layouts. Unfavourable: - Favourable: -
GSIM	H	N/A	Unfavourable: many interconnection devices, higher power rating of interconnection elements.
MPSC	M	N/A	

H - high; M - medium; L - low

Table 6.1: Layout architecture vs. cost

Line technology

As commented before, the operation cost will depend on the generation cost and on the power losses. The generation cost will depend on the generator technology and on the market which will define the optimum generation schedule for all generators. Hence, the generation cost cannot be compared in function of the line technology. On the other hand, the power losses (and therefore, the system efficiency) will be dependent on the line technology, its power rating and the number of conversion stages.

The efficiency of distribution systems for AC and DC grids has been analysed in [107]. The results show that DC grids can be more efficient than AC ones, resulting in lower operation costs. Another approach comparing costs is performed in [111]. For the same power transmission and the same power losses, DC lines can be smaller and thus cheaper than AC lines.

In particular, the power losses due to power conversion -conversion losses-within AC or DC microgrids are compared in [112]. They are significantly affected by the number of conversion stages. In this sense, DC microgrids have been attracting interest for increasing the system efficiency. This is due to the low number of power conversions when feeding DC loads and the lower cost in converters investment [113]. However, conversion stages would also be needed for the integration of AC loads. Therefore, a future scenario that merges both AC and DC microgrids is envisioned. Taking into account that both AC and DC microgrids will coexist, it makes also sense to

consider both AC and DC line technologies for their interconnections. The cost comparison in function of line technology is summarized in Table 6.2.

Line technology	Material cost	Operation Cost	Overall cost	Comments
DC (large cable approach [111])	M	L	L	Favourable: higher efficiency than other options. Unfavourable: investment cost compared to other DC option. Favourable: cheaper cables than other options.
DC (small cable approach [107])	L	M	L	Unfavourable: lower efficiency than DC large cable approach. Favourable: -
AC	M	M	M	Unfavourable: lower efficiency, smaller cable rating for the same section.

H - high; M - medium; L - low

Table 6.2: Line technology vs. cost

Interconnection technology

It is well known that power electronics are more costly than power transformers. But their advantage in controllability makes these devices essential for smart grids applications. In [114], the cost of a classical low-frequency power transformer and a solid state transformer -its equivalent based on power electronics- is compared. The result shows that the cost of power electronics based transformers can be up to 4.5 times the cost of classical power transformers. But on the other hand, power electronics offer a high level of controllability and thus, they can improve the power quality providing ancillary services. Furthermore, it can be observed that depending on the topology of the solid state transformer, it can include a high frequency classical transformer. This provides galvanic isolation between the two sides of the solid state transformer as a conventional one does. Table 6.3 compares the cost of the interconnection technology.

6.3.2 Scalability

In this study, scalability is referred as the capacity of a system to accept new elements as generators, loads or microgrids. The new loads and generators are considered to be placed inside the microgrids. So, two main scalability concepts are considered: i) the capacity to accept a growth of the existing microgrids and ii) the capacity to accept the connection of new microgrids.

6.3 Qualitative comparison of architectures

Interface technology	Cost	Comments
Classical transformer	L	Not possible for AC-DC, DC-DC or DC-AC interfaces.
Power converter	H	Advanced features on controllability. Possible for AC-DC, DC-DC and DC-AC interfaces.

H - high; M - medium; L - low

Table 6.3: Interconnection technology vs. cost

The scalability of smart grids projects has recently been reviewed in [115]. In this study, several factors affecting the scalability have been identified. The most remarkable factors are i) technical, ii) economic and iii) regulation.

Regarding the technical factors, the most important is the modularity ¹, but the interface and software integration require to be taken into account. The number of interactions between elements should grow accordingly with the size, otherwise the system may turn complex in excess. On the other hand, software tools should cope with the increased size. In this case, the technological progress plays a favourable role. The economic factor is related to the viability of an scaling-up project in terms of cost and revenues. Finally, the regulation can affect the scaling capacity (e.g. in Spain, PV installations at domestic level are restricted to a maximum capacity).

Layout

The growth of the existing microgrids can influence on the need of importing and exporting electric power, which can be increased or lowered depending on the new elements installed. For any microgrid clustering layout, the increase of importing or exporting requirements is limited by the power rating of the interconnection points, being possible to upgrade them assuming an additional cost. On the other hand, if the existing microgrids become more self-sufficient, the power flows through links and external grids will reduce, which will have a positive effect on the scaling capacity. So, the lower the dependence of the microgrids on the external grid, the higher the capacity of scalability of the overall system. In this direction, regarding the growth of a microgrid, these architectures that can exchange power through more interconnections should have a favourable scaling capacity. Hence, the GSIM and the MPSC layout architectures could provide a better acceptance of microgrid's growth.

¹Modularity refers to whether a solution can be divided into interdependent components [115]

On the other hand, the installation of new microgrids will affect the number of interactions and hence, the complexity of the system. In this direction, the PCM is the layout architecture that will have the lowest increment of complexity. This is due to the fact that each new microgrid will add just one interaction with external elements. In contrast, the added power exchange may saturate the external grid. So, regarding the scalability, the advantage of the simplicity of the PCM is limited by the possible saturation of the external network. This can be avoided in the MPSC layout as it can exist more than 1 electrical path to import or export electricity. In addition, this layout, as well as the GSIM has higher modularity as it can form sub-clusters (e.g. see Figure 6.1(c)). Table 6.4 compares the scalability for the different layout architectures.

Layout architecture	Microgrid growing capacity	New microgrid integration capacity	Overall scaling capacity	Comments
PCM	L	M	L	Favourable: simplicity. Unfavourable: low flexibility, 1 power exchange paths, lower modularity.
GSIM	H	M	M	Favourable: modularity, flexibility, >1 power exchange paths. Unfavourable: complexity.
MPSC	H	H	H	Favourable: modularity, flexibility, >1 power exchange paths, external grid support. Unfavourable: complexity (lower than GSIM).

H - high; M - medium; L - low

Table 6.4: Layout architecture vs. scaling capacity

Line technology

DC lines have higher power transmission capacity, lower voltage drops and lower cost than AC lines [107, 109] (the overall cost taking into account the interconnection power converter can be greater than AC technology with power transformer). According to these proprieties, DC lines should better withstand an increase of power flows and hence, providing better scalability for both concepts: growth of microgrids and connection of new microgrids. If the power flows through the interconnection links or through the external grid increase, higher voltage drops will occur. This can lead to an unacceptable power quality and the need of additional equipment (and cost) to compensate this effect. In this case, the lower voltage drops of DC technol-

6.3 Qualitative comparison of architectures

ogy play a favourable role. On the other hand, for the same increment of active power, AC technology will require more capacity due to the reactive power, which is not advantageous for scaling up the whole system. Table 6.5 compares the scalability versus the line technology.

Line technology	Microgrid growing capacity	New microgrid integration capacity	Overall scaling capacity	Comments
DC	H	H	H	Favourable: low voltage drop, cable cost, high power capacity. Unfavourable: -
AC	L	L	L	Favourable: possible to use power transformers for interconnecting elements (lower cost). Unfavorable: cable cost, high voltage drops, low power capacity.

* H - high; M - medium; L - low

Table 6.5: Line technology vs. scaling capacity

Interconnection technology

As stated before, the growth of existing microgrids can increase the power exchange requirements. In this case, as power transformers have the capacity to withstand periods of overloads, it is more likely that they better accept the growth of the existing microgrids avoiding the installation of new equipment. On the other hand, power electronics technology is more expensive and can not be overloaded. So, in the case the power exchange requirements increase over the rated power, an additional power converter must be placed. As a consequence, the growth of a microgrid can be limited by the economic factor.

Regarding the installation of new microgrids, the limitation of using power electronics as an interface element is the cost, which can turn the interconnection of the new microgrid unattractive. Table 6.6 compares power transformer and power converter interconnection technology regarding the scalability.

6.3.3 Protection

All electric power systems must be protected against electrical failures through an Electrical Protection System (EPS). The EPS should avoid the possibility that an electrical failure is expanded through the electrical network, affect-

Interconnection technology	Microgrid growing capacity	New microgrid integration capacity	Overall scaling capacity	Comments
Transformer	H	H	H	Favourable: cost, overload withstand. Unfavourable: low controllability.
Power converter	L	M	L	Favourable: high controllability. Unfavourable: cost.

* H - high; M - medium; L - low

Table 6.6: Interconnection technology vs. scaling capacity

ing the rest of the power system [116–118]. In addition, the EPS has to safeguard people, assets and facilities in the affected area, reducing at least the possibility of causing any damage. In general, the basic requirements for EPSs are [116–118]: i) reliability. It is the feature that guarantees that the protection will be operative in any case; ii) selectivity or discrimination. This means that the EPS should only disconnect and isolate the damaged part of network, this feature is directly related to the protection’s coordination; and iii) sensitivity. It is the capability to be accurate on the fault detection and it also affects to the protection’s coordination; iv) response time. It is the ability to isolate the fault in a short period of time; and finally v) stability. Meaning that the system must remain stable even while an eventuality is affecting a protective zone.

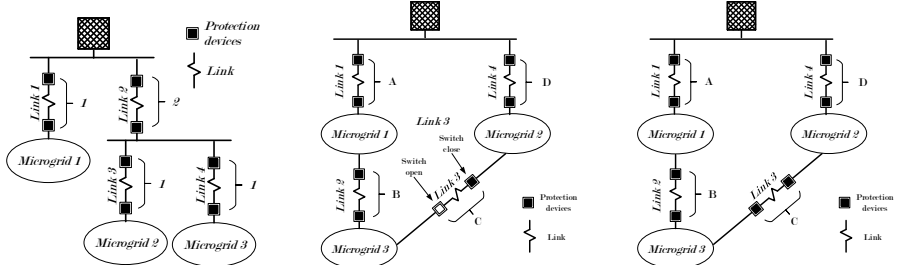
Typically, the EPS is defined according to power system technical aspects like the type of electricity generation, voltage level, grid topology, weather conditions, among others. In addition, strategic and economic aspects are also taken into account in order to select the most adequate EPS. For instance, the EPS for a highly interconnected transmission system where millions of clients are connected should be customized, automatized and sophisticated to guarantee the maximum continuity of supply, while the EPS for distribution systems can be very simple [116–118]. In the present study, the protection system for the cluster of microgrids is studied and treated according to the three defined architecture levels.

Layout

The layout defines how microgrids are interconnected. In this sense, the EPS must ensure a good performance of the interconnected system. An important point for microgrids is that they can export or import energy from an external grid. The protection and coordination of protections have to take into account such bidirectionality of power flows. This issue has been analyzed in [28, 119–123]. For the layout PCM, the microgrids' behavior may approach to radial power system operation. Considering high penetration of distributed resources, the radial operation favors the presence of bidirectional power flows. So for this case, it is particularly important that the EPS is designed to be sensitive to this phenomenon. For this layout though, the EPS coordination is simple, easily guarantying a good selectivity and discrimination, accurate sensitivity and fast protection actuation. However, the general reliability of the system is reduced while compared to meshed options, because there is a unique electrical path to the external grid or to other microgrids [28, 116, 121, 124]. So, any electric failure at the interconnection element would produce a complete isolation of the microgrid. In terms of selectivity, Figure 6.4(a) presents a simple example of parallel configuration, where there are three microgrids connected in parallel to an external grid. In addition, there are four interconnection links, numbered as 1 to 4, which are protected through protection devices, numbered as 1 and 2. In order to guarantee a good selectivity, links 1, 3 and 4 must actuate before the link 2. In contrast, for the rest of microgrids mixed interconnections –GSIM and MPSC layouts– (depicted in Figures 6.4(b) and 6.4(c)), protections and their coordination is more complex, and some considerations should be taken into account to ensure the mentioned requirements. In particular, for the case represented in Figure 6.4(b), all microgrid subclusters are parallel connected to the external grid. The opened switch at link 3 guarantees an open-loop operation of the system and this facilitates the coordination of protections, and at the same time, avoids microgrid isolation in case of experiencing faults during maintenance works. This ensures the continuity of supply to loads [28, 116, 121, 124].

Finally, the last case, depicted in Figure 6.4(c), combines mixed interconnections and microgrids are operated in closed-loop. For this case, if it is required a coordination between protections, a good communication system would be needed. The main advantage of this system is that reliability is very high. The main drawback is the complexity that will increase the cost. In this case, the fault location and its isolation present many challenges, which are described in [28, 121, 124]. For the example presented in Figure

6.4(c), in case of experiencing a failure at link 3, the protection C must act before the rest, while if the failure is located in the microgrid 3, the protections B and C must act at the same time.



(a) The parallel interconnection of microgrids operating as a radial system (b) The series and mixed interconnection of microgrids operating as an open-loop (c) The series and mixed interconnection of microgrids operating as a close-loop

Figure 6.4: Protections schemes in function of the layout

Table 6.7 compares the fulfillment of protection requirements for the different layout architectures.

Layout architecture	Selectivity applicability	Coordination requirements	Overall protection difficulty	Comments
PCM radial	H	L	L	Favourable: simplicity. Unfavourable: -
GSIM/MPSC open-loop	M	M	M	Favourable: possibility of system reconfiguration after a fault. Unfavourable: required communications and higher cost.
GSIM/MPSC close-loop	L	H	H	Favourable: system reconfiguration after a fault is not required. Unfavourable: robust communication system required, complex operation.

H - high; M - medium; L - low

Table 6.7: Layout architecture vs. protections requirements

Line technology

It is known that, depending on line technology (AC or DC systems), the EPS has to consider different aspects to effectively protect the facilities and people. This section focuses on the most typical protection devices, which

6.3 Qualitative comparison of architectures

are relays, disconnectors, circuit breakers and fuses [125, 126]. These protections exist in both systems, but there are some differences in terms of (i) the variety, (ii) the requirements and (iii) the performance.

The major part of electrical power systems are AC. Accordingly, in terms of variety, there are many manufactures, standards and solutions for any rated power, voltage level and rated current. At the present, DC systems are growing in interest. Therefore, manufacturers and legislators are introducing this technology in the electrical power system. But currently, the variety in DC technology is lower than AC technology and presents some limitations in terms of power, voltage and current ratings.

In terms of requirements, AC and DC faults are different. According to [127], AC faults are classified into symmetrical faults (three-phase faults) and asymmetrical faults (single-phase-to-ground, phase-to-phase and double-phase-to-ground faults). In contrast, DC faults are divided into pole-to-pole faults and pole-to-ground faults. Hence, the AC technology must identify a higher number of faults. Additionally, the microgrid interconnections present new challenges compared to the traditional distribution links. This implies that the EPS should be able to detect the power flow direction and to identify the fault current level. The power flow direction between microgrids or between a microgrid and an external grid can vary depending on the local load and generation at each instant. Therefore, the EPS must take into account the power flow direction at the moment when an electrical fault occurs. On the other hand, when a fault occurs, the fault current is supplied by the local DG and by the external link (other microgrids or external grid). So, the external link fault current can vary depending on the local generators contribution. In case of DC systems, there is an additional challenge. To interconnect microgrids under DC systems, power electronics interface is required. Power electronics cannot contribute to supply fault currents because they do not support overloads as power transformers do. So, a very fast detection and disconnection is required. For example in this case, traditional fuses are not suitable as their response time would be too long [125]. Therefore, it is necessary to select more sensitive DC relays, fuses, etc. which are able to detect sudden load, voltage, current and impedance variations and to perform a fast fault isolation.

Finally, as a consequence of the different fault interruption methods, the AC and DC protection performance are different. In case of DC technology, it is difficult to interrupt the current as it does not presents a zero value. In contrast, AC technology current crosses the zero value two times per period [128]. Table 6.8 compares three AC/DC aspects of protections in function of line technology.

Line technology	Variety	Requirements	Performance	Overall applicability	Comments
DC	M	H	M	M	Favourable: less fault types. Unfavourable: less mature technology, very sensitive and fast protections requirements, difficult to interrupt the current.
AC	H	H	H	H	Favourable: a plenty of economic and reliable options, mature technology. Unfavourable: high variety of fault types.

H - high; M - medium; L - low

Table 6.8: Line technology vs. protections

Interconnection technology

In terms of protection, power converters and transformers are sensible elements that require special attention to guarantee their proper operating conditions. Both interconnection devices must be protected against short-circuit currents and voltages surges as well as under voltage events. In addition, power converters can withstand overvoltages and overcurrents during less time than transformers. Power transformers are able to withstand a fault during 2-5 seconds, and their protection level depends on their rated power. While small transformers (below 500 kW) are only protected through fuses, the larger ones are also protected through differential, earth fault, overvoltage, current and thermal overload, overexcitation, high/low impedance protections, among others protections [129]. For power converters though, protections are more stringent because they should ensure faster response than the case of transformers, demanding more accurate protections [125, 126]. According to this analysis, it is expected that the cost of protecting a power converter would be higher than for power transformers. Table 6.9 compares power transformer and power converter interconnection technologies regarding protection needs.

6.3.4 Reliability

According to [130], the reliability of a system covers two concepts: its security and its adequacy, which are basically distinguished by the time frame considered. Operational security applies for the short-term and represents the ability of a system to withstand sudden disturbances such as electric short-circuits or unanticipated loss of system elements. Adequacy applies for the long-term and is the ability of the system to supply the aggregate electrical demand of customers at all times, taking into account scheduled and

6.3 Qualitative comparison of architectures

Interconnection technology	Required protection level	Required sensitivity of protections	Overload capacity	Overall applicability*	Comments
Power transformer	M	L	H	H	Favourable: mature technology. Overload capacity, which implies lower requirements. Unfavourable: - Favourable: -
Power converter	H	H	L	L	Unfavorable: sensitive to overloads, which implies high protection requirements.

H - high; M - medium; L - low

*The given values are to differentiate both technologies. But both technologies can be effectively protected

Table 6.9: Interconnection technology vs. protections

reasonably expected unscheduled outages [131]. Therefore, while adequacy implies that generation is able to meet the demand for contingencies (and reflects static performance), security indicates that the power system will be able to deal with outages or equipment failures in steady state, remaining intact even after their occurrence (and reflects dynamic performance).

For the present study, reliability can be evaluated in a single microgrid or in the system constituted by several microgrids. The reliability in a single microgrid will depend on the elements it contains and on how they are operated and controlled. The reliability in a cluster of microgrids, focus of the present section, will be influenced by the reliability of each single microgrid, but also by the cluster layout, the line technology and the interconnection technology.

The reliability of the system can then be evaluated through different metrics, based mainly on probabilistic and deterministic methodologies. Indices that use concepts like failure rate, average outage duration, average annual unavailability or average annual outage time are probabilistic. As they represent expected or average values linked to a probability, they characterise long-run average values and cannot always reflect the impact of a system outage [132]. An example of this index is the LOLE (Loss of Load Expectation), which is the probability that demand exceeds the capacity of the system in a specific period.

In order to reflect the severity of disturbances, the deterministic indices defined in the standard [133] can be used. They are customer oriented and some of the most common ones are the SAIDI (System Average Interruption Duration Index), which is calculated as the sum of customer-sustained interruption durations per year divided by the total customers served, the SAIFI (System Average Interruption Frequency Index), which represents the num-

ber of customer interruptions divided by the total customers served and the CAIDI (Customer Average Interruption Duration Index), which indicates the total number of customer interruption durations divided by the total number of customers interrupted. The latter is in fact the ratio between the SAIDI and the SAIFI.

The reliability in active distribution systems with multiple microgrids is evaluated in [134] through a probabilistic approach. The concept of virtual power plant (VPP) is used to model microgrids with intermittent generation. The microgrid components are aggregated in a single entity, a VPP, so as to obtain a simplified equivalent model that facilitates the reliability evaluation in grids consisting of many microgrids. Each microgrid is understood as a power source if it provides more power than the local demand and becomes a customer when the demand exceeds the available output. The application of this methodology is interesting when details of the network consisting of microgrids are available, which is not the case of the present study. In this sense, next sections perform a qualitative analysis of the reliability for different microgrid clusters as a function of their layout, line technology and interconnection technology.

Layout

When a contingency occurs, the power being generated or consumed in the affected and surrounding buses is modified or no longer available. So, a reinforcement for reliability is given by the connection paths and redundancy of the system. Those layouts presenting many connection nodes with the macro grid could take advantage of these connection paths if a contingency occurs there, to help to reach a safe operation during and after its occurrence. This is the case of layouts PCM and MPSC where the microgrids are connected with an external grid. In this sense, layout MPSC and GSIM could benefit of the connections with other microgrids to overcome a disturbance. The question rising is if it is better in terms of security to be connected to the main grid or to other microgrids. This will depend on the type, number and strength of the connections. The stronger is the grid, the smaller the voltage changes that can occur [135], so it contributes to the voltage stability of the system.

Strong grids imply high short-circuit power (and high short-circuit ratio). The short-circuit power or capacity reflects the maximum power that a network can provide to an installation during a fault. Therefore, it is key for the redundancy in the sense of compliance with (N-1) criteria [136]. Taking into account the actual deployment of microgrids, the short-circuit capacity

6.3 Qualitative comparison of architectures

of the macro-grid is in most of the cases higher than the one of a single microgrid or a cluster of microgrids. Therefore, layout PCM would probably be more redundant than GSIM, which is not connected to the macro grid. The most redundant layout would be MPSC for having interconnections with the main grid, but also among microgrids.

The connection with the macro grid or other microgrids would be a drawback if the contingency occurs inside the connected entity and the protection coordination cannot ensure the fault isolation, facilitating failure propagation. However, assuming all the microgrids provide stability support and protections are properly sized and coordinated, a higher number of connections with the main grid and among microgrids leads to a higher reliability. A qualitative evaluation of the reliability depending on the layout architecture is depicted in Table 6.10.

Layout architecture	Reliability	Comments
PCM	M	Favourable: Grid strength at all PCC. Unfavourable: Null interconnectivity among microgrids.
GSIM	L	Favourable: High interconnectivity among microgrids. Unfavourable: Null connection to the main AC grid.
MPSC	H	Favourable: Grid strength at all PCC and high interconnectivity among microgrids. Unfavourable:-

H - high; M - medium; L - low

Table 6.10: Layout architecture vs. Reliability

Line technology

The type of line technology affects the security of the microgrid clustering in the sense that it might imply additional equipment and condition the failure rate of the interconnection lines. The number of contingencies in lines is usually given in km/year. It depends, for instance on the internal configuration of the conductors, type of insulation and number of circuits. It also varies if it is the case of cables or overhead lines. As reflected in [137], the failure rate is very low and similar for HVDC and EHVAC lines. For instance, according to this study the risk of permanent HVDC bipolar faults should be the same as for double-circuit faults of EHVAC lines (0.003/100 km/year). Regarding LV levels, the study [138] analyses the possibility of

a transition from AC to DC-LV distribution networks, remarking the need for further reliability studies for a better understanding of how the cables will behave under DC in an aged condition. Therefore, it is difficult to state if one of the technologies is more reliable than the other. This qualitative evaluation of the reliability depending on the line technology is depicted in Table 6.11.

Line technology	Reliability	Comments
AC	N/A	Favourable: mature technology in power system transmission. Unfavourable: reactive power consumption/generation.
DC	N/A	Favourable: no reactive power. Unfavourable: requires power electronics to connect to the conventional system.

H - high; M - medium; L - low

Table 6.11: Line technology vs. Reliability

Interconnection technology

The interconnection technology, mainly transformers and power electronics, used in the boundaries of the microgrids also have an effect in the reliability of the clustering. The failure rate of a transformer is lower than the failure rate of a converter [139] and, again depending on the type of transformer and type of converter installed, the number of failures will change. On the other hand, the fact that the clustering interconnection includes power electronics adds controllability: for instance, VSC (Voltage Source Converters) contribute to active and reactive power control. Nevertheless, systems with high penetration of power electronics are characterized by low inertia, which implies challenges in frequency response. In any case, the parallelization of equipment will improve the reliability of the system, at the expense of higher costs. A qualitative evaluation of the reliability depending on the interconnection technology architecture is depicted in Table 6.12.

6.3 Qualitative comparison of architectures

Interconnection technology	Reliability	Comments
Transformer	H	Favourable: Lower failure rate than converters, microgrid inertia is not decoupled. Unfavourable: Low controllability.
Power converter	M	Favourable: High controllability (active and reactive power control), enables renewable generation integration. Unfavourable: Higher failure rate than transformers, inertia from AC side is decoupled.

H - high; M - medium; L - low

Table 6.12: Interconnection technology vs. Reliability

6.3.5 Stability

As a general definition, the stability of a power system refers to its ability to return to a steady state after a disturbance. According to CIGRÉ/IEEE [140], the network stability can refer to three main types of phenomena: i) voltage stability; ii) frequency stability; iii) and rotor angle stability. Voltage stability refers to short and long term dynamics of the voltage levels in the system. For instance, voltage stability includes the capability of maintaining a voltage in the buses of the network within admissible limits. Frequency stability in turn refers to the ability of the system to maintain the electrical frequency within admissible levels while in an excursion or transient state due to an imbalance between generation and demand. Finally, rotor angle stability refers to the behaviour of oscillatory modes of the rotor of generators while synchronized in electrical networks.

The following sections briefly discuss on the stability of a cluster of microgrids addressing their layout, line technology and interconnection technology.

Layout

According to the architectures proposed for a cluster of microgrids in Figure 6.1, the architecture MSPC would be potentially the most stable one among the ones presented. This architecture mimics the way conventional power systems have been developed worldwide in the sense that microgrids are connected in parallel to an external grid (as for the architecture PCM). But it also enhances the stability by adding further interconnections between microgrids. The stability of this architecture mainly decays on the external grid. This external grid is intended to include power reserves provided by

synchronized generators and storage systems, as well as synchronized inertia and other equipment to effectively ensure the balance between generation and demand in the whole network at all times, so in other words, to satisfy the required stability in frequency and voltage levels. The microgrids, while connected to this external grid, may provide ancillaries for an enhanced network stability, but they are not supposed to principally sustain it. In case of any eventuality in a microgrid, it could be grid disconnected, without affecting the stability of the rest of the network. Also for this case, the stability of such grid disconnected microgrid can be supported by the series connection with other microgrids.

The centre of gravity of network stability could be moved from the main grid to the microgrids in the architecture GSIM. In fact, this architecture is characterized by the absence of a proper power system interconnecting microgrids, so all balancing mechanisms (power reserves, synchronized inertia, reactive power sources, etcetera) of the network are included in the microgrids. This way, and from the network stability point of view, the unavailability of a single microgrid could be critical for the rest of the system. This does not necessarily mean that this architecture is potentially less stable than the rest of architectures, provided that the distribution of balancing sources among the microgrids is sufficient and conveniently planned. Anyhow, the critical role of microgrids in network stability tasks is also exacerbated by the fact that microgrids could be connected in series. Because of this series disposition, the unavailability of a single microgrid could break the unique path or access to balancing sources for the rest of microgrids and in this sense, this architecture may be the less stable among presented. Table 6.13 compares the stability for the different layout architectures.

Line technology

There are mainly two types of line technology interconnecting microgrids: AC and DC. While the AC technology is the widely and conventionally adopted solution for the development of power systems worldwide, DC technology is gaining importance by the hand of power electronics-interfaced systems, such as, for instance, offshore wind power plants [110, 141] and microgrids [142].

From a stability point of view, AC line technologies cannot be defined as intrinsically more stable than DC line technologies and vice versa. However, it is interesting to point out some aspects around these technologies that directly impact on network stability.

For the stability of AC line technology-based grids, associated control

6.3 Qualitative comparison of architectures

Layout architecture	Stability	Comments
PCM	M	Favourable: stability is provided by the external grid, microgrids can provide stability support, in case of a microgrid fault its disconnection does not affect the stability of the system. Unfavourable: -
GSIM	L	Favourable: - Unfavourable: loss of a microgrid can be critical for the rest of the system, absence of an external grid capable to respond to disturbances.
MPSC	H	Favourable: stability is provided by the external grid, microgrids can provide stability support and also, the stability of the microgrids disconnected from the main grid is enhanced by the fact that they may still be connected in series to other microgrids. Unfavourable: -

H - high; M - medium; L - low

Table 6.13: Layout architecture vs. stability

systems should manage two electrical variables: voltage levels and voltage frequency. The management of voltage levels is usually associated to the regulation of reactive power flows within the network, while the regulation of voltage frequency is related to the management of active power flows. This problem is somehow simplified in DC line technology-based grids in the sense that there are no reactive power flows to control.

Apart from this kind of an apparent advantage, the absence of reactive power flows further favours DC line technology-based grids from a stability point of view. The thing is that the inductive nature of AC lines is translated in an important consumption of reactive power in them. This reactive components increase the magnitude of the currents flowing through the lines and thus increase the thermal losses. At the end, this actually limits the effective power transmission capacity of the line from one point to another: a percentage of the ampacity of lines is used not to transmit active power but to simply heat the lines. The higher the inductive component of lines, the higher the reactive power consumed, and the shorter the distance the lines can transmit power in a cost effective way. Such diminishment in transport capacity of lines and the increased power losses, also diminish the effectiveness of the provision of power reserves in the network for balancing purposes, i.e. for electrical frequency stability purposes. The balancing needs in the network should be oversized taking into account the losses in AC line technology-based systems. Such oversize is potentially lower for DC ones, due to the reduced losses. Table 6.14 compares the stability versus the line technology.

Line technology	Stability	Comments
AC	Can not be compared to DC technology	Favourable: mature technology, large experience from the conventional power system. Unfavourable: two variables must be controlled (P and Q), reactive power consumption in power lines which diminishes the effectiveness of provision of power reserves.
DC	Can not be compared to AC technology	Favourable: One one variable to be controlled (P), no reactive power flows. Unfavourable: new technology in power transmission, low experience.

H - high; M - medium; L - low

Table 6.14: Line technology vs. stability

Interconnection technology

The magnitude and slow dynamics of the electrical frequency, which are required for the proper functioning of sensible equipment of consumers depend on the amount of synchronized inertia of the network, i.e. on the quantity and size of connected synchronized generators. A well-known problem related to the replacement of conventional generation by renewable-based power plants is the reduction of the synchronized inertia of the system [143]. The reason is that renewable-based power plants are grid connected through power electronics, which from the point of view of the network, have no inertia.

Microgrids, while grid connected through power electronics as renewable-based power plants, reduce the effective synchronized inertia of the network. So in general terms, and for all proposed architectures in Figure 5, the usage of power electronics as interconnection technology of microgrids can be translated into volatile levels and fast dynamics in the electrical frequency (and voltage), thus reducing network stability.

However, modern power electronics could be equipped with control algorithms that permit microgrids to mimic the behaviour of conventional synchronized generators or loads in terms of inertial response. This way, a microgrid could transiently and instantaneously increase or decrease its power exchange with an external grid in response of a frequency excursion in the network. This kind of inertial response –or as commonly known synthetic inertia–, smooths out the dynamics of electrical frequency as the rotating masses of synchronized generators do. Apart of doing so, power electronics can also manage reactive power flows so they can actively reg-

6.3 Qualitative comparison of architectures

ulate voltage levels at the connection point of microgrids. At the end, the controllability and capabilities of power electronics for network stability is remarkable and the development of control rules for power converters as interconnection technology of microgrids and renewable-based power plants are principal research lines nowadays [144].

The problem of ensuring network stability is exacerbated in the extreme that all microgrids in the network are interconnected through power electronics and there is no a proper power network in between (so there is no a synchronized generator with a big and heavy rotor governing the 50/60 Hz for the frequency of the system). This is the case of the GSIM architecture. This architecture can be managed in a centralized or decentralized way. In the case the power electronics interconnecting microgrids are managed in a decentralized way, each one should be equipped with the so-called droop control-type governors. They regulate the active power exchanged with the network function of its electrical frequency, and the reactive power function of the voltage levels. Despite the numerous advantages of this concept (minimum communication needs, network flexibility, etcetera), such droop-based control systems are known to yield stability problems for large values of control gains for the active power / electrical frequency droop [145, 146]. Moreover, such droop-based control systems are well performed considering all power converters interfacing microgrids connected in parallel. In the case converters are connected in series, coordination between them is fundamental, and for sure, controllability needs are to be distributed between them for coherence. Table 6.15 compares power transformer and power converter interconnection technology regarding the stability.

Interconnection technology	Stability	Comments
Transformer	H	Favourable: mature technology, microgrid inertia is not decoupled. Unfavourable: lower controllability.
Power converter	M	Favourable: active voltage regulation, potential to provide synthetic inertia. Unfavourable: low experience, reduction of synchronized inertia.

H - high; M - medium; L - low

Table 6.15: Interconnection technology vs. stability

6.3.6 Communications

The operation and control of a microgrid cluster requires a coordination of the different DERs and, accordingly, it requires a communication infrastructure.

Several approaches have been proposed for the control and operation of a microgrid. These approaches are named centralized, decentralized and distributed respectively [8, 79]. In the centralized approach, the information of the DERs and loads are collected in a central aggregator. Then, this information is processed and setpoints are sent back to each DER through direct communication links. On the other hand, the decentralized architecture does not use direct communication links, they use the power lines to communicate by means of varying the voltage and frequency. Finally, in the distributed control, the coordination is done through direct communication links. But in this case, the communication is done between units [79].

As stated previously, from the main grid operator viewpoint, microgrids can be seen as single controllable entities capable to react to external requests. Hence, the same approaches (centralized, decentralized and distributed) can be adopted to coordinate the cluster of microgrids. For example, the 'More MicroGrids' project has addressed this issue using a centralized approach [96,98]. This section will discuss the communication needs for the operation of the cluster of microgrids. Following the indications in [98], and as stated in Chapter 5 it is be considered that microgrids operate under a hierarchical control scheme where, at the end, it is managed by a central controller.

Layout

Figures 6.5 and 6.6 show the possible communication architectures for the PCM and GSIM layouts respectively. The centralised control layout collects all data regarding the external grid state as well as the microgrid information. Then it computes the required setpoints optimizing the system operation and send them to microgrid central controllers as well as to other DERs that may exist at the external grid. The central unit can optimize, effectively, the system operation in relatively small multi-microgrid systems. The communication and computation needs by the central controller increases when the amount of DERs and interconnected microgrids increase [147]. In addition, the geographic extensions of microgrid clusters may lead communication challenges which could turn the central topology infeasible [8]. On the other hand, the fully decentralised architecture is not recommended be-

6.3 Qualitative comparison of architectures

cause of the strong coupling between the different units of the system, which requires a certain level of coordination [8]. An intermediate solution could be the distributed control architecture [148].

In the case there is a contingency in the PCM architecture, microgrids can be isolated and perform their autonomous operation. In the case of GSIM architecture, microgrids can be isolated but also sub-clusters can be formed improving the isolated operation performance. In this later case and considering the central architecture as shown in Figure 6.6(a), sub-central controllers can become in charge of the sub-clusters operation. In contrast if the control is distributed, the sub-cluster operation should be adapted to the new configuration. In this direction, more studies are required.

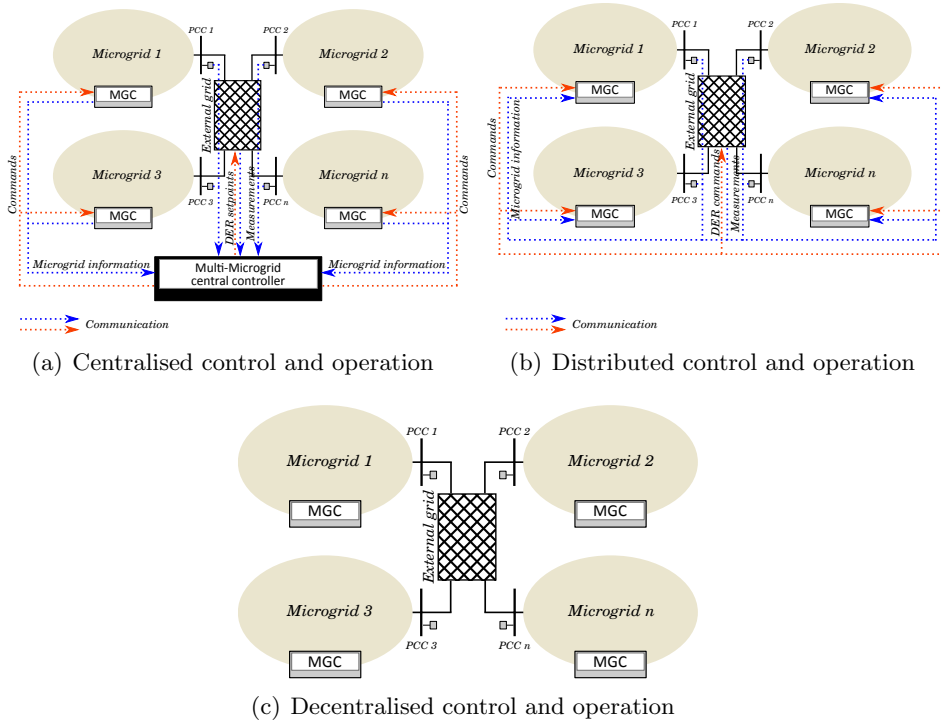


Figure 6.5: Communication architectures for PCM layout

The MPSC and GSIM could operate under centralised or distributed architectures as PCM does. But in these cases, the advantages of the distributed and central controllers could be combined obtaining a better performance. Considering the MPSC layout (but the same concept could be applicable to the GSIM), each sub-cluster could have a central controller

Chapter 6 Multi-microgrid architectures

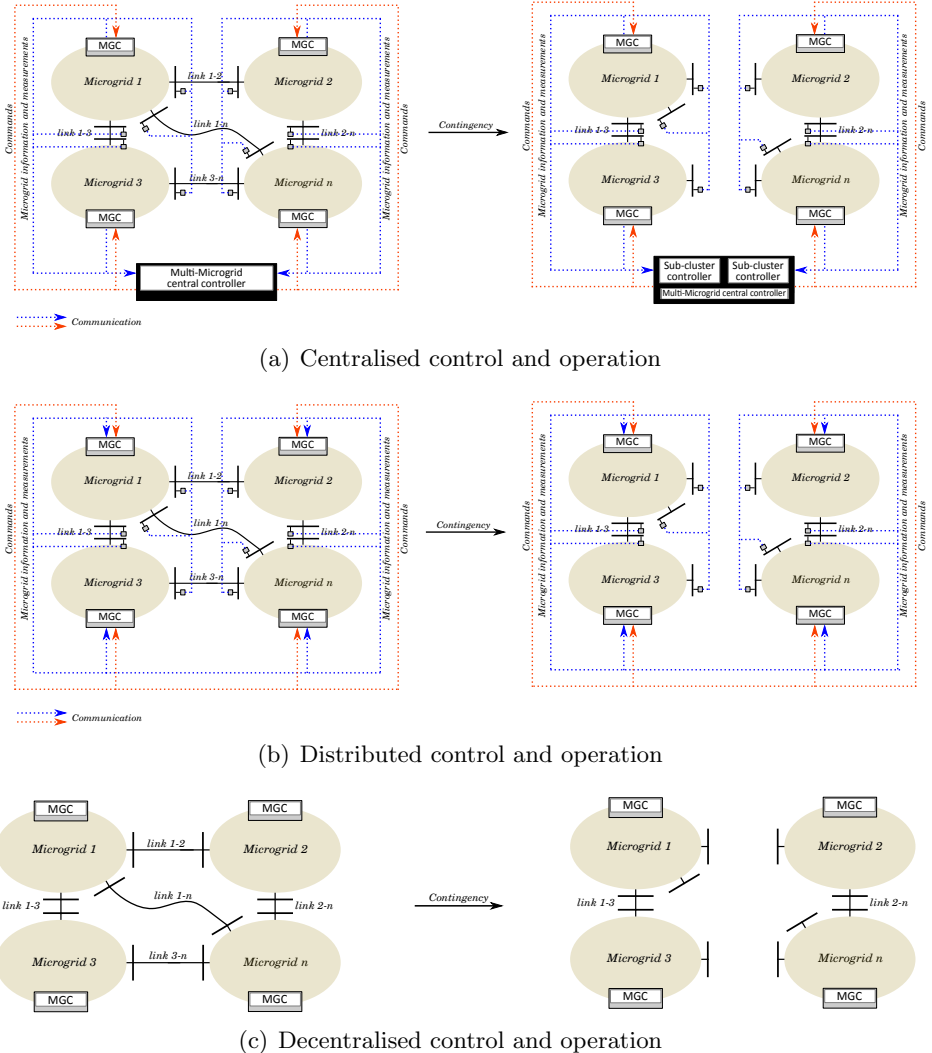


Figure 6.6: Communication architectures for GSIM layout

which interacts with the main multi-microgrid controller as shown in Figure 6.7. In this manner, the number of communication links and interactions required by the main multi-microgrid central controller can be reduced, being able to be applied even in large systems.

Table 6.16 compares the communication requirements and the optimal operation performance between the different layout architectures.

6.3 Qualitative comparison of architectures

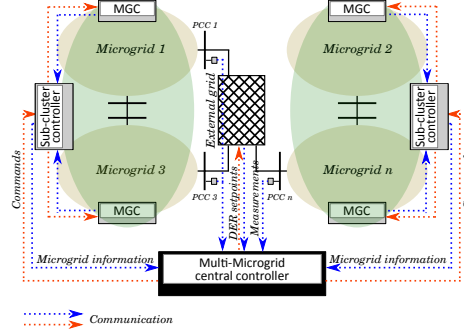


Figure 6.7: 2-level communication architecture for MPSC layout

Layout architecture	Communication requirements/ optimal operation performance	Comments
PCM centralized	H/M	Favourable: effective optimum operation in normal conditions. Unfavourable: high communication requirements. Its applicability can depend on the number of elements to be controlled, Microgrids operate isolated after a contingency.
PCM distributed	M/L	Favourable: lower communication requirements. Applicable for large systems. Unfavourable: Probably, the operation is not as optimum as in the central architecture. Microgrids operate isolated after a contingency.
GSIM centralized (1 - level)	H/H	Favourable: effective optimum operation in normal conditions. After a contingency, sub-clusters may be formed for improving isolated operation performance. Unfavourable: high communication requirements. Its applicability can depend on the number of elements to be controlled.
GSIM - centralized (2 - level)	M/H	Favourable: effective optimum operation in normal conditions. After a contingency, sub-clusters may be formed for improving isolated operation performance. Lower communication requirements than 1-level architecture. Unfavourable: - Favourable: lower communication requirements than central architecture. Applicable for large systems. After contingency, sub-clusters can be formed for improving isolated operation performance.
GSIM distributed	M/M	Unfavourable: Probably, the operation is not as optimum as in the central architecture.
MPSC	Same characteristics than GSIM	Same characteristics than GSIM
PCM/GSIM/MPSC decentralized	L/NA	Not recommended [8]

H - high; M - medium; L - low

Table 6.16: Layout vs. communications and operation

Line technology

The problem of concerning different types of line technology (AC or DC lines) interfacing microgrids in regard of communications has to do with the difficulty of developing proper control systems managing power flows between these lines. For AC systems, system stability is ensured by maintaining a constant electrical frequency in the distribution grid, i.e. in the network interfacing all microgrids. Since the electrical frequency is the same throughout the network, it can be measured locally by those agents (generators) in charge of providing power reserves for frequency control purposes. Ideally, no communications are needed for this purpose, at least while providing so-called primary power reserves [149], since activated locally through power - frequency droops. However, for the provision of secondary reserves, communications may be needed between microgrids and a central manager of the whole network, since being this a market regulated service. System stability for DC networks cannot be ensured by locally measuring electrical frequency (this is zero in this case). Other signals need to be sent to the microgrids to act in consequence and maintain constant voltage levels everywhere. Different control systems are developed in literature for this purpose. Voltage - power control droops for power converters are proposed and this results in a system with low communication requirements [150]. However, the scarcity of exogenous measurements and control signals through communication platforms affects the performance of the above described control algorithms for voltage and frequency levels. Thus, improving the performance of such control algorithms through the coordination of the different participating agents, communications are principal. This is one aspect addressed in [87]. This work proposed a hybrid AC and DC system so as to interface different microgrids. Exploiting communications, the architecture of the whole system could be change so different microgrids can be connected and disconnected according to operational objectives. Among the advantages of such hybrid system over a distribution system between microgrids in AC, the authors claim better operational flexibility and improved integration capacity of DG (optimized power sharing throughout). Table 6.17 compares the communication requirements and the operation performance versus the line technology.

Interconnection technology

Communications (and the level of enhanced controllability they provide) can be different for various interconnection technology between microgrids. In

6.3 Qualitative comparison of architectures

Line technology	Communication requirements/ Control and operation performance	Comments
AC	H/H	Favourable: for providing stability (primary power reserves), frequency is a control signal that can be measured locally without additional communication links. Unfavourable: communications are required for secondary power reserves among other regulated activities and for improving the performance of the control algorithms.
DC	H/M	Favourable: DC voltage can be used as a control signal, which can be measured locally. Unfavourable: communication are required for regulated activities and for improving the performance of the control algorithms. Low experience.

H - high; M - medium; L - low

Table 6.17: Line technology vs. communications and operation

fact, power electronics, as interconnection interfaces, are usually equipped with local communication devices that permits to effectively receive exogenous inputs from other microgrids and/or a centralized manager of the whole network. In addition, such power electronics can be also equipped with local intelligence that permit to autonomously take decisions from local measurements (i.e. measurements of the status and needs of the agents of the microgrid it is connected to), and act in consequence. A practical example of this is the research done in the FP7 project Smart Rural Grid [151]. In this project, a power electronics device equipped with batteries serve as the link between a microgrid (or part of a rural distribution grid) with the rest of the network. This power converter receives inputs from the network operator through wireless communication paths and also from the agents (e.g. DG and controllable loads) of the microgrid it is connected to. All of this permit the power converter to provide diverse services related to the security of supply to consumers in case of mains failure and performance improvement of the distribution network by peak load alleviation, voltage and frequency control, and others. The profitability of communication devices in a cluster of microgrids is clearly benefited from installing such flexible and controllable power electronics as interconnection technology. With conventional transformers, communications could be exploited just for isolation purposes of microgrids in case of grid eventualities and some control actions, as the adjustment of tap changers for voltage control purposes. Table 6.18 compares the communication requirements and the operation performance

versus the interconnection technology.

Interconnection technology	Communication requirements/Control & operation performance	Comments
Transformer	L/L	Favourable: low communications requirements. Unfavourable: the control and operation of a power transformer is limited to microgrid isolation and tap changer adjustment.
Power converter	H/H	Favourable: high capacity of control and good operation performance. Can provide additional services to the external grid and to the microgrid. Unfavourable: high communication requirements

H - high; M - medium; L - low

Table 6.18: Interconnection technology vs. communications and operation

6.3.7 Business models

The multiple microgrids deployment and the corresponding regulatory framework are an opportunity to create new business models to promote the installation of DERs.

The business model aim is to describe how to create value with a certain product or technology. In this case, the business model approach must identify potential values in different microgrid cluster architectures. Moreover, regulatory agencies must define the regulatory framework including responsibilities and roles. This would constitute a stable environment to deploy multi-microgrid projects.

The present section is focused on the business model value configuration according to the approach of [152, 153] and this work delves into business model activities and resources. Business model activities include the energy trading mechanisms and ancillary services to keep the grid on-going. Business model resources are all technology components needed to deploy the microgrids network as line and interconnection elements.

Business models for microgrids have been deeply analysed in different works. In [154], a business model related to a deployment of a single microgrid is described. Additionally, the study performed in [155] analyses the business model of 24 microgrids identifying 29 combinations of elements. In contrast to the previous work, this section is focused on the interactions between multiple microgrids in different cases. As commented earlier, microgrids are seen in this chapter as a single entity capable to provide energy and flexibility for ancillary services. Therefore, internal business model and operations within a single microgrid are not part of this work.

6.3 Qualitative comparison of architectures

Related to energy trading at the daily or hourly basis between multiple microgrids or local energy communities with two-way communications, there are two energy management approaches: centralized optimization and Transactive Energy control [156]. The U.S. Department of Energy's Grid-wise Architecture Council defined Transactive Energy in [157] as a set of economic and control mechanisms that allows the dynamic balance of supply and demand across the entire electrical infrastructure using value as a key operational parameter. Transactive Energy requires a microgrid central controller to manage the microgrid and interact with other microgrid controllers exchanging messages with prices and energy quantities in a two-way negotiation. In contrast, the centralized optimization approach assumes that a central entity takes decisions for all microgrids.

Reference [158] describes a centralized minimization-cost algorithm to settle energy transactions between microgrids without revealing cost functions of each microgrid either considering grid constraints. In contrast, the study performed in [159] has presented a centralized micro-market for energy exchange between grid nodes considering grid constraints and the day-ahead wholesale market for main grid connected microgrids. The micro or local market proposition for local energy communities is introduced in [160]. This is a centralized optimization peer-to-platform approach enabling inter-microgrid energy trading with a central entity managing the local market.

Compared to the centralized approach, the work performed in [161] proposed a Transactive Energy system for real-time energy trading between microgrids to address the imbalances leftover in the previous inter-microgrid auction based electricity market.

Layout

The three clustering layouts proposed in this work open a new approach related to the corresponding business models and regulations. PCM and MPSC layouts imply that there is an external grid operator who is responsible to the feasible operation. This operator could require technical assistance to operate the grid and then microgrids could provide ancillary services. In this case, the value proposition of microgrids are the ancillary services to the grid operator. These services could be required through grid codes and external signals like TSO does nowadays or through other mechanisms not developed yet. For example, in [162] it is proposed a microgrid scheduling model to offer ancillary services to the grid operator within the current regulatory framework.

In contrast, GSIM layouts at the early stage could be developed without

a central entity. Therefore, a third-party should take the grid operator role and establish a reward mechanism for microgrids providing ancillary services. The grid operator role is mandatory in order to operate the microgrid interconnections safely ensuring voltage and, if required, frequency stability.

Additionally, layout options have implications about interconnector ownership. In PCM layout, the single external connection could be owned by the microgrid responsible and the grid operator could own the rest of the grid. This is a similar model like the power generators have in some European power system.

In contrast, building up new direct lines between microgrids at the early stage GSIM and MPSC layouts could be complicated due to cost sharing negotiation. In such cases, one party could get more benefits with the direct line than the other. Therefore, the payment agreement between microgrids could be difficult to reach. This could be a similar negotiation process like nowadays TSO do before building a new connection line between them. However, microgrids could have difficulties quantifying the benefits of the project. For instance, if there is a grid operator, all lines could be owned by it. Alternative models could be explored to avoid dominant positions in cases without a grid operator dominated by transactive energy processes.

Line technology

Independently of the line technology used, microgrids can provide ancillary services to support grid operations. In case of AC external networks, it is necessary to implement an active and reactive power control in the microgrid and grid operator sides. Note that power exchanges are limited to the interconnection capacity. Hence, reactive power requirements could limit the active power transactions. Therefore, a local market for reactive power control could be developed in order to reward the efforts provided by each microgrid. This possibility should be developed deeply in further works.

In contrast, DC external networks only uses active power as control variable and the local reactive power market is not needed.

Interconnection technology

In case of AC external networks using a power converter as interconnection technology, the controllability would improve in front of using a power transformer. It would promote a faster ancillary services market inside the cluster of microgrids.

Note that if the microgrids are interconnected through DC technology, the requirement of power converters would be mandatory.

In both cases, the grid operator sends requests to each microgrid.

6.3.8 Summary

The overall comparison between microgrid clustering architectures to form the multi-microgrid electric power systems is shown in Table 6.19, where business models have been excluded because they can be adapted to each architecture.

	Layout			Line technology		Interconnection technology		
	PCM	GSIM	MPSC	AC	DC	Transformer	Power converter	
Cost	L	H	M	M	L	L	H	
Scalability	L	M	H	L	H	H	L	
Protection	L ⁽¹⁾	M-H ⁽¹⁾	M-H ⁽¹⁾	H ⁽²⁾	M ⁽²⁾	H ⁽²⁾	L ⁽²⁾	
Reliability	M	L	H	N/A	N/A	H	M	
Stability	M	L	H	N/A	N/A	H	M	
Communication requirements	N/A ⁽³⁾	N/A ⁽³⁾	N/A ⁽³⁾	H	H	L	H	
Operation performance	N/A ⁽³⁾	N/A ⁽³⁾	N/A ⁽³⁾	H	M	L	H	

H - high; M - medium; L - low

⁽¹⁾ refers to the difficulty of protection

⁽²⁾ refers to the applicability

⁽³⁾ depend on the control architecture

Table 6.19: Overall comparison between the presented microgrid clustering architectures

6.4 Conclusion

Taking into account the recent developments, a massive roll out of microgrids can be expected in the near future. This will lead to the electric power system transformation, from the current centralized system to a multi-microgrid based decentralized system. Hence, now there is the opportunity to design how our future electric system should look like. Accordingly, this chapter has defined the possible multi-microgrid architectures and their potential benefits. From this work, the following conclusions can be drawn:

- The use of the existing electric installations to integrate microgrids can avoid huge expenses on building a completely new infrastructure. Hence, the PCM and MPSC layouts with AC line technology seem to be the most probable architectures for these areas that are currently

electrified. On the other hand, the interconnection technology will depend on the particular requirements of each area.

- In non-electrified areas, planning a new infrastructure will be a challenge and an opportunity. The initial decisions can affect the performance of the system and it should be done according to the particular requirements of the region. For example, regions with low financial resources should try to avoid multi-microgrid architectures with higher costs. But if these regions are under expansion, the scalability should be taken into consideration. Hence, an equilibrium between cost and scalability will determine the best multi-microgrid architecture for the particular regions of this example.
- In general, the PCM layout architecture is considered the simplest one. This architecture is expected to offer simple protection systems, acceptable reliability and stability in front of disturbances and reduced investment cost. In contrast, the scalability can be affected. To deal with scalability, the MPSC architecture could be selected. In this case, the cost would increase. From the analysed architectures, the GSIM layout does not offer significant advantages in front of the MPSC microgrid. In addition, despite its expected acceptable scalability, the high costs and the expected low performance in terms of protection, reliability and stability make the GSIM architecture uncompetitive to the PCM layout. Hence, the use of the GSIM layout is not recommended.
- Regarding the line technology, AC architecture results in higher installation and O&M cost and lower performance of scalability than the DC line technology. In contrast, the AC protection technology is more mature than DC technology. In addition, the protection requirements of power transformers (AC) are less restrictive. Hence, it is expected that AC systems can be protected easier than DC systems. The stability is difficult to be compared. The advantage of the AC line technology is that the associated protection becomes simpler and cheaper as well as the possibility to use power transformers as interface technology. The use of power transformers could compensate the cost difference between AC and DC line technology being, overall, cheaper than if the DC line technology is used.

The AC line technology is the most used one. The reason being is its larger maturity as the transmission and distribution has been traditionally done in AC. However, DC technology development is ex-

pected to occur fast because of its advantages. Hence, for planning new multi-microgrids in non-electrified areas, it should be considered and analysed both AC and DC line technologies.

- The interconnection technology can also affect the overall multi-microgrid system performance. The use of power transformers presents better system scalability, reliability, stability and lower protection requirements. Taking into account these advantages and the reduced cost in comparison to power converters, it seems that power transformers should be recommended in most of the cases. Nevertheless, due to the high controllability of power converters, the grid capacity to integrate renewable power generation can increase. Hence, a mix of microgrids interconnected by means of transformers and power converters may result in a good solution for low carbon multi-microgrid systems.
- Communication systems will play a key role for the operability of the microgrid clusters. The amount of communications required is an important factor to consider and will be mainly affected by the control type. Centralised controllers can lead to better system performance but it can increase the communication and computational needs. The hierarchical approach presented in this chapter could reduce these requirements being capable of operating large multi-microgrids. On the other hand, distributed control approaches can avoid extra computational efforts and communication requirements.
- Changing the current electric power system to a multi-microgrid system opens new opportunities in terms business models, which will need to be adapted to the grid architecture.

According to these results, future investigations for the development of multi-microgrid systems should focus on the PCM and MPSC layout architectures taking into account any interface technology. Despite the AC line technology is the most used nowadays, the benefits of DC technology are well determined. Hence, both technologies are now of interest to be applied in the future multi-microgrids: the AC technology to benefit from the current infrastructure reducing additional investment costs; and DC technology to benefit from lower power losses, simplicity and cost.

Finally, the comparison done in this chapter is obtained from the current state of the art. It means that further technological development could modify some of the features presented here. In addition, due to the low

development of multi-microgrids, further detailed works could be done to study the architecture's potential by means of case studies.

Chapter 7

Optimal feeder flow control for grid connected microgrids

7.1 Introduction

As explained before, the control of the active power exchange between a microgrid with its external grid, i.e. the FFC, can be required by the external grid operators. This control can help grid operators to plan their distribution grid operation. As stated in [104], *from the utility's point of view, it is desirable if a portion of their networks consume constant electric power as scheduled or commanded*. In essence, a feeder flow controlled microgrid is a true dispatchable system from the utility's point of view [163].

The FFC in microgrids has recently been studied in [104, 164–169]. In [104], the minimum feeder flow setpoint at the connection point of the microgrid is determined and an algorithm is developed to comply with the setpoint, but its optimal operation is not considered. In [164], the FFC under different conditions (load variation during grid connected and islanded modes and the transition mode) is studied. In addition, a method to determine the frequency - feeder flow droop constants is defined in order to avoid higher frequency deviations during transition (grid connected-islanded) mode. One important conclusion is that multiple DGs operating under FFC mode are better for fulfilling the setpoints during load variations. But again, the optimal economic operation is not considered. In [165] and [166], a centralized feeder flow controller based on a fuzzy PI controller to minimize the power deviations during various load changes is proposed. The proposed scheme consists on all DGs operating under UPC mode, and the centralized feeder flow controller modifies each active power setpoint to maintain the desired feeder flow at the microgrid's point of connection. In [167], an economic dispatch optimization problem is formulated considering a microgrid based on different control areas, where each control area performs a FFC. The objective is to minimize the cost ensuring the stability,

but the network power flow equations are not considered.

The economic optimization of the power systems operation can be performed considering the power flow equations (optimal power flow) or without them (optimal economic dispatch). The optimal economic dispatch for feeder flow controlled microgrids has been studied in [167], but the optimal power flow problem for feeder flow controlled microgrids has not been formulated before. To find a global optimum for the optimal power flow problem in radial grids, relaxation techniques have been used, leading to second order cone problems (SOCP) [170]. In addition, conditions for the objective function have been found to ensure the relaxed problem holds [170]. When these conditions are not accomplished, the optimal solution has no physical sense. To solve it, an iterative algorithm is suggested in [171], where some terms of the objective function are moved to an additional constraint to make the relaxation hold, but under some conditions the algorithm can converge to a local optimum. This happens because the optimal power flow formulation does not consider the real cost function. Traditionally, economic dispatch algorithms or optimal power flows have been formulated taking into account that generators operate under UPC mode (constant active power setpoint) [172]. So, the optimal power setpoints that minimize the cost will be maintained constant. In the FFC mode, the power generated will depend on the output of the optimization algorithm but also on the load and non-dispatchable generators variations. So, when a load variation occurs the dispatchable generators outputs will vary and the optimal operating points can be lost.

The present study addresses the before described problems. On one hand, the formulation of a relaxed optimal power flow problem for feeder flow controlled microgrids is proposed. The problem is based on a MISOCP and to avoid the loss of the optimal operation point, the uncertainty is considered by means of stochastic formulation. On the other hand, an algorithm for obtaining a feasible global optimum solution from the relaxed optimal power flow problem is proposed. The proposed algorithm maintains all the cost terms in the objective function, being able to find the global optimum solution.

7.2 Formulation of the optimal feeder flow problem

This section presents the formulation of the optimal operation of a feeder flow controlled microgrid and how it can be solved to find a global optimum. The objective is to present the concept of how the operation of feeder flow

controlled microgrids can be optimized. Hence, a single period is considered in the present study. But this formulation can be easily extended to multi-period optimization problem. Note that for the sake of simplicity just loads, dispatchable generators and non-dispatchable generators (as PV) are considered. In such system, the decision variables are the active and reactive power setpoints of the UPC generators and the active and reactive power flow setpoints of the FFC generators.

7.2.1 Notation

Tables 7.1, 7.2 and 7.3 show the sets, variables and parameters used in the proposed optimal feeder flow problem formulation. Note that the voltage and current variables represent square values, avoiding the need of using non-conic constraints [170, 171].

Table 7.1: Sets definition

Sets	Description
N	Grid nodes $n \in N$ (for slack: $n = 1$)
S	Scenarios
L	Lines (n, m) ; $n, m \in N$, n = up-stream, m = down-stream
$u(n)$	Nodes $m \in N$ that comply both: i) up-stream node $n \in N$ and ii) directly connected to $n \in N$. i.e. all node $m \in N$ that complies $(m, n) \in L$
$d(n)$	Nodes $m \in N$ that comply both: i) down-stream node $n \in N$ and ii) directly connected to $n \in N$. i.e. all node $m \in N$ that complies $(n, m) \in L$
UPC	Nodes $n \in N$ with generators under Unit output Power Control mode
FFC	Nodes $n \in N$ with generators under Feeder Flow Control mode

7.2.2 Stochastic formulation

The formulation considers different scenarios s , which are generated based on the PV generation and load predictions. This way, uncertainty can be considered. To obtain a global optimum, the objective function will consider the sum of the objective functions of each scenario.

7.2.3 Power flow equations

First of all, and for the sake of comprehension, the scheme of the DistFlow formulation model [173] for optimal power flow formulation is introduced in Figure 7.1. In this Figure, the sub-index corresponding to each scenario $s \in S$ is omitted. Also, the external active and reactive power flow setpoints are depicted. The net consumption (P_n^{net} and Q_n^{net}) is drawn as a load, but

Table 7.2: Variables definition

Real variables	Description
P_{ns}^G, Q_{ns}^G	Active and reactive power generation at node $n \in N$ and scenario $s \in S$
P_{nms}, Q_{nms}	Active and reactive power flow from node $n \in N$ to node $m \in N$ at scenario $s \in S$. $(n, m) \in L$
$P_{ns}^{net}, Q_{ns}^{net}$	Net active and reactive power consumption at node $n \in N$ at scenario $s \in S$
P_n^{G*}, Q_n^{G*}	Active and reactive power setpoint at generator connected at node $n \in UPC$
FFP_n^*, FFQ_n^*	Active and reactive power flow setpoint at generator connected at node $n \in FFC$
$\Delta FFP_{ns}, \Delta FFQ_{ns}$	Active and reactive power flow deviation at generator connected at node $n \in FFC$ at scenario $s \in S$
ΔC	Auxiliary variable for the convexification of the objective function
ΔC_1	Total fixed generation cost
ΔC_2	Total variable penalty cost for feeder flow setpoint violation
ΔC_3	Total fix penalty cost for feeder flow setpoint violation
Positive variables	Description
i_{nms}	Square of the current flowing from node $n \in N$ to node $m \in N$ at scenario $s \in S$. $(n, m) \in L$
v_{ns}	Square of the voltage of node $n \in N$ at scenario $s \in S$
DP_{1s} and DP_{2s}	Auxiliary variables for linearise the absolute value: $ \Delta FFP_s = DP_{1s} + DP_{2s}, s \in S$
DQ_{1s} and DQ_{2s}	Auxiliary variables for linearise the absolute value: $ \Delta FFQ_s = DQ_{1s} + DQ_{2s}, s \in S$
Binary variables	Description
y_n	State of generator connected at node $n \in N$. Connected = 1, disconnected = 0
zps, zqs	Status of the active and reactive power flow compliance at slack node and scenario $s \in S$. 0 = compliant, 1 = non-compliant
$zp1_{ns}, zp2_{ns}$	Auxiliary variables for linearising the condition: if $P_n^{Gmin} < P_{ns}^G < P_n^{Gmax}$ then $\Delta FFP_{ns} = 0$, $n \in FFC, s \in S$
$zq1_{ns}, zq2_{ns}$	Auxiliary variables for linearising the condition: if $Q_n^{Gmin} < Q_{ns}^G < Q_n^{Gmax}$ then $\Delta FFQ_{ns} = 0$, $n \in FFC, s \in S$
zdp_s, zdq_s	Auxiliary variables for linearising the absolute values: $ \Delta FFP_s $ and $ \Delta FFQ_s $, $s \in S$

note that generators can also be installed. Generation is considered as a negative net consumption.

The active and reactive power balance constraints at the slack node are expressed as (7.1) and (7.2), respectively. The power balance at the rest of the nodes is expressed as (7.3) and (7.4), respectively. The net consumption at node n is equal to the input power minus the output power.

7.2 Formulation of the optimal feeder flow problem

Table 7.3: Parameters definition

Parameters	Description
r_{nm}, x_{nm}	Resistance and reactance of the line $(n, m) \in L$
P_{ns}^C, Q_{ns}^C	Active and reactive power consumption forecast at node $n \in N$ at scenario $s \in S$
v_{min}, v_{max}	Minimum and maximum square voltage
v^*	Slack voltage
i_{nm}^{max}	Maximum square current flow through line $(n, m) \in L$
P_n^{Gmin}, P_n^{Gmax}	Minimum and maximum active power generation at node $n \in N$ when the corresponding generator is connected.
Q_n^{Gmin}, Q_n^{Gmax}	Minimum and maximum reactive power generation at node $n \in N$ when the corresponding generator is connected.
$FFP_n^* _{n=1}$	External active power flow setpoint at node $n = 1$
$FFQ_n^* _{n=1}$	External reactive power flow setpoint at node $n = 1$
M_1, M_2, M_3	Large values used for modelling integer constraints
C_n^{ag}, C_n^{bg}	Fix and variable generation cost parameters at node $n \in N$
C^{affp}, C^{bfff}	Fix and variable cost parameters of active power flow non-compliance at node $n = 1$
C^{affq}, C^{bfffq}	Fix and variable cost parameters of reactive power flow non-compliance at node $n = 1$

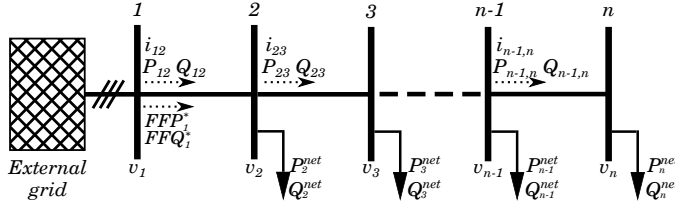


Figure 7.1: Scheme of the DistFlow model

$$P_{ns}^G = \sum_{m \in d(n)} P_{nms} \quad \forall s \in S; \quad n = 1 \quad (7.1)$$

$$Q_{ns}^G = \sum_{m \in d(n)} Q_{nms} \quad \forall s \in S; \quad n = 1 \quad (7.2)$$

$$P_{ns}^{net} = \sum_{m \in u(n)} (P_{mns} - r_{mn} \cdot i_{mns}) - \sum_{m \in d(n)} P_{nms} \quad \forall s \in S; \quad \forall n \in N \setminus \{1\} \quad (7.3)$$

$$Q_{ns}^{net} = \sum_{m \in u(n)} (Q_{mns} - x_{mn} \cdot i_{mns}) - \sum_{m \in d(n)} Q_{nms} \quad \forall s \in S; \quad \forall n \in N \setminus \{1\} \quad (7.4)$$

The net power consumption is calculated as (7.5) and (7.6), respectively. It represents the forecasted load minus the generated power (which can be forecasted in case of non-dispatchable generation or a decision variable in case of dispatchable generation).

$$P_{ns}^{net} = P_{ns}^C - P_{ns}^G \quad \forall n \in N; \quad \forall s \in S \quad (7.5)$$

$$Q_{ns}^{net} = Q_{ns}^C - Q_{ns}^G \quad \forall n \in N; \quad \forall s \in S \quad (7.6)$$

The voltage drops can be expressed as (7.7). Then, the voltages must be constrained between upper and lower limits as shown in (7.8). The slack voltage, i.e. the point of the microgrid interconnection, is fixed according to constraint (7.9).

$$v_{ms} = v_{ns} - 2(r_{nm}P_{nms} + x_{nm}Q_{nms}) + i_{nms}(r_{nms}^2 + x_{nms}^2) \quad \forall n \in N; \quad \forall m \in d(n); \quad \forall s \in S \quad (7.7)$$

$$v_{min} \leq v_{ns} \leq v_{max} \quad \forall n \in N; \quad \forall s \in S \quad (7.8)$$

$$v_{ns} = v^* \quad \forall s \in S; \quad n = 1 \quad (7.9)$$

The square of the currents flowing through the lines are also constrained, as shown in (7.10).

$$i_{nms} \leq i_{nm}^{max} \quad \forall n \in N; \quad \forall m \in d(n); \quad \forall s \in S \quad (7.10)$$

The generation limits are expressed as (7.11)-(7.14), being y_n the connection/disconnection binary variable.

$$P_n^{Gmin} \cdot y_n \leq P_{ns}^G \quad \forall n \in N; \quad s \in S \quad (7.11)$$

$$P_{ns}^G \leq P_n^{Gmax} \cdot y_n \quad \forall n \in N; \quad s \in S \quad (7.12)$$

$$Q_n^{Gmin} \cdot y_n \leq Q_{ns}^G \quad \forall n \in N; \quad s \in S \quad (7.13)$$

$$Q_{ns}^G \leq Q_n^{Gmax} \cdot y_n \quad \forall n \in N; \quad s \in S \quad (7.14)$$

The current can be calculated as (7.15). This constraint is clearly non linear and non-convex. This leads to the need of using non linear programming (NLP) solvers, which rarely find the global optimum. To solve this issue, this constraint is relaxed as (7.16), becoming a second order cone constraint.

$$i_{nms} = \frac{P_{nms}^2 + Q_{nms}^2}{v_{ns}} \quad \forall n \in N; \quad \forall m \in d(n); \quad \forall s \in S \quad (7.15)$$

$$i_{nms} v_{ns} \geq P_{nms}^2 + Q_{nms}^2 \quad \forall n \in N; \quad \forall m \in d(n); \quad \forall s \in S \quad (7.16)$$

7.2.4 UPC and FFC constraints

Generators of the microgrid can operate under FFC or UPC modes. For generators operating under UPC mode, the active and reactive power generation must be the same for all scenarios. This is expressed with constraints (7.17) and (7.18).

$$P_{ns}^G = P_n^{G*} \quad \forall n \in UPC; \quad \forall s \in S \quad (7.17)$$

$$Q_{ns}^G = Q_n^{G*} \quad \forall n \in UPC; \quad \forall s \in S \quad (7.18)$$

For those generators under FFC mode, the power flow upstream their associated bus must be equal to the setpoint for all scenarios. This can be expressed by the constraints (7.19) and (7.20).

$$FFP_n^* = \sum_{m \in d(n)} (P_{nms}) + P_{ns}^{net} \quad \forall n \in N; \quad \forall s \in S; \quad \forall n \in FFC \quad (7.19)$$

$$FFQ_n^* = \sum_{m \in d(n)} (Q_{nms}) + Q_{ns}^{net} \quad \forall n \in N; \quad \forall s \in S; \quad \forall n \in FFC \quad (7.20)$$

The above equations enforce the power flow through the controlled lines to be constant for all scenarios. This can lead to an infeasible solution. If the downstream loads variations between scenarios are large enough, the active power generation required from the feeder flow controlled generators can be greater than their maximum power (constraints (7.12) and (7.14)) or lower than their minimum power (constraints (7.11) and (7.13)). To solve this, without losing the convexity of the OPF problem, the feeder flow constraints are rewritten as (7.21)-(7.25) for the active power and as (7.26)-(7.30) for the reactive power. Particularly, constraints (7.19) and (7.20) are modified so that the variables ΔFFP_{ns} and ΔFFQ_{ns} (defined as the feeder flow setpoint deviation) are included as shown in (7.21) and (7.26). The rest of the additional constraints (7.22)-(7.25) and (7.27)-(7.30) are to model the feeder flow control operation, in which the power flow will be equal to the power flow setpoint if the power generation of the FFC generator is not at

its limits; and a power flow deviation can occur if the power generation of the FFC generator is at its limits. More details are given below.

$$FFP_n^* + \Delta FFP_{ns} = \sum_{m \in d(n)} (P_{nms}) + P_{ns}^{net} \quad \forall n \in FFC; \quad \forall s \in S \quad (7.21)$$

$$P_{ns}^G - P_n^{Gmin} \leq P_n^{Gmax} \cdot zp1_{ns} \quad \forall s \in S; \quad \forall n \in FFC \quad (7.22)$$

$$P_n^{Gmax} - P_{ns}^G \leq P_n^{Gmax} \cdot zp2_{ns} \quad \forall s \in S; \quad \forall n \in FFC \quad (7.23)$$

$$\Delta FFP_{ns} \leq M_1(2 - zp1_{ns} - zp2_{ns}) \quad \forall s \in S; \quad \forall n \in FFC \quad (7.24)$$

$$\Delta FFP_{ns} \geq M_1(zp1_{ns} + zp2_{ns} - 2) \quad \forall s \in S; \quad \forall n \in FFC \quad (7.25)$$

$$FFQ_n^* + \Delta FFQ_{ns} = \sum_{m \in d(n)} (Q_{nms}) + Q_{ns}^{net} \quad \forall n \in FFC; \quad \forall s \in S \quad (7.26)$$

$$Q_{ns}^G - Q_n^{Gmin} \leq Q_n^{Gmin} \cdot zq1_{ns} \quad \forall s \in S; \quad \forall n \in FFC \quad (7.27)$$

$$Q_n^{Gmax} - Q_{ns}^G \leq Q_n^{Gmax} \cdot zq2_{ns} \quad \forall s \in S; \quad \forall n \in FFC \quad (7.28)$$

$$\Delta FFQ_{ns} \leq M_1(2 - zq1_{ns} - zq2_{ns}) \quad \forall s \in S; \quad \forall n \in FFC \quad (7.29)$$

$$\Delta FFQ_{ns} \geq M_1(zq1_{ns} + zq2_{ns} - 2) \quad \forall s \in S; \quad \forall n \in FFC \quad (7.30)$$

If the constraints for the FFC of the active power (7.21)-(7.25) are considered . Equation (7.21) reflects that all scenarios have the same active power flow setpoint (FFP_n^*), but they can present different deviations (ΔFFP_{ns}). Equations (7.22) and (7.23) say that i) if P_{ns}^G is strictly greater than P_n^{Gmin} , then $zp1_{ns}$ is equal to 1 and ii) if P_{ns}^G is strictly lower than P_n^{Gmax} , then $zp2_{ns}$ is equal to 1. So, if the power generation P_{ns}^G is not at its limits, then the condition (7.31) is fulfilled. If M_1 is large enough, equation (7.24) says that if the condition (7.31) is fulfilled, then ΔFFP_{ns} is lower or equal to 0. Otherwise, ΔFFP_{ns} can take any value. The same way, equation (7.25) says that if the condition (7.31) is fulfilled, then ΔFFP_{ns} is greater or equal to 0. Otherwise, ΔFFP_{ns} can take any value. Hence, if condition (7.31) is fulfilled, then $\Delta FFP_{ns} = 0$ which means that the active power flow setpoint is fulfilled by the scenario s . Otherwise, if the condition (7.31) is not fulfilled, then ΔFFP_{ns} can take any value.

$$zp1_{ns} + zp2_{ns} = 2 \quad (7.31)$$

Reactive power feeder flow constraints (7.26)-(7.30) behave in the same manner. Note that these equations are linear integer constraints which suits well with the MISOCP formulation.

7.2.5 Objective function

The active and reactive power exchanges between the grid and the microgrid will be determined by an external agent. In this case, the internal operation cost minimization is considered to be the most interesting objective function. The operation cost can be written as (7.32). The first term represents the generation cost function, which considers linear generation costs. In addition, as an external feeder flow setpoint is required, a penalty for feeder flow setpoint deviations is also included. This penalty is linear with the absolute value of the corresponding deviation. The second and third terms represent the penalty cost for not complying with the external active and reactive feeder flow setpoints, respectively.

$$f = \sum_{s \in S} \left[\sum_{n \in N} \left(C_n^{ag} \cdot y_n + C_n^{bg} \cdot P_{ns}^G \right) \right] + \sum_{s \in S} \left[C^{affp} \cdot zp_s + C^{bfff} \cdot |\Delta FFP_s| \right] + \sum_{s \in S} \left[C^{affq} \cdot zq_s + C^{bfff} \cdot |\Delta FFQ_s| \right] \quad (7.32)$$

where $|\Delta FFP_s| = |FFP^* - FFP_s|$ and $|\Delta FFQ_s| = |FFQ^* - FFQ_s|$ are the feeder flow setpoint deviations at the slack node.

The objective function is not linear and it contains binary variables. This function is reformulated so that it can be solved as a MISOCP optimization problem. The above cost function is rewritten as (7.33) with the additional constraints (7.34)-(7.46). The new objective function is linear as all binary variables and absolute values have been removed. ΔC is a variable that substitutes the removed costs terms. This variable is constrained as (7.34). In this constraint, the right side represents all the costs that have been removed from the objective function. The terms of the right side will be defined later. Despite the inequality nature of the constraint 7.34, the solver will find the solution $\Delta C = \Delta C_1 + \Delta C_2 + \Delta C_3$. This can be ensured due to the minimization nature of the problem. Hence, this new objective function is completely equivalent to the one represented by (7.32).

$$f = \sum_{s \in S} \left[\sum_{n \in N} \left(C_n^{bg} \cdot P_{ns}^G \right) \right] + \Delta C \quad (7.33)$$

$$\Delta C \geq \Delta C_1 + \Delta C_2 + \Delta C_3 \quad (7.34)$$

The total activation cost of generators (ΔC_1) is expressed as (7.35).

$$\Delta C_1 = \sum_{s \in S} \left[\sum_{n \in N} (C_n^{ag} \cdot y_n) \right] \quad (7.35)$$

The variable cost of feeder flow setpoint deviation is linearised as follows. Equation (7.36) represents the variable cost for the active and reactive power flow deviation while constraints (7.37)-(7.43) are for linearising the absolute values. The terms $DP_{1s} + DP_{2s}$ and $DQ_{1s} + DQ_{2s}$ in constraint (7.36) are equivalent to the absolute values that appear in the original objective function (7.32), i.e. $|\Delta FFP_s| = DP_{1s} + DP_{2s}$ and $|\Delta FFQ_s| = DQ_{1s} + DQ_{2s}$. Note that these terms are linear. If M_2 is large enough, constraints (7.38) and (7.39) only imposes that if $DP_{1s} > 0$ then $DP_{2s} = 0$ and vice versa. Note that DP_{1s} and DP_{2s} are defined as non-negative variables and zdp_s is a binary variable. Considering this and observing constraint (7.37), it is evident that $|\Delta FFP_s| = |P_{ns}^G - FFP^*| = DP_{1s} + DP_{2s}$. The same deduction can be done for the reactive power.

$$\Delta C_2 = \sum_{s \in S} \left[(DP_{1s} + DP_{2s}) \cdot C^{bfffq} + (DQ_{1s} + DQ_{2s}) \cdot C^{bfffq} \right] \quad (7.36)$$

$$P_{ns}^G - FFP^* = DP_{1s} - DP_{2s} \quad \forall s \in S; n = 1 \quad (7.37)$$

$$DP_{1s} \leq M_2 \cdot zdp_s \quad \forall s \in S \quad (7.38)$$

$$DP_{2s} \leq M_2 \cdot (1 - zdp_s) \quad \forall s \in S \quad (7.39)$$

$$Q_{ns}^G - FFQ^* = DQ_{1s} - DQ_{2s} \quad \forall s \in S; n = 1 \quad (7.40)$$

$$DQ_{1s} \leq M_2 \cdot zdq_s \quad \forall s \in S \quad (7.41)$$

$$DQ_{2s} \leq M_2 \cdot (1 - zdq_s) \quad \forall s \in S \quad (7.42)$$

$$DP_{1s}, DP_{2s}, DQ_{1s}, DQ_{2s} \geq 0 \quad (7.43)$$

The fixed cost of feeder flow setpoint deviation is expressed as (7.44). Constraints (7.45) and (7.46) determine if the scenario s fulfils (or not) the external setpoints through the binary variables zps and zqs . Note that the right side of these constraints represents the absolute values of the feeder flow setpoint deviation. Hence, if M_3 is large enough and there is a violation

of the external feeder flow setpoint, the right side is positive and accordingly, the binary variables are equal to 1. If the right side is 0, the binary variables become free variables, but due to the minimization nature of the optimization problem, they will be equal to 0.

$$\Delta C_3 = \sum_{s \in S} [zp_s \cdot C^{affp} + zq_s \cdot C^{affq}] \quad (7.44)$$

$$DP_{1s} + DP_{2s} \leq M_3 \cdot zp_s \quad \forall s \in S \quad (7.45)$$

$$DQ_{1s} + DQ_{2s} \leq M_3 \cdot zq_s \quad \forall s \in S \quad (7.46)$$

7.2.6 Optimal feeder flow problem

In [170], the second order cone relaxation for the optimal power flow problem is studied. The authors prove that the relaxed problem is exact under the following conditions:

- A1) The network graph is connected.
- A2) The objective function is convex.
- A3) The objective function is strictly increasing in i , non increasing in load, and independent of the apparent power.
- A4) The original optimal power flow problem is feasible.

Being exact means that every optimal solution of the relaxed problem satisfies equation (7.15). Hence, as the optimal solution is feasible for the non-relaxed problem, then it is the global optimum.

The optimal feeder flow problem is defined as following and denoted in this thesis as **OFFP**:

$$[MIN]f$$

Subject to (7.1)-(7.14), (7.16)-(7.18), (7.21)-(7.30), (7.34)-(7.46).

Condition A1 is expected to occur always and can be checked a priory. Condition A4 is a basic requirement to find a solution and will depend on the grid design. Hence, only conditions A2 and A3 have to be checked. In the proposed problem, the objective function is convex (A2). On the other hand, condition A3 may not be always satisfied. Note that the penalty cost terms, despite being linearised, represent absolute values. This motivates to find an alternative solution for solving the OFFP.

The proposed solution consists on applying a penalty to the objective function so that the global optimum is forced to be at the surface of the cone represented by the relaxed constraint (7.16), i.e. forcing the relaxed constraint to be active. If the relaxation does not hold, it means that the objective function can be improved if the power losses are artificially increased, leading to a non-meaningful solution. This could occur for example when the feeder flow setpoint is not fulfilled but increasing the power losses it can be fulfilled diminishing the corresponding penalties. Hence, the solution consists on adding the currents to the objective function with a penalty weight w . The objective function is redefined as (7.47).

$$f' = f + w \cdot \sum_{s \in S} \sum_{n \in N} \sum_{m \in d(n)} i_{nms} \quad (7.47)$$

Then, the corresponding optimal feeder flow problem, denoted in this thesis as **OFFP-w**, is defined as:

$$[MIN] f'$$

Subject to (7.1)-(7.14), (7.16)-(7.18), (7.21)-(7.30), (7.34)-(7.46).

The main difficulty is still to determine the value of w . If the relaxation does not hold, it means that increasing artificial losses still improves the objective function (the penalty w is too low). On the other hand, if the relaxation holds but w is too large, the problem will be solved to obtain the minimum currents and not the minimum costs represented by f . To find the appropriate weight, i.e. the minimum w that makes the relaxation hold, the algorithm 1 is developed.

The algorithm begins with no penalty. So, the OFFP-w is equivalent to the OFFP. If relaxation does not hold, then high and low bounds of the penalty weight are found. The initial range is set between 0 and the value which would make the penalty contribution to be equal to 10 times the objective function. The next iteration will hold thanks to this large penalty weight. Then at each iteration, w is set at the middle of the range $[low - high]$. If the problem is solved and the relaxation does not hold, w is too small and the *low* value is updated. Otherwise, the *high* value is updated. Note that at each iteration this range is reduced by half. The algorithm terminates when w cannot vary more than 5% or when the objective function is smaller than the lower bound found at the first optimization + 1c€.

The OFFP and the OFFP-w problems are MISOCP optimization problems. These can be efficiently solved by the CPLEX solver using the Branch

Algorithm 1 Global optimum

```

1:  $w \leftarrow 0$ 
2:  $f^* = \text{solve OFFP-w}$ 
3: if relaxation holds then
4:   save results
5:   go to 25
6: else
7:    $f_{min}^* \leftarrow f^*$ 
8:    $f^* \leftarrow 2 \cdot f^*$ 
9:    $low \leftarrow w$ 
10:   $high \leftarrow 10 \cdot f^* / \left( \sum_{s \in S} \sum_{n \in N} \sum_{m \in d(n)} i_{nms} \right)$ 
11:   $err \leftarrow (high - low) / high$ 
12: end if
13: while  $err > 0.05$  AND  $f^* - f_{min}^* > 0.01$  do
14:    $w \leftarrow low + (high - low) / 2$ 
15:    $f^{**} = \text{solve OFFP-w}$ 
16:   if relaxation holds then
17:      $f^* \leftarrow f^{**} - \text{penalty contribution}$ 
18:     save results
19:      $high \leftarrow w$ 
20:   else
21:      $low \leftarrow w$ 
22:   end if
23:    $err \leftarrow (high - low) / high$ 
24: end while
25: return Results

```

and Cut method [171]. In this thesis the CPLEX solver is used under the GAMS environment.

7.3 Case study

The test system is based on the IEEE 33-Bus distribution system [174] as shown in Figure 7.2. In addition, 6 PV generators and 8 dispatchable generators have been included. According to [167], a multi-FFC configuration suits better for microgrids without dominant generators. Considering this, generators identified as 2, 6 and 26 are operated under FFC mode, while the rest of dispatchable generators operate under UPC mode. The total power consumption is around 3.7 MW, while the installed power generation is 5 MW. The base case and grid data is shown in the Appendix D.

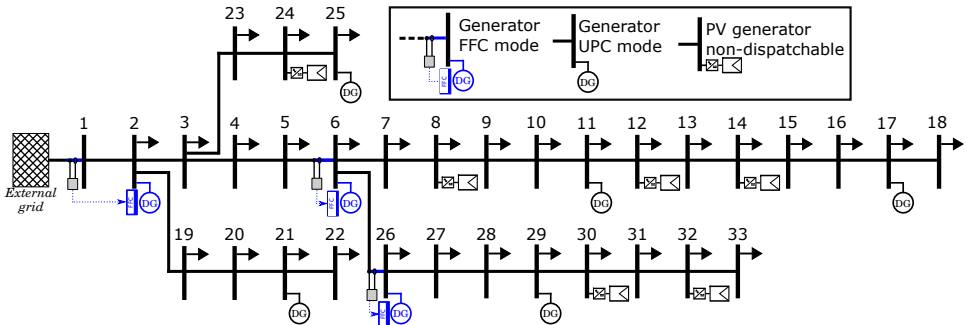


Figure 7.2: Scheme of IEEE 33-Bus distribution system

It is considered that PV generators operate under MPPT control mode. Hence, their active power generation is forced to be equal to the corresponding prediction.

7.4 Results

This section presents the results of the proposed optimization problem. First, the proposed algorithm for solving the OFFP is validated showing it converges and finds a global optimum. Then the proposed stochastic formulation is compared to a non-stochastic formulation, showing it finds better solutions for the feeder flow controlled microgrids.

7.4.1 Convergence

First, the forecasted scenario (active and reactive power for loads and active power for PV units) is used to generate ns random scenarios. For this purpose, it is considered that forecast errors follow a Gaussian distribution with a standard deviation of 0.35 p.u. These ns scenarios are used for testing the proposed optimization algorithm. A total of $ns = 10$ scenarios are considered (Figure 7.3) as it allows finding the optimal solution within a reasonable computation time.

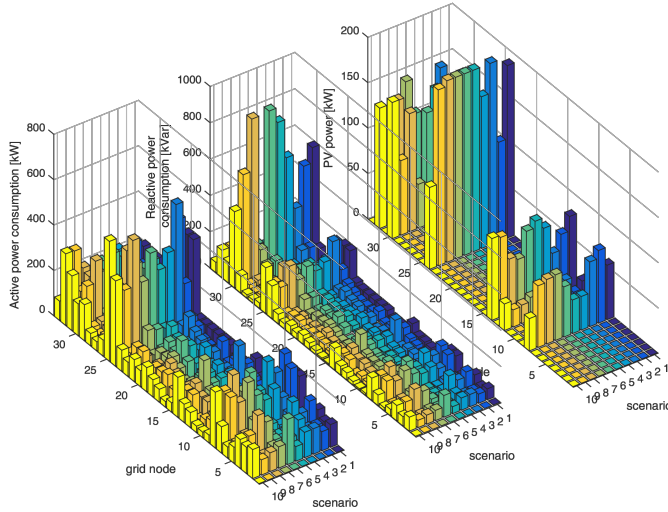


Figure 7.3: Scenarios used for the optimization problem

To test the solution algorithm convergence, the feeder flow setpoints are fixed to $(FFP_n^*|_{n=1}, FFQ_n^*|_{n=1}) = (1350 \text{ kW}, 900 \text{ kvar})$. Figure 7.4 shows the convergence of the algorithm. In this case, the OFFP relaxation has not hold, but has provided a lower bound of the objective function of 3085€ (dashed black line). As a result the *low* and *high* values are calculated and w is updated at each iteration. As it can be observed, when the relaxation holds, the *high* value is decreased. Otherwise, the *low* value is increased. The algorithm requires just 8 iterations, terminating because $err < 0.05$. A total cost of 3086€ has been obtained. According to the lower bound found, it can be assumed to be the global optimum. The proposed algorithm can converge even faster, without degrading the solution in excess, if the termination criteria is modified to be less restrictive. For example, iteration 2 has found a solution of 3086€ which has not been improved during

the next iterations. This solution is just 1€ worst than the lower bound found.

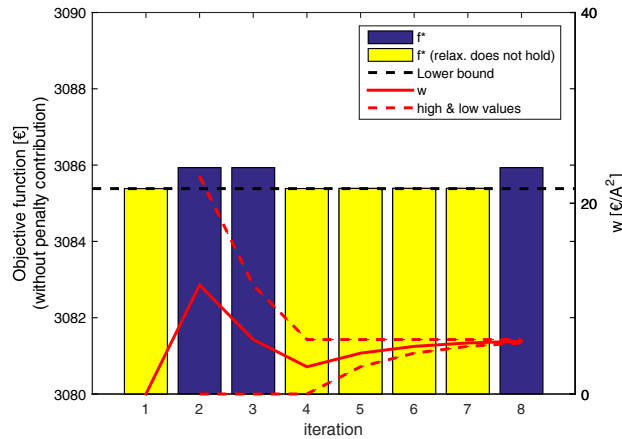


Figure 7.4: Convergence process of the proposed algorithm

Once the convergence process has been shown, the performance of the algorithm is further analysed in Figure 7.5. The top plot in Figure 7.5 shows a sensibility analysis of the relaxation gap, ϵ_r , in front of the weight w in blue markers and the w values at each iteration in black circles. The relaxation gap has been defined as (7.48). This gap measures how far is the relaxed solution from the non-relaxed equality constraint (7.15), i.e. the OFFP-w holds only if $\epsilon_r = 0$, otherwise, the optimal solution of the relaxed problem has no physical meaning. The bottom plot shows a sensibility analysis of the objective function in front of w . The objective function of the original OFFP is shown in blue, and the added penalty in the modified OFFP-w is shown in red.

$$\epsilon_r = \sum_{s \in S} \sum_{n \in N} \sum_{m \in d(n)} [i_{nms} v_{ns} - (P_{nms}^2 + Q_{nms}^2)] \quad (7.48)$$

The top plot in Figure 7.5 shows how for w greater than 5.5, the OFFP-w holds, i.e. $\epsilon_r = 0$. As the relaxation has not hold (iteration 1), an initial large w is calculated (iteration 2), and then, the proposed algorithm searches for the minimum w that makes the relaxation holds. According to the bottom plot, which shows that the real objective function increases with w , the algorithm has found the best possible solution.

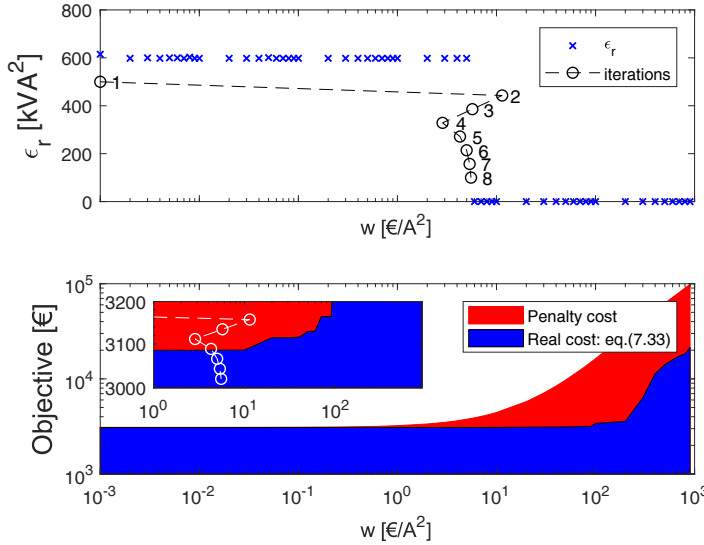


Figure 7.5: Algorithm evolution. Analysis of the relaxation gap and the objective function

7.4.2 Feeder flow control performance

This section presents the benefits of the presented OFFP formulation considering uncertainty (stochastic formulation). For this purpose, the load and PV forecast errors (standard deviation) are set to realistic values. For PV forecast it can be expected a root mean square error between 10% to 15% [175, 176]. A PV forecast error of 15% is assumed in this thesis. On the other hand, the load forecast errors can be assumed to be between 5% to 12% in microgrid buildings [177]. A 10% of load forecast errors is considered in this thesis.

After optimizing again the case study, Table 7.4 depicts the output set-points of the optimal feeder flow problem results considering 1 scenario and 10 scenarios respectively. The first case does not consider uncertainty as it only uses the predicted values. The second case considers uncertainty by generating randomly a total of 10 possible scenarios. It can be observed that for both cases all UPC generators are ON. On the other hand, only the first FFC generator is ON. These results are reasonable due to the high fixed costs of FFC generators. In the case of generator 2, its connection is explained because despite its high costs, it avoids penalties due to the feeder flow setpoint deviations. The main difference between both cases is

that considering 1 scenario, the UPC generators work at their rated power (these generators have lower costs), while when stochastic optimization is considered, this power is lower, i.e. generator 21 is not at its maximum. As a result, generation at generator 2 is higher (due to its FFC mode). This solution is better because of the minimum power generation of generator 2. If the load consumption is lower or PV production is higher than the predicted one, generator 2 will need to reduce its generation, being possible to reach its minimum value and hence violating the feeder flow setpoints. To illustrate this, a total of 25 scenarios (independent from the ones generated at the optimization process) are simulated using the setpoints of Table 7.4. Figure 7.6 shows the power generation of generator 2 and the active power feeder flow (from node 1 to node 2). As it can be observed, when the uncertainty is not considered, a total of 6 scenarios do not comply with the setpoint because P_2^{Gmin} is reached, leading to a penalty. In contrast, when 10 scenarios are used for optimizing, only 4 scenarios do not comply, and for these scenarios, power deviations are lower. This leads to lower penalty costs. On average, the cost for the 10 scenario optimization is improved by around 3.5%. This value could be greater with increased feeder flow penalty costs.

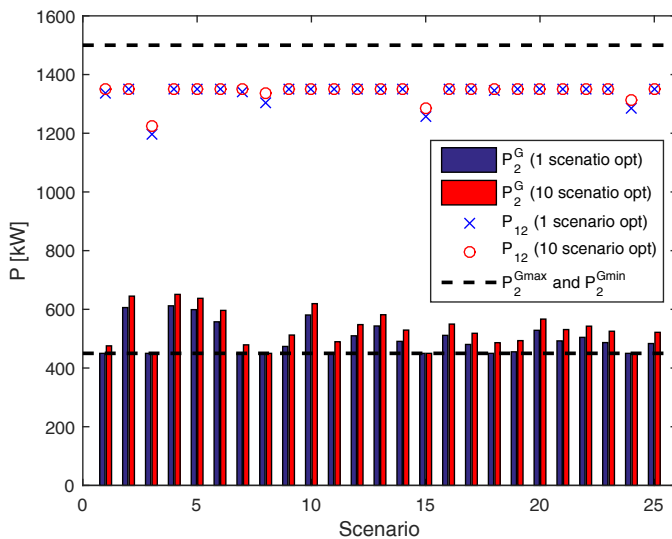


Figure 7.6: Active power generation (generator 2) and active power feeder flow for 25 random scenarios. $(FFP_n^*|_{n=1}, FFQ_n^*|_{n=1}) = (1350 \text{ kW}, 900 \text{ kvar})$

Table 7.4: Optimal setpoints.
(1350 kW, 900 kvar)

Number of scenarios = 1 Computation time = 1.7 s							
Gen	Type	Status	$P_n^{G^*}$ [kW]	$Q_n^{G^*}$ [kvar]	FFP_n^* [kW]	FFQ_n^* [kvar]	
2	FFC	ON	-	-	1350	900	
6	FFC	OFF	-	-	-	-	
8	PV	ON	-	40	-	-	
11	UPC	ON	200	100	-	-	
12	PV	ON	-	15	-	-	
14	PV	ON	-	45	-	-	
17	UPC	ON	250	125	-	-	
21	UPC	ON	400	115.6	-	-	
24	PV	ON	-	100	-	-	
25	UPC	ON	200	100	-	-	
26	FFC	OFF	-	-	-	-	
29	UPC	ON	300	150	-	-	
30	PV	ON	-	75	-	-	
32	PV	ON	-	75	-	-	

Number of scenarios = 10 Computation time = 35.9 s							
Gen	Type	Status	$P_n^{G^*}$ [kW]	$Q_n^{G^*}$ [kvar]	FFP_n^* [kW]	FFQ_n^* [kvar]	
2	FFC	ON	-	-	1350	900	
6	FFC	OFF	-	-	-	-	
8	PV	ON	-	9.4	-	-	
11	UPC	ON	200	100	-	-	
12	PV	ON	-	15	-	-	
14	PV	ON	-	45	-	-	
17	UPC	ON	250	125	-	-	
21	UPC	ON	366.4	119.5	-	-	
24	PV	ON	-	100	-	-	
25	UPC	ON	200	100	-	-	
26	FFC	OFF	-	-	-	-	
29	UPC	ON	300	150	-	-	
30	PV	ON	-	0	-	-	
32	PV	ON	-	75	-	-	

A second scenario supposes a larger power consumption. The load forecasts for the lines 6-18 and 26-33 are now increased 1.5 times and higher feeder flow setpoints are considered. In addition, the voltage at the slack node is 0.98 p.u. This leads to a challenging situation where the voltage could exceed the limits due to the larger voltage drops, specially downstream node 6. Again, Table 7.5 shows the optimal outputs. Comparing with the previous case, when uncertainty is not considered, generator 25 is switched off, while the FFC generator 26 is turned on. In addition, the feeder flow setpoint at generator 26 is small enough to ensure it operates at its maximum power. This permits to diminish the voltage drop from node 1 to node 26 improving the voltage profile. Nevertheless, deviations from the forecast can produce voltage violations as shown in Figure 7.7 in blue lines, which represents the corresponding simulation for 25 random scenarios. On the other hand, when considering uncertainty, these voltage violations are mitigated thanks to the connection of the FFC generator 6, as shown in red in Figure 7.7. In this case, the average cost for the 10 scenario optimization is improved by 1%.

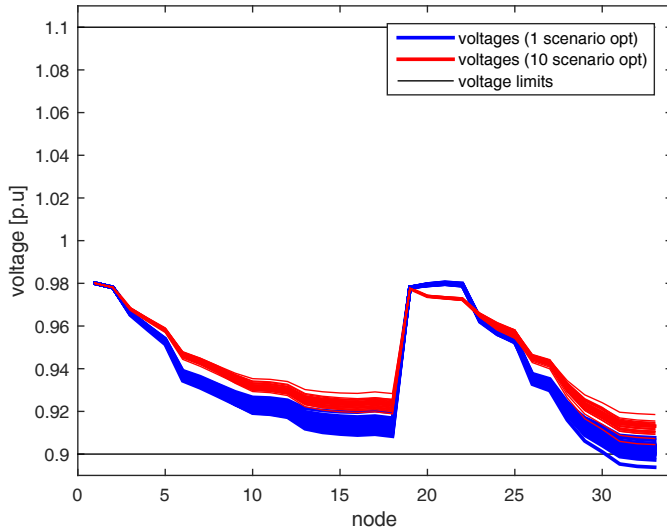


Figure 7.7: Voltages for 25 random scenarios

Table 7.5: Optimal setpoints. $(FFP_n^*|_{n=1}, FFQ_n^*|_{n=1}) = (2500 \text{ kW}, 1500 \text{ kvar})$

Number of scenarios = 1							
Computation time = 1.6 s							
Gen	Type	Status	$P_n^{G^*}$ [kW]	$Q_n^{G^*}$ [kvar]	FFP_n^* [kW]	FFQ_n^* [kvar]	
2	FFC	ON	-	-	2500	1500	
6	FFC	OFF	-	-	-	-	
8	PV	ON	-	40	-	-	
11	UPC	ON	200	100	-	-	
12	PV	ON	-	15	-	-	
14	PV	ON	-	45	-	-	
17	UPC	ON	250	125	-	-	
21	UPC	ON	400	116.2	-	-	
24	PV	ON	-	100	-	-	
25	UPC	OFF	-	-	-	-	
26	FFC	ON	-	-	669.2	801.2	
29	UPC	ON	300	150	-	-	
30	PV	ON	-	75	-	-	
32	PV	ON	-	75	-	-	

Number of scenarios = 10							
Computation time = 40.2 s							
Gen	Type	Status	$P_n^{G^*}$ [kW]	$Q_n^{G^*}$ [kvar]	FFP_n^* [kW]	FFQ_n^* [kvar]	
2	FFC	ON	-	-	2500	1500	
6	FFC	ON	-	-	1384.1	745.4	
8	PV	ON	-	40	-	-	
11	UPC	ON	200	100	-	-	
12	PV	ON	-	15	-	-	
14	PV	ON	-	45	-	-	
17	UPC	ON	250	125	-	-	
21	UPC	OFF	-	-	-	-	
24	PV	ON	-	100	-	-	
25	UPC	OFF	-	-	-	-	
26	FFC	ON	-	-	618.7	662.9	
29	UPC	ON	300	150	-	-	
30	PV	ON	-	75	-	-	
32	PV	ON	-	75	-	-	

7.5 Conclusion

This study has presented a novel optimal power flow problem formulation for feeder flow controlled microgrids based on the second order cone relaxation of the DistFlow equations, which has been named OFFP-w.

Additionally, and in contrast to other studies which try to determine the objective function requirements to ensure the solution of the relaxed problem is also the solution of the non-relaxed problem, this chapter presents a novel algorithm for solving the relaxed problem to ensure finding a meaningful solution without imposing conditions into the objective function.

In the particular case of feeder flow controlled microgrids, uncertainty may not only lead to a voltage or current limits violation, but also can produce the loss of the optimal operation point. The presented stochastic formulation permits finding a better solution improving the average objective function while maintaining the system voltages and currents within their limits. The better performance of the objective function mainly comes from the feeder flow setpoints penalties. The presented improvement can be even greater if the cost of violating the feeder flow constraints increases.

Chapter 8

Conclusions

In this thesis, different methods for the control of the power flow through the main feeders in LS-PVPPs as well as in microgrids are studied. This chapter describes the main findings and contributions of this thesis and includes insights for future works.

8.1 Contributions

The main findings are detailed per chapter.

- In Chapter 3 a central power plant controller for coordinating all the PV inverters, capacitor banks and FACTS devices within a LS-PVPP is proposed, where the aim of the controller is to fulfil the new grid code requirements. The active power requirements are met thanks to a central PI controller and a ramp rate limiter. But as energy storage is not included, those grid support functions which depend on the power reserves cannot be guaranteed. This issue is addressed in the next chapter. On the other hand, a new reactive power dispatch method is designed to control the reactive power injection through the LS-PVPP feeder. It has been observed that the operation of capacitor banks can compromise the stability when the voltage droop support function is required. To solve this, an hysteresis method for deciding the connection of capacitor banks combined with a low pass filter in the voltage measurement is proposed. The advantages of the proposed method are shown through simulations, where the reactive power oscillations and multiple capacitor banks connections and disconnections are avoided. The PPC controller has been implemented in several LS-PVPPs around the world, passing all the grid code tests and being, now, operative.
- In Chapter 4 the central controller has been enhanced so that it complies with the strictest grid code requirements. For this purpose, the

installation of a centralised energy storage system is proposed. The controller coordinates the PV power generation with the power delivered or stored by the energy storage device. For limiting the fast PV power variations, a direct ramp rate control is proposed. It has been found that, due to the delay between the time the setpoint is sent and the time the desired value is reached, this technique can produce a power ripple during ramp rate events. This effect is eliminated with the proposed filter. On the other hand, the controller also manages the SOC of the storage device. If the reference SOC setpoint is computed so that it is proportional to the PV power generated, the desired operation range is kept within the established limits during more time, which is beneficial for reducing the ageing of the battery.

- Until now, multi-microgrid systems have been studied in terms of control, operation and management. The influence of the interconnection architectures is studied in Chapter 6, where they have been defined and compared. The architectures are classified according to the layout, the line technology and the interconnection technology. Due to the low development of multi-microgrids, the comparison has been performed qualitatively. This comparison considers the main parameters that define the system performance: cost, scalability, protection, reliability, stability, communications and business models. It has been identified that for electrified areas, the most promising architectures, are the PCM and the MSPC layouts with AC line technology, while the use of power transformers or power converters as interconnection interface device will depend on the particular requirements of each area. On the other hand, for non-electrified areas, the PCM and MSPC layouts are also the recommended architectures. But in this case, both, the AC and the DC line technologies are recommended depending on the specific requirements of the area. The same happens with the interconnection technology: both possible solutions (power transformers and power converters) are interesting for the future multi-microgrid systems.
- The feeder flow control in microgrids can be an interesting solution for planning the operation of the future multi-microgrid systems. In this direction, in Chapter 6 a novel optimal power flow problem formulation for the feeder flow controlled microgrids is proposed. To improve the microgrid operation and to obtain the optimal operating point, the load and PV power uncertainty is considered by generating a set

of scenarios that are optimized simultaneously. On the other hand, to solve the non linearities of the power flow equations and to be able to find a global optimum, these constraints have been relaxed, leading to a MISOCP formulation. In addition, for ensuring that the optimum solution found for the relaxed optimization problem is also a solution of the original non-relaxed problem, the objective function has been reformulated and an iterative algorithm has been proposed. The results have shown that the proposed formulation combined with the proposed algorithm converges and is capable of finding the optimal setpoints.

8.2 Future work

The integration of LS-PVPPs into the electric power system has to deal with a set of challenges derived from the grid codes. For this purpose, the use and coordination of support equipment as capacitor banks, FACTS and storage devices has been considered in this thesis. Nevertheless, the control performance studies could be extended in the following direction:

- In this thesis, the active and reactive power setpoints obtained from the centralized PI controller (α and β) are dispatched equal for all PV inverters. This dispatch could be improved by developing an optimization method so that the power losses are minimized.
- The tuning of the centralized PI controllers of the PPC has been performed by an empirical method. Further work could develop a specific method for obtaining the controllers parameters.
- Currently, PV forecast systems estimate the future generation in a time frame from 5 to 15 minutes or even in an hourly time frame. This is not practical for limiting the PV power fluctuations in a time frame of seconds. Developing forecast systems with more resolution could be useful for limiting the ramp rates while reducing the storage requirements.

Regarding the multi-microgrid systems, the following studies can be continued:

- This thesis has performed a qualitative analysis of the different multi-microgrid architectures. This study could be extended by performing a numerical analysis of the most promising architectures.

Chapter 8 Conclusions

- The formulated MISOCP for FFC microgrids could be extended by including load flexibility, transformer tap changers, energy storage systems and daily forecast. In this case, a multi-period optimization should be performed.
- The FFC is presented in the literature as an interesting control method for planning the operation of multi-microgrid systems. In this direction, the study of multi-microgrid systems including feeder flow controlled microgrids could be studied.

Bibliography

- [1] E. Commission, *Communication from the commission to the European Council and the European Parliament - An energy policy for Europe*. Commission of the European Communities, 2007. 1
- [2] ——, *Communication from the commission to the European Parliament, the Council, the European Economic and Social Committee and the Committee of the Regions - A policy framework for climate and energy in the period from 2020 to 2030*. Commission of the European Communities, 2014. 1
- [3] M. Aragüés Peñalba, “Operation and control of transmission systems for offshore wind power plants,” Doctoral Thesis, Universitat Politècnica de Catalunya, April 2016. 1
- [4] Solar Power Europe, “Global market outlook for solar power 2017-2021,” 2017. 1, 9, 10
- [5] N. Hatzigergiou, H. Asano, R. Iravani, and C. Marnay, “Microgrids,” *IEEE Power and Energy Magazine*, vol. 5, no. 4, pp. 78–94, July 2007. 2, 69
- [6] J. M. Guerrero, J. C. Vasquez, J. Matas, L. G. de Vicuna, and M. Castilla, “Hierarchical control of droop-controlled AC and DC microgrids - a general approach toward standardization,” *IEEE Transactions on Industrial Electronics*, vol. 58, no. 1, pp. 158–172, Jan 2011. 2, 69
- [7] D. Pattabiraman, R. H. Lasseter, and T. M. Jahns, “Feeder flow control method with improved power sharing performance in microgrids,” in *2017 IEEE Power Energy Society General Meeting*, July 2017, pp. 1–5. 2
- [8] D. E. Olivares, A. Mehrizi-Sani, A. H. Etemadi, C. A. Cañizares, R. Iravani, M. Kazerani, A. H. Hajimiragh, O. Gomis-Bellmunt, M. Saeedifard, R. Palma-Behnke, G. A. Jiménez-Estevez, and N. D.

Bibliography

- Hatziaargyriou, “Trends in microgrid control,” *IEEE Transactions on Smart Grid*, vol. 5, no. 4, pp. 1905–1919, July 2014. 2, 69, 70, 76, 104, 105, 107
- [9] United Nations, “Kyoto protocol to the united nations framework convention on climate change,” 1998. 9
- [10] International Energy Agency, “CO₂ emissions from fuel combustion - Highlights,” 2017. 9
- [11] Wind Europe, “Wind in power 2017. Annual combined onshore and offshore wind energy statistics,” 2018. 9, 10
- [12] F. Katiraei and J. R. Aguero, “Solar PV integration challenges,” *IEEE Power and Energy Magazine*, vol. 9, no. 3, pp. 62–71, May 2011. 11
- [13] T. Ackermann, G. Andersson, and L. Söder, “Distributed generation: a definition,” *Electric Power Systems Research*, vol. 57, no. 3, pp. 195 – 204, 2001. [Online]. Available: <http://www.sciencedirect.com/science/article/pii/S0378779601001018> 11
- [14] K. Komoto, K. Kurokawa, T. Nishimura, K. Kato, K. Otani, M. Ito, M. Ermer, C. Beneking, G. Kalenbach, K. Weltzien, D. Otto, C. Schneider, T. Nowicki, A. Beneking, P. V. D. Vleuten, L. A. Verhoef, B. Bessais, M. Arraras, C. Itoiz, M. Olite, J. P. Ganiguer, D. Faiman, D. Raviv, R. Rosenstreich, N. Enebish, J. Song, S. Wang, S. Ma, D. Singh, J. S. MacDonald, T. Hansen, H. Hayden, F. Paletta, and A. Sarno, “IEA PVPS task 8: Project proposals on very large scale photovoltaic power generation (VLS-PV) systems in deserts,” in *2006 IEEE 4th World Conference on Photovoltaic Energy Conference*, vol. 2, May 2006, pp. 2359–2362. 11
- [15] M. Mendelsohn, T. Lowder, B. Canavan, and N. R. E. L. (U.S.), *Utility-scale Concentrating Solar Power and Photovoltaics Projects: A Technology and Market Overview*, ser. NREL/TP. National Renewable Energy Laboratory, 2012. 11
- [16] M. Tripathy, P. Sadhu, and S. Panda, “A critical review on building integrated photovoltaic products and their applications,” *Renewable and Sustainable Energy Reviews*, vol. 61, pp. 451 – 465, 2016. [Online]. Available: <http://www.sciencedirect.com/science/article/pii/S1364032116300259> 12

- [17] T. Markvart, L. Castaner, L. Castañer, and A. McEvoy, *Practical Handbook of Photovoltaics: Fundamentals and Applications*, ser. Electronics & Electrical. Elsevier, 2003. 12
- [18] A. Cabrera-Tobar, E. Bullich-Massagué, M. Aragüés-Peñaiba, and O. Gomis-Bellmunt, “Topologies for large scale photovoltaic power plants,” *Renewable and Sustainable Energy Reviews*, vol. 59, pp. 309 – 319, 2016. [Online]. Available: <http://www.sciencedirect.com/science/article/pii/S1364032116000289> 12, 13, 16
- [19] H.-L. Tsai, C.-S. Tu, and Y.-J. Su, “Development of generalized photovoltaic model using MATLAB SIMULINK,” in *Proceedings of the World Congress on Engineering and Computer Science*, Oct 2008. 12
- [20] M. Meinhardt, G. Cramer, B. Burger, and P. Zacharias, “Multi-string-converter with reduced specific costs and enhanced functionality,” *Solar Energy*, vol. 69, pp. 217 – 227, 2001, EUROSUN 2000 Selected Proceedings. [Online]. Available: <http://www.sciencedirect.com/science/article/pii/S0038092X01000676> 13
- [21] M. Díez-Mediavilla, M. Dieste-Velasco, M. Rodríguez-Amigo, T. García-Calderón, and C. Alonso-Tristán, “Performance of grid tied pv facilities based on real data in spain. central inverter versus string system,” *Energy Conversion and Management*, vol. 86, pp. 1128 – 1133, 2014. 13
- [22] M. D. Prada-Gil, J. L. Domínguez-García, L. Trilla, and O. Gomis-Bellmunt, “Technical and economic comparison of various electrical collection grid configurations for large photovoltaic power plants,” *IET Renewable Power Generation*, vol. 11, no. 3, pp. 226–236, 2017. 13
- [23] A. Egea-Alvarez, A. Junyent-Ferré, and O. Gomis-Bellmunt, *Active and Reactive Power Control of Grid Connected Distributed Generation Systems*. Berlin, Heidelberg: Springer Berlin Heidelberg, 2012, pp. 47–81. [Online]. Available: https://doi.org/10.1007/978-3-642-22904-6_3 14
- [24] A. Samadi, M. Ghandhari, and L. Söder, “Reactive power dynamic assessment of a pv system in a distribution grid,” *Energy Procedia*, vol. 20, pp. 98 – 107, 2012, technoport 2012 - Sharing Possibilities and 2nd Renewable Energy Research Conference (RERC2012). [Online]. Available: <http://www.sciencedirect.com/science/article/pii/S1876610212007424> 14

Bibliography

- [25] B. S. Kumar and K. Sudhakar, "Performance evaluation of 10 MW grid connected solar photovoltaic power plant in India," *Energy Reports*, vol. 1, pp. 184 – 192, 2015. [Online]. Available: <http://www.sciencedirect.com/science/article/pii/S2352484715000311> 15
- [26] E. Bullich-Massagué, R. Ferrer-San-José, M. Aragüés-Peñalba, L. Serrano-Salamanca, C. Pacheco-Navas, and O. Gomis-Bellmunt, "Power plant control in large-scale photovoltaic plants: design, implementation and validation in a 9.4 MW photovoltaic plant," *IET Renewable Power Generation*, vol. 10, no. 1, pp. 50–62, 2016. 15, 18, 41
- [27] C. Verdugo, J. I. Candela, A. Luna, and P. Rodriguez, "Power station for large scale photovoltaic power plants," in *2017 IEEE 6th International Conference on Renewable Energy Research and Applications (ICRERA)*, Nov 2017, pp. 768–773. 15
- [28] O. Gomis-Bellmunt, J. Liang, J. Ekanayake, R. King, and N. Jenkins, "Topologies of multiterminal HVDC-VSC transmission for large offshore wind farms," *Electric Power Systems Research*, vol. 81, no. 2, pp. 271 – 281, 2011. [Online]. Available: <http://www.sciencedirect.com/science/article/pii/S0378779610002166> 16, 91
- [29] Danfoss, "String inverters for pv power plants," Technical Report. 2009. 18
- [30] S. Shivashankar, S. Mekhilef, H. Mokhlis, and M. Karimi, "Mitigating methods of power fluctuation of photovoltaic (PV) sources - a review," *Renewable and Sustainable Energy Reviews*, vol. 59, pp. 1170 – 1184, 2016. [Online]. Available: <http://www.sciencedirect.com/science/article/pii/S1364032116000897> 19
- [31] R. van Haaren, M. Morjaria, and V. Fthenakis, "An energy storage algorithm for ramp rate control of utility scale PV (photovoltaics) plants," *Energy*, vol. 91, pp. 894 – 902, 2015. 19, 45, 46, 51, 58
- [32] M. J. E. Alam, K. M. Muttaqi, and D. Sutanto, "A novel approach for ramp-rate control of solar PV using energy storage to mitigate output fluctuations caused by cloud passing," *IEEE Transactions on Energy Conversion*, vol. 29, no. 2, pp. 507–518, June 2014. 19, 25, 45, 46

- [33] V. Salehi and B. Radibratovic, "Ramp rate control of photovoltaic power plant output using energy storage devices," in *PES General Meeting — Conference Exposition, 2014 IEEE*, July 2014, pp. 1–5. 19, 45, 46
- [34] K. Prompinit and S. Khomfoi, "Ramp rate consideration of a BESS using active power control for PV generation," in *Electrical Machines and Systems (ICEMS), 2015 18th International Conference on*, Oct 2015, pp. 1676–1680. 19, 45, 46, 48
- [35] S. Abdollahy, A. Mammoli, F. Cheng, A. Ellis, and J. Johnson, "Distributed compensation of a large intermittent energy resource in a distribution feeder," in *Innovative Smart Grid Technologies (ISGT), 2013 IEEE PES*, Feb 2013, pp. 1–6. 19, 45, 46
- [36] C. S. Lai, Y. Jia, L. L. Lai, Z. Xu, M. D. McCulloch, and K. P. Wong, "A comprehensive review on large-scale photovoltaic system with applications of electrical energy storage," *Renewable and Sustainable Energy Reviews*, vol. 78, pp. 439 – 451, 2017. [Online]. Available: <http://www.sciencedirect.com/science/article/pii/S1364032117305622> 19
- [37] M. Obi and R. Bass, "Trends and challenges of grid-connected photovoltaic systems - a review," *Renewable and Sustainable Energy Reviews*, vol. 58, pp. 1082 – 1094, 2016. [Online]. Available: <http://www.sciencedirect.com/science/article/pii/S136403211501672X> 19
- [38] H. Berndt, M. Hermann, H. D. Kreye, R. Reinisch, U. Scherer, and J. Vanzetta, *Transmission code 2007 - Network and system rules of the German transmission system operators*. Verband der Netzbetreiber - VDN - e.V. beim VDEW, 2007. 19
- [39] *Technical transmission grid code of the Romanian power system*. Romanian Power Grid Company TRANSELECTRICA S.A., 2004. 19, 26
- [40] *Grid connection code for renewable power plants (RPPs) connected to the electricity transmission system (TS) or the distribution system (DS) in South Africa*, 2012. 19, 20, 26, 29
- [41] Z. Li, H. Han, C. Niu, and Z. Chen, "Comparative assessment of standards for grid-connected PV system in China, the U.S. and European countries," in *2nd IET Renewable Power Generation Conference (RPG 2013)*, Sept 2013, pp. 1–4. 19

Bibliography

- [42] A. Cabrera-Tobar, E. Bullich-Massagué, M. Aragüés-Peñaiba, and O. Gomis-Bellmunt, “Review of advanced grid requirements for the integration of large scale photovoltaic power plants in the transmission system,” *Renewable and Sustainable Energy Reviews*, vol. 62, pp. 971 – 987, 2016. [Online]. Available: <http://www.sciencedirect.com/science/article/pii/S136403211630154X> 19, 21, 22, 23
- [43] *Minimum technical requirements for interconnection of photovoltaic (PV) facilities*. Puerto Rico Electric Power Authority. PREPA, 2012. 19, 26
- [44] A. Cabrera-Tobar, E. Bullich-Massagué, M. Aragüés-Peñaiba, and O. Gomis-Bellmunt, “Capability curve analysis of photovoltaic generation systems,” *Solar Energy*, vol. 140, pp. 255 – 264, 2016. [Online]. Available: <http://www.sciencedirect.com/science/article/pii/S0038092X16305291> 21
- [45] V. Gevorgian and S. Booth, *Review of PREPA Technical Requirements for Interconnecting Wind and Solar Generation*, ser. NREL/TP, 2013. 24
- [46] C. Koch-Ciobotaru, A. S. de Ibarra, E. Martinez-Laserna, D. I. Stroe, M. Swierczynski, and P. Rodriguez, “Second life battery energy storage system for enhancing renewable energy grid integration,” in *2015 IEEE Energy Conversion Congress and Exposition (ECCE)*, Sept 2015, pp. 78–84. 24, 57
- [47] “Minimum technical requirements compliance procedure proposal: APER’s proposed compliance procedure for frequency and ramp-rate,” *APER’s Technical Compliance Committee, 2014*, 2013. 24
- [48] S. Teleke, M. Baran, S. Bhattacharya, and A. Huang, “Rule-based control of battery energy storage for dispatching intermittent renewable sources,” *IEEE Transactions on Sustainable Energy*, vol. 1, no. 3, pp. 117–124, Oct 2010. 25
- [49] H. Gaztanaga, J. Landaluze, I. Etxeberria-Otadui, A. Padros, I. Berazaluce, and D. Cuesta, “Enhanced experimental PV plant grid-integration with a mw lithium-ion energy storage system,” in *2013 IEEE Energy Conversion Congress and Exposition (ECCE)*, Sept 2013, pp. 1324–1329. 25

- [50] R. van Haaren, M. Morjaria, and V. Fthenakis, “Utility scale PV plant variability and energy storage for ramp rate control,” in *2013 IEEE 39th Photovoltaic Specialists Conference (PVSC)*, June 2013, pp. 0973–0979. 25
- [51] G. Wang, M. Ciobotaru, and V. Agelidis, “Power smoothing of large solar PV plant using hybrid energy storage,” *IEEE Transactions on Sustainable Energy*, vol. 5, no. 3, pp. 834–842, July 2014. 25
- [52] W. Xiao, K. Torchyan, M. El Moursi, and J. Kirtley, “Online supervisory voltage control for grid interface of utility-level PV plants,” *IEEE Transactions on Sustainable Energy*, vol. 5, no. 3, pp. 843–853, July 2014. 25
- [53] E. Bullich-Massagué, M. Aragüés-Peñaiba, R. Ferrer-San-José, L. Serrano-Salamanca, C. Pacheco-Navas, and O. Gomis-Bellmunt, “Power plant control experience in large scale PV plant. Modelling, control, simulation and implementation,” in *4th International Workshop on Integration of Solar into Power Systems, Berlin*, November 2014. 25, 26
- [54] J. Martínez, P. Rodriguez, P. C. Kjær, and R. Teodorescu, “Design and coordination of a capacitor and on-load tap changer system for voltage control in a wind power plant of doubly fed induction generator wind-turbines,” *Wind Energy*, vol. 15, no. 4, pp. 507–523, 2012. [Online]. Available: <http://dx.doi.org/10.1002/we.474> 25
- [55] J. Jung, A. Onen, R. Arghandeh, and R. P. Broadwater, “Coordinated control of automated devices and photovoltaic generators for voltage rise mitigation in power distribution circuits,” *Renewable Energy*, vol. 66, no. 0, pp. 532 – 540, 2014. [Online]. Available: <http://www.sciencedirect.com/science/article/pii/S096014811400010X> 25, 26
- [56] R. Varma, S. Rahman, and T. Vanderheide, “New control of PV solar farm as STATCOM (PV-STATCOM) for increasing grid power transmission limits during night and day,” *IEEE Transactions on Power Delivery*, vol. PP, no. 99, pp. 1–1, 2014. 25
- [57] L. Yaoyuan, Z. Chengbi, M. Hong, and F. Wenwen, “Research on a new method to achieve low voltage ride through of PV,” in *2014 International Conference on Power System Technology (POWERCON)*, Oct 2014, pp. 1064–1070. 25

Bibliography

- [58] M. Datta, T. Senju, A. Yona, T. Funabashi, and C.-H. Kim, “A co-ordinated control method for leveling PV output power fluctuations of PV-diesel hybrid systems connected to isolated power utility,” *Energy Conversion, IEEE Transactions on*, vol. 24, no. 1, pp. 153–162, March 2009. 29
- [59] “EHS annual monitoring report. 2012.” 34
- [60] <http://en.grupotsk.com/proyectos/vanju-mare> [accessed in january 2015]. 34
- [61] <http://www.schrack-seconet.com> [accessed in january 2015]. 35
- [62] J. Marcos, L. Marroyo, E. Lorenzo, D. Alvira, , and E. Izco, “From irradiance to output power fluctuations: the PV plant as a low pass filter,” *Progress in Photovoltaics: Research and Applications*, vol. 19, no. 1, pp. 505–510, 2011. 46, 57
- [63] J. Marcos, I. n. de la Parra, M. García, and L. Marroyo, “Control strategies to smooth short-term power fluctuations in large photovoltaic plants using battery storage systems,” *Energies*, vol. 7, no. 10, p. 6593, 2014. [Online]. Available: <http://www.mdpi.com/1996-1073/7/10/6593> 47
- [64] I. de la Parra, J. Marcos, M. García, and L. Marroyo, “Control strategies to use the minimum energy storage requirement for PV power ramp-rate control,” *Solar Energy*, vol. 111, pp. 332 – 343, 2015. 50
- [65] M. Sengupta and A. Andreas, “(2010) Oahu solar measurement grid (1-year archive), nrel report no. da-5500-56506.” [Online]. Available: <http://dx.doi.org/10.5439/1052451> 57
- [66] C. Schwaegerl and L. Tao, *The Microgrids Concept*. John Wiley and sons, 2013. 69
- [67] S. Parhizi, H. Lotfi, A. Khodaei, and S. Bahramirad, “State of the art in research on microgrids: A review,” *IEEE Access*, vol. 3, pp. 890–925, 2015. 69
- [68] E. Hossain, E. Kabalci, R. Bayindir, and R. Perez, “A comprehensive study on microgrid technology,” *International Journal of Renewable Energy Research*, vol. 4, no. 4, pp. 1094–1107, 2014. 69, 70

- [69] A. Banerji, D. Sen, A. K. Bera, D. Ray, D. Paul, A. Bhakat, and S. K. Biswas, "Microgrid: A review," in *Global Humanitarian Technology Conference: South Asia Satellite (GHTC-SAS), 2013 IEEE*, Aug 2013, pp. 27–35. 69, 70
- [70] J. M. Guerrero, M. Chandorkar, T. L. Lee, and P. C. Loh, "Advanced control architectures for intelligent microgrids - part i: Decentralized and hierarchical control," *IEEE Transactions on Industrial Electronics*, vol. 60, no. 4, pp. 1254–1262, April 2013. 69, 70
- [71] J. M. Guerrero, P. C. Loh, T. L. Lee, and M. Chandorkar, "Advanced control architectures for intelligent microgrids - part ii: Power quality, energy storage, and AC/DC microgrids," *IEEE Transactions on Industrial Electronics*, vol. 60, no. 4, pp. 1263–1270, April 2013. 69, 70
- [72] R. Jain and A. Arya, "A comprehensive review on micro grid operation, challenges and control strategies," in *Proceedings of the 2015 ACM Sixth International Conference on Future Energy Systems*, ser. e-Energy '15. New York, NY, USA: ACM, 2015, pp. 295–300. [Online]. Available: <http://doi.acm.org/10.1145/2768510.2768514> 69, 70
- [73] P. Borazjani, N. I. A. Wahab, H. B. Hizam, and A. B. C. Soh, "A review on microgrid control techniques," in *2014 IEEE Innovative Smart Grid Technologies - Asia (ISGT ASIA)*, May 2014, pp. 749–753. 69, 70
- [74] E. Unamuno and J. A. Barrena, "Hybrid ac/dc microgrids - part i: Review and classification of topologies," *Renewable and Sustainable Energy Reviews*, vol. 52, pp. 1251 – 1259, 2015. [Online]. Available: <http://www.sciencedirect.com/science/article/pii/S1364032115008412> 69, 70
- [75] ——, "Hybrid ac/dc microgrids - part ii: Review and classification of control strategies," *Renewable and Sustainable Energy Reviews*, vol. 52, pp. 1123 – 1134, 2015. [Online]. Available: <http://www.sciencedirect.com/science/article/pii/S1364032115008333> 69, 70
- [76] T. S. Ustun, C. Ozansoy, and A. Zayegh, "Recent developments in microgrids and example cases around the world - a review,"

Bibliography

- Renewable and Sustainable Energy Reviews*, vol. 15, no. 8, pp. 4030 – 4041, 2011. [Online]. Available: <http://www.sciencedirect.com/science/article/pii/S1364032111002735> 69, 70
- [77] N. Lidula and A. Rajapakse, “Microgrids research: A review of experimental microgrids and test systems,” *Renewable and Sustainable Energy Reviews*, vol. 15, no. 1, pp. 186 – 202, 2011. [Online]. Available: <http://www.sciencedirect.com/science/article/pii/S136403211000328X> 69, 70
- [78] H. Jiayi, J. Chuanwen, and X. Rong, “A review on distributed energy resources and microgrid,” *Renewable and Sustainable Energy Reviews*, vol. 12, no. 9, pp. 2472 – 2483, 2008. [Online]. Available: <http://www.sciencedirect.com/science/article/pii/S1364032107001025> 69, 70
- [79] T. Dragićević, X. Lu, J. C. Vasquez, and J. M. Guerrero, “DC microgrids - part i: A review of control strategies and stabilization techniques,” *IEEE Transactions on Power Electronics*, vol. 31, no. 7, pp. 4876–4891, July 2016. 69, 70, 76, 104
- [80] ——, “DC microgrids - part ii: A review of power architectures, applications, and standardization issues,” *IEEE Transactions on Power Electronics*, vol. 31, no. 5, pp. 3528–3549, May 2016. 69, 70
- [81] M. S. Mahmoud, M. S. U. Rahman, and F. M. A. L. Sunni, “Review of microgrid architectures - a system of systems perspective,” *IET Renewable Power Generation*, vol. 9, no. 8, pp. 1064–1078, 2015. 69, 70
- [82] T. Strasser, F. Andrén, J. Kathan, C. Cecati, C. Buccella, P. Siano, P. Leitão, G. Zhabelova, V. Vyatkin, P. Vrba, and V. Mařík, “A review of architectures and concepts for intelligence in future electric energy systems,” *IEEE Transactions on Industrial Electronics*, vol. 62, no. 4, pp. 2424–2438, April 2015. 69, 70
- [83] I. Patrao, E. Figueres, G. Garcerá, and R. González-Medina, “Microgrid architectures for low voltage distributed generation,” *Renewable and Sustainable Energy Reviews*, vol. 43, pp. 415 – 424, 2015. [Online]. Available: <http://www.sciencedirect.com/science/article/pii/S1364032114009939> 69, 70

- [84] D. of Energy Office of Electricity Delivery and E. Reliability, “Summary report: 2012 DOE microgrid workshop,” 2012. [online] <http://energy.gov/sites/prod/files/2012%20Microgrid%20Workshop%20Report%2009102012.pdf>. Accessed May. 18, 2016. 70
- [85] A. G. Madureira, “Coordinated and optimized voltage management of distribution networks with multi-microgrids,” Doctoral Thesis, Universidade do Porto, April 2010. 72
- [86] S. Chowdhury, *Microgrids and Active Distribution Networks*, ser. Energy Engineering. Institution of Engineering and Technology, 2009. [Online]. Available: <http://digital-library.theiet.org/content/books/po/pbrn006e> 72
- [87] P. Wu, W. Huang, N. Tai, and S. Liang, “A novel design of architecture and control for multiple microgrids with hybrid AC/DC connection,” *Applied Energy*, vol. 210, pp. 1002 – 1016, 2018. [Online]. Available: <http://www.sciencedirect.com/science/article/pii/S0306261917308838> 74, 75, 79, 80, 108
- [88] A. G. Anastasiadis, A. G. Tsikalakis, and N. D. Hatziargyriou, “Operational and environmental benefits due to significant penetration of microgrids and topology sensitivity,” in *IEEE PES General Meeting*, July 2010, pp. 1–8. 75
- [89] W. Saad, Z. Han, and H. V. Poor, “Coalitional game theory for cooperative micro-grid distribution networks,” in *2011 IEEE International Conference on Communications Workshops (ICC)*, June 2011, pp. 1–5. 75
- [90] L. Che, M. Shahidehpour, A. Alabdulwahab, and Y. Al-Turki, “Hierarchical coordination of a community microgrid with AC and DC microgrids,” *IEEE Transactions on Smart Grid*, vol. 6, no. 6, pp. 3042–3051, Nov 2015. 75
- [91] L. Che, X. Zhang, M. Shahidehpour, A. Alabdulwahab, and A. Abu-sorrah, “Optimal interconnection planning of community microgrids with renewable energy sources,” *IEEE Transactions on Smart Grid*, vol. 8, no. 3, pp. 1054–1063, May 2017. 75
- [92] M. Goyal and A. Ghosh, “Microgrids interconnection to support mutually during any contingency,” *Sustainable Energy, Grids and Networks*, vol. 6, no. Supplement C, pp. 100 – 108, 2016. 75

Bibliography

- [93] L. Meng, Q. Shafiee, G. F. Trecate, H. Karimi, D. Fulwani, X. Lu, and J. M. Guerrero, "Review on control of DC microgrids and multiple microgrid clusters," *IEEE Journal of Emerging and Selected Topics in Power Electronics*, vol. 5, no. 3, pp. 928–948, Sept 2017. 75, 79
- [94] P. Kou, D. Liang, and L. Gao, "Distributed EMPC of multiple microgrids for coordinated stochastic energy management," *Applied Energy*, vol. 185, pp. 939 – 952, 2017. [Online]. Available: <http://www.sciencedirect.com/science/article/pii/S0306261916313964> 75, 79, 80
- [95] N. Nikmehr, S. Najafi-Ravadanegh, and A. Khodaei, "Probabilistic optimal scheduling of networked microgrids considering time-based demand response programs under uncertainty," *Applied Energy*, vol. 198, pp. 267 – 279, 2017. [Online]. Available: <http://www.sciencedirect.com/science/article/pii/S0306261917304774> 75, 79, 80
- [96] N. J. Gil and J. A. P. Lopes, "Hierarchical frequency control scheme for islanded multi-microgrids operation," in *Power Tech, 2007 IEEE Lausanne*, July 2007, pp. 473–478. 75, 79, 80, 81, 104
- [97] A. G. Madureira and J. A. P. Lopes, "Coordinated voltage support in distribution networks with distributed generation and microgrids," *IET Renewable Power Generation*, vol. 3, no. 4, pp. 439–454, December 2009. 75, 79, 80, 81
- [98] A. G. Madureira, J. C. Pereira, N. J. Gil, J. A. P. Lopes, G. N. Korres, and N. D. Hatziargyriou, "Advanced control and management functionalities for multi-microgrids," *European Transactions on Electrical Power*, vol. 21, no. 2, pp. 1159–1177, 2011. [Online]. Available: <http://dx.doi.org/10.1002/etep.407> 75, 79, 80, 81, 104
- [99] F. O. Resende, N. J. Gil, and J. A. P. Lopes, "Service restoration on distribution systems using multi-microgrids," *European Transactions on Electrical Power*, vol. 21, no. 2, pp. 1327–1342, 2011. [Online]. Available: <http://dx.doi.org/10.1002/etep.404> 75, 79, 80, 81
- [100] F. Shahnia and S. Bourbour, "A practical and intelligent technique for coupling multiple neighboring microgrids at the synchronization stage," *Sustainable Energy, Grids and Networks*, vol. 11, pp. 13 – 25, 2017. [Online]. Available: <http://www.sciencedirect.com/science/article/pii/S235246771630162X> 75, 79, 80

- [101] M. Goyal and A. Ghosh, "Microgrids interconnection to support mutually during any contingency," *Sustainable Energy, Grids and Networks*, vol. 6, pp. 100 – 108, 2016. [Online]. Available: <http://www.sciencedirect.com/science/article/pii/S2352467716000175> 75, 79, 80, 82
- [102] S. Bala and G. Venkataramanan, "Autonomous power electronic interfaces between microgrids," in *2009 IEEE Energy Conversion Congress and Exposition*, Sept 2009, pp. 3006–3013. 75, 79, 80, 82
- [103] M. He and M. Giesselmann, "Reliability-constrained self-organization and energy management towards a resilient microgrid cluster," in *2015 IEEE Power Energy Society Innovative Smart Grid Technologies Conference (ISGT)*, Feb 2015, pp. 1–5. 75, 79, 80
- [104] K.-L. Nguyen, D.-J. Won, S.-J. Ahn, and I.-Y. Chung, "Power sharing method for a grid connected microgrid with multiple distributed generators," *Journal of Electrical Engineering and Technology*, vol. 7, no. 4, pp. 459 – 467, 2012. 76, 117
- [105] J.-M. Rodriguez-Bernuz, E. Prieto-Araujo, F. Girbau-Llistuella, A. Sumper, R. Villafafila-Robles, and J.-A. Vidal-Clos, "Experimental validation of a single phase intelligent power router," *Sustainable Energy, Grids and Networks*, vol. 4, pp. 1 – 15, 2015. [Online]. Available: <http://www.sciencedirect.com/science/article/pii/S2352467715000405> 81, 82
- [106] I. U. Nutkani, "Power flow control of intertied ac microgrids," *IET Power Electronics*, vol. 6, pp. 1329–1338(9), August 2013. [Online]. Available: <http://digital-library.theiet.org/content/journals/10.1049/iet-pel.2012.0640> 82
- [107] D. Nilsson and A. Sannino, "Efficiency analysis of low- and medium-voltage DC distribution systems," in *Power Engineering Society General Meeting, 2004. IEEE*, June 2004, pp. 2315–2321 Vol.2. 82, 85, 86, 88
- [108] D. J. Hammerstrom, "AC versus DC distribution systems - Did we get it right?" in *Power Engineering Society General Meeting, 2007. IEEE*, June 2007, pp. 1–5. 82
- [109] D. M. Larruskain, I. Zamora, A. J. Mazón, O. Abarregui, and J. Monasterio, "Transmission and distribution networks: AC versus

Bibliography

- DC,” in *9th Spanish-Portuguese Congress on Electrical Engineering*, 2005. 82, 88
- [110] M. D. P. Gil, J. Domínguez-García, F. Díaz-González, M. Aragüés-Peñaiba, and O. Gomis-Bellmunt, “Feasibility analysis of offshore wind power plants with DC collection grid,” *Renewable Energy*, vol. 78, pp. 467 – 477, 2015. [Online]. Available: <http://www.sciencedirect.com/science/article/pii/S0960148115000609> 82, 100
- [111] T. Kaipia, P. Salonen, J. Lassila, and J. Partanen, “Possibilities of the low voltage DC distribution systems,” in *NORDAC 2006 conference, Stockholm*, Aug 2006. 85, 86
- [112] D. Chen and L. Xu, *AC and DC microgrid with distributed energy resources*. Springer, 2017, pp. 39–64. 85
- [113] P. Wang, J. Xiao, C. Jin, X. Han, and W. Qin, *Hybrid AC/DC Micro-Grids: Solution for High Efficient Future Power Systems*. Springer, 2017, pp. 23–40. 85
- [114] J. E. Huber and J. W. Kolar, “Volume/weight/cost comparison of a 1MVA 10 kV/400 V solid-state against a conventional low-frequency distribution transformer,” in *2014 IEEE Energy Conversion Congress and Exposition (ECCE)*, Sept 2014, pp. 4545–4552. 86
- [115] L. Sigrist, K. May, A. Mørch, P. Verboven, P. Vingerhoets, and L. Rouco, “On scalability and replicability of smart grid projects - a case study,” *Energies*, vol. 9, no. 3, p. 195, 2016. [Online]. Available: <http://www.mdpi.com/1996-1073/9/3/195> 87
- [116] B. Ravindranath and M. Chander, *Power system protection and switchgear*. New Age International, 1977. 90, 91
- [117] U. A. Bakshi and M. V. Bakshi, *Protection And Switchgear*. Technical Publications, 2009. 90
- [118] Y. G. Paithankar and S. Bhide, *Fundamentals of power system protection*. PHI Learning Pvt. Ltd., 2010. 90
- [119] H. Nikkhajoei and R. H. Lasseter, “Microgrid protection,” in *Power Engineering Society General Meeting, 2007. IEEE*. IEEE, 2007, pp. 1–6. 91

- [120] N. Hatziargyriou, *Microgrids: architectures and control*. Wiley Online Library, 2014. 91
- [121] S. A. Gopalan, V. Sreeram, and H. H. Iu, “A review of coordination strategies and protection schemes for microgrids,” *Renewable and Sustainable Energy Reviews*, vol. 32, pp. 222–228, 2014. 91
- [122] E. Sortomme, S. Venkata, and J. Mitra, “Microgrid protection using communication-assisted digital relays,” *IEEE Transactions on Power Delivery*, vol. 25, no. 4, pp. 2789–2796, 2010. 91
- [123] G. Buigues, A. Dyško, V. Valverde, I. Zamora, and E. Fernández, “Microgrid protection: Technical challenges and existing techniques,” in *International Conference on Renewable Energies and Power Quality (ICREPQ '13)*, 2013. 91
- [124] S. Mirsaeidi, D. M. Said, M. W. Mustafa, M. H. Habibuddin, and K. Ghaffari, “Progress and problems in micro-grid protection schemes,” *Renewable and Sustainable Energy Reviews*, vol. 37, pp. 834–839, 2014. 91
- [125] J. J. Justo, F. Mwasilu, J. Lee, and J.-W. Jung, “AC-microgrids versus DC-microgrids with distributed energy resources: A review,” *Renewable and Sustainable Energy Reviews*, vol. 24, pp. 387–405, 2013. 93, 94
- [126] E. Planas, J. Andreu, J. I. Gárate, I. M. de Alegría, and E. Ibarra, “AC and DC technology in microgrids: A review,” *Renewable and Sustainable Energy Reviews*, vol. 43, pp. 726–749, 2015. 93, 94
- [127] M. Monadi, M. A. Zamani, J. I. Candela, A. Luna, and P. Rodriguez, “Protection of AC and DC distribution systems embedding distributed energy resources: A comparative review and analysis,” *Renewable and Sustainable Energy Reviews*, vol. 51, pp. 1578–1593, 2015. 93
- [128] S. Khan, *Power system protection*. Shahriar Khan, 2013. 93
- [129] ABB. Transformer protection. [Online]. Available: <http://new.abb.com/substation-automation/systems/protection-solutions/transformer-protection> 94
- [130] N. A. E. R. Council, “Reliability concepts in bulk power electric systems,” 1985. 94

Bibliography

- [131] M. Shahidehpour, F. Tinney, and Y. Fu, "Impact of security on power systems operation," in *Proceedings of the IEEE*, 2005, pp. 2013 – 2025. 95
- [132] R. Billinton and R. Allan, *Reliability evaluation of power systems*. Pitman Advanced Publishing Program, 1984. 95
- [133] "IEEE guide for electric power distribution reliability indices - red-line," *IEEE Std 1366-2012 (Revision of IEEE Std 1366-2003) - Red-line*, pp. 1–92, May 2012. 95
- [134] Z. Bie, P. Zhang, G. Li, B. Hua, M. Meehan, and X. Wang, "Reliability evaluation of active distribution systems including microgrids," in *2013 IEEE Power Energy Society General Meeting*, July 2013, pp. 1–1. 96
- [135] A. Golieva, "Low short circuit ratio connection of wind power plants," Master of Science Thesis, Delft Technical University, 2015. 96
- [136] M. Bollen, *Integration of Distributed Generation in the Power System*, ser. IEEE Press Series on Power Engineering. John Wiley & Sons, 2011. 96
- [137] K. Lindén, B. Jacobson, M. Bollen, and J. Lundquist, "Reliability study methodology for HVDC grids," in *B4-108 CIGRÉ*, 2010. 97
- [138] D. Antoniou, A. Tzimas, and S. M. Rowland, "Transition from alternating current to direct current low voltage distribution networks," *IET Generation, Transmission Distribution*, vol. 9, no. 12, pp. 1391–1401, 2015. 97
- [139] J.-F. Bessède, *Eco-friendly Innovations in Electricity Transmission and Distribution Networks*, ser. Woodhead Publishing Series in Energy. Elsevier, 2014. 98
- [140] P. Kundur, J. Paserba, V. Ajjarapu, G. Andersson, A. Bose, C. Canizares, N. Hatziargyriou, D. Hill, A. Stankovic, C. Taylor, T. V. Cutsem, and V. Vittal, "Definition and classification of power system stability IEEE/CIGRE joint task force on stability terms and definitions," *IEEE Transactions on Power Systems*, vol. 19, no. 3, pp. 1387–1401, Aug 2004. 99
- [141] M. A. Peñalba, O. Gomis-Bellmunt, and M. Martins, "Coordinated control for an offshore wind power plant to provide fault ride through

- capability,” *IEEE Transactions on Sustainable Energy*, vol. 5, no. 4, pp. 1253–1261, Oct 2014. 100
- [142] A. Colet-Subirachs, O. Gomis-Bellmunt, D. Clos-Costa, G. Martin-Segura, A. J. Ferre, and L. F. Marti, “Electromechanical modelling and control of a micro-wind generation system for isolated low power DC micro grids,” in *Power Electronics and Applications, 2009. EPE '09. 13th European Conference on*, Sept 2009, pp. 1–10. 100
- [143] J. Bömer, K. Burges, and C. Nabe, “All island tso facilitation of renewables studies,” accessed on 18-11-2016. [Online]. Available: <http://www.ecofys.com/en/publication/all-island-tso-facilitation-of-renewables-studies/> 102
- [144] F. M. Uriarte, C. Smith, S. VanBroekhoven, and R. E. Hebner, “Microgrid ramp rates and the inertial stability margin,” *IEEE Transactions on Power Systems*, vol. 30, no. 6, pp. 3209–3216, Nov 2015. 103
- [145] S. V. Iyer, M. N. Belur, and M. C. Chandorkar, “A generalized computational method to determine stability of a multi-inverter microgrid,” *IEEE Transactions on Power Electronics*, vol. 25, no. 9, pp. 2420–2432, Sept 2010. 103
- [146] E. Barklund, N. Pogaku, M. Prodanovic, C. Hernandez-Aramburu, and T. C. Green, “Energy management in autonomous microgrid using stability-constrained droop control of inverters,” *IEEE Transactions on Power Electronics*, vol. 23, no. 5, pp. 2346–2352, Sept 2008. 103
- [147] M. Yazdanian and A. Mehrizi-Sani, “Distributed control techniques in microgrids,” *IEEE Transactions on Smart Grid*, vol. 5, no. 6, pp. 2901–2909, Nov 2014. 104
- [148] J. Wu and X. Guan, “Coordinated multi-microgrids optimal control algorithm for smart distribution management system,” *IEEE Transactions on Smart Grid*, vol. 4, no. 4, pp. 2174–2181, Dec 2013. 105
- [149] F. Díaz-González, M. Hau, A. Sumper, and O. Gomis-Bellmunt, “Participation of wind power plants in system frequency control: Review of grid code requirements and control methods,” *Renewable and Sustainable Energy Reviews*, vol. 34, no. Supplement C, pp. 551 – 564, 2014. [Online]. Available: <http://www.sciencedirect.com/science/article/pii/S1364032114002019> 108

Bibliography

- [150] J. Pegueroles-Queralt, F. Bianchi, and O. Gomis-Bellmunt, "Optimal droop control for voltage source converters in islanded microgrids," *IFAC Proceedings Volumes*, vol. 45, no. 21, pp. 566 – 571, 2012, 8th Power Plant and Power System Control Symposium. [Online]. Available: <http://www.sciencedirect.com/science/article/pii/S1474667016320316> 108
- [151] FP7 smart rural grid project. Accessed: 22/11/2017. [Online]. Available: <http://smartruralgrid.eu/> 109
- [152] A. Osterwalder, Y. Pigneur, and C. Tucci, "Clarifying Business Models: Origins, Present, and Future of the Concept," *Communication of the association for Information Systems*, vol. 16, Article 1, pp. 1–25, 2005. 110
- [153] A. Osterwalder and Y. Pigneur, *A handbook for visionaries, game changers, and challengers*. John Wiley & Sons, 2010. 110
- [154] K. Ubilla, G. A. Jiménez-Estévez, R. Hernández, L. Reyes-Chamorro, C. H. Irigoyen, B. Severino, and R. Palma-Behnke, "Smart microgrids as a solution for rural electrification: Ensuring long-term sustainability through cadastre and business models," *IEEE Transactions on Sustainable Energy*, vol. 5, no. 4, pp. 1310–1318, Oct 2014. 110
- [155] J. Knuckles, "Business models for mini-grid electricity in base of the pyramid markets," *Energy for Sustainable Development*, vol. 31, pp. 67 – 82, 2016. [Online]. Available: <http://www.sciencedirect.com/science/article/pii/S0973082615001349> 110
- [156] K. Kok and S. Widergren, "A society of devices: Integrating intelligent distributed resources with transactive energy," *IEEE Power and Energy Magazine*, vol. 14, no. 3, pp. 34–45, May 2016. 111
- [157] The GridWise Architecture Council, "GridWise Transactive Energy Framework Version 1.0," Tech. Rep., 2015. [Online]. Available: https://www.gridwiseac.org/pdfs/te_framework_report_pnnl-22946.pdf 111
- [158] D. Gregoratti and J. Matamoros, "Distributed energy trading: The multiple-microgrid case," *IEEE Transactions on Industrial Electronics*, vol. 62, no. 4, pp. 2551–2559, April 2015. 111
- [159] P. Olivella-Rosell, G. Viñals-Canal, A. Sumper, R. Villafafila-Robles, B. A. Bremsdal, I. Ilieva, and S. Ø. Ottesen, "Day-ahead micro-market

- design for distributed energy resources,” in *2016 IEEE International Energy Conference (ENERGYCON)*, April 2016, pp. 1–6. 111
- [160] I. Ilieva, B. Breindal, S. Ø. Ottesen, J. Rajasekharan, and P. Olivella-Rosell, “Design characteristics of a smart grid dominated local market,” in *CIRED Workshop 2016*, June 2016, pp. 1–4. 111
- [161] H. S. V. S. K. Nunna and D. Srinivasan, “Multiagent-based transactive energy framework for distribution systems with smart microgrids,” *IEEE Transactions on Industrial Informatics*, vol. 13, no. 5, pp. 2241–2250, Oct 2017. 111
- [162] A. Majzoobi and A. Khodaei, “Application of microgrids in providing ancillary services to the utility grid,” *Energy*, vol. 123, pp. 555 – 563, 2017. [Online]. Available: <http://www.sciencedirect.com/science/article/pii/S0360544217301202> 111
- [163] P. Piagi and R. H. Lasseter, “Autonomous control of microgrids,” in *2006 IEEE Power Engineering Society General Meeting*, 2006, pp. 8 pp.–. 117
- [164] S. J. Ahn, J. W. Park, I. Y. Chung, S. I. Moon, S. H. Kang, and S. R. Nam, “Power-sharing method of multiple distributed generators considering control modes and configurations of a microgrid,” *IEEE Trans. on Power Delivery*, vol. 25, no. 3, pp. 2007–2016, July 2010. 117
- [165] V. R. Pandi, A. Al-Hinai, and A. Feliachi, “Adaptive coordinated feeder flow control in distribution system with the support of distributed energy resources,” *International Journal of Electrical Power and Energy Systems*, vol. 85, pp. 190 – 199, 2017. 117
- [166] ——, “Coordinated control of distributed energy resources to support load frequency control,” *Energy Conversion and Management*, vol. 105, pp. 918 – 928, 2015. 117
- [167] S. J. Ahn, S. R. Nam, J. H. Choi, and S. I. Moon, “Power scheduling of distributed generators for economic and stable operation of a microgrid,” *IEEE Trans. on Smart Grid*, vol. 4, no. 1, pp. 398–405, March 2013. 117, 118, 130
- [168] Z. xia Xiao, J. M. Guerrero, J. Shuang, D. Sera, E. Schaltz, and J. C. Vásquez, “Flat tie-line power scheduling control of grid-connected hybrid microgrids,” *Applied Energy*, 2017. 117

Bibliography

- [169] R. Majumder, A. Ghosh, G. Ledwich, and F. Zare, “Power management and power flow control with back-to-back converters in a utility connected microgrid,” *IEEE Trans. on Power Systems*, vol. 25, no. 2, pp. 821–834, May 2010. 117
- [170] M. Farivar and S. H. Low, “Branch flow model: Relaxations and convexification - part i,” *IEEE Trans. on Power Systems*, vol. 28, no. 3, pp. 2554–2564, Aug 2013. 118, 119, 127
- [171] B. P. Swaminathan, “Operational Planning of Active Distribution Networks - Convex Relaxation under Uncertainty,” Theses, Université Grenoble Alpes, Sep. 2017. 118, 119, 130
- [172] Y. Levron, J. M. Guerrero, and Y. Beck, “Optimal power flow in microgrids with energy storage,” *IEEE Transactions on Power Systems*, vol. 28, no. 3, pp. 3226–3234, Aug 2013. 118
- [173] M. Baran and F. F. Wu, “Optimal sizing of capacitors placed on a radial distribution system,” *IEEE Trans. on Power Delivery*, vol. 4, no. 1, pp. 735–743, Jan 1989. 119
- [174] M. E. Baran and F. F. Wu, “Network reconfiguration in distribution systems for loss reduction and load balancing,” *IEEE Trans. on Power Delivery*, vol. 4, no. 2, pp. 1401–1407, Apr 1989. 130
- [175] C. Monteiro, T. Santos, L. A. Fernandez-Jimenez, I. J. Ramirez-Rosado, and M. S. Terreros-Olarde, “Short-term power forecasting model for photovoltaic plants based on historical similarity,” *Energies*, vol. 6, no. 5, pp. 2624–2643, 2013. 133
- [176] D. P. Larson, L. Nonnenmacher, and C. F. Coimbra, “Day-ahead forecasting of solar power output from photovoltaic plants in the american southwest,” *Renewable Energy*, vol. 91, pp. 11 – 20, 2016. 133
- [177] H. Chitsaz, H. Shaker, H. Zareipour, D. Wood, and N. Amjady, “Short-term electricity load forecasting of buildings in microgrids,” *Energy and Buildings*, vol. 99, pp. 50 – 60, 2015. 133

Chapter 9

Publications

9.1 Related journal articles

- Eduard Bullich-Massagué, Ricard Ferrer-San-José, Mònica Aragüés-Peñaiba, Luis Serrano-Salamanca, Carlos Pacheco-Navas, Oriol Gomis-Bellmunt, “Power plant control in large-scale photovoltaic plants: design, implementation and validation in a 9.4 MW photovoltaic plant”, IET Renewable Power Generation, Vol. 10, no. 1, pp. 50-62, Jan. 2016, doi:10.1049/iet-rpg.2015.0113.
- Eduard Bullich-Massagué, Mònica Aragüés-Peñaiba, Andreas Sumper, Oriol Boix-Aragones, “Active power control in a hybrid PV-storage power plant for frequency support”, Solar Energy, Elsevier, Vol. 144 (Mar. 2017), pp. 49-62, doi:10.1016/j.solener.2016.12.033.
- Eduard Bullich-Massagué, Francisco Díaz-Gonzàlez, Mònica Aragüés-Peñaiba, Francesc Girbau-Llistuella, Pol Olivella-Rosell, Andreas Sumper, “Microgrid clustering architectures”, Applied Energy, Elsevier, Vol. 212 (Feb. 2018), pp. 340-361, doi:10.1016/j.apenergy.2017.12.048.
- Eduard Bullich-Massagué, Mònica Aragüés-Peñaiba, Eduardo Prieto-Araujo, Andreas Sumper, Raphael Caire, “Optimal Feeder flow control for grid connected microgrids”, IEEE trans. on Smart Grid, *under review*.

9.2 Related conference papers

- Eduard Bullich-Massagué, Ricard Ferrer-San-José, Mònica Aragüés-Peñaiba, Luis Serrano-Salamanca, Carlos Pacheco-Navas, Oriol Gomis-Bellmunt, “Power plant control experience in large scale PV plant.

Modelling, control, simulation and implementation” in 4th Solar integration workshop, Berlin, Germany, November 2014. *Best papers award.*

9.3 Other Publications

This section presents other relevant journal and conference publications not directly related to the thesis.

9.3.1 Other journal articles

- Eduard Bullich-Massagué, Andreas Sumper, Roberto Villafafila-Robles, Joan Rull-Duran, “Optimization of surge arrester locations in overhead distribution networks”, Power Delivery, IEEE Transactions on, Vol. 30, no. 2, pp. 674-683, Apr. 2015, doi: 10.1109/TPWRD.2014.2312077.
- Ana Cabrera-Tobar, Eduard Bullich-Massagué, Mònica Aragüés-Peñalba, Oriol Gomis-Bellmunt, “Topologies for large scale photovoltaic power plants”, Renewable and Sustainable Energy Reviews, Elsevier, Vol. 59 (Jun. 2016), pp. 309-319, doi:10.1016/j.rser.2015.12.362.
- Ana Cabrera-Tobar, Eduard Bullich-Massagué, Mònica Aragüés-Peñalba, Oriol Gomis-Bellmunt, “Review of advanced grid requirements for the integration of large scale photovoltaic power plants in the transmission system”, Renewable and Sustainable Energy Reviews, Elsevier, Vol. 62 (Sep. 2016), pp. 971-987, doi:10.1016/j.rser.2016.05.044.
- Ana Cabrera-Tobar, Eduard Bullich-Massagué, Mònica Aragüés-Peñalba, Oriol Gomis-Bellmunt, “Capability curve analysis of photovoltaic generation systems”, Solar Energy, Elsevier, Vol. 140 (Dec. 2016), pp. 255-264, doi:10.1016/j.solener.2016.11.014.
- Pau Lloret-Gallego, Mònica Aragüés-Peñalba, Lien Van Schepdael, Eduard Bullich-Massagué, Pol Olivella-Rosell, Andreas Sumper, “Methodology for the evaluation of resilience of ICT systems for smart distribution grids”, Energies, Vol. 10, no. 9 (Aug. 2017), doi:10.3390/en10091287.
- Pol Olivella-Rosell, Eduard Bullich-Massagué, Mònica Aragüés-Peñalba, Andreas Sumper, Stig Ødegaard Ottesen, Josep-Andreu Vidal-Clos,

Roberto Villafáfila-Robles, “Optimization problem for meeting distribution system operator requests in local flexibility markets with distributed energy resources”, Applied Energy, Elsevier, Vol. 210 (Jan. 2018), pp. 881-895, doi:10.1016/j.apenergy.2017.08.136.

9.3.2 Other conference papers

- Ana Cabrera-Tobar, Eduard Bullich-Massagué, Mònica Aragüés-Peñaiba, Oriol Gomis-Bellmunt, “Reactive power capability analysis of a photovoltaic generator for large scale power plants”, in 5th IET International Conference on Renewable Power Generation (RPG) 2016, London, UK, September 2016, doi:10.1049/cp.2016.0574.
- Eduard Bullich-Massagué, Mònica Aragüés-Peñaiba, Pol Olivella-Rosell, Pau Lloret-Gallego, Josep-Andreu Vidal-Clos, Andreas Sumper, “Architecture definition and operation testing of local electricity markets. The EMPOWER project”, in 2017 International Conference on Modern Power Systems (MPS), Cluj-Napoca, Romania, June 2017, doi:10.1109/MPS.2017.7974447.
- Marc Galceran-Feixas, Mònica Aragüés-Peñaiba, Eduard Bullich-Massagué, Josep-Andreu Vidal-Clos, Oriol Gomis-Bellmunt, “Multi-period power management optimization for operating isolated hybrid microgrids”, in 2017 IEEE PES Innovative Smart Grid Technologies Conference Europe (ISGT-Europe), Torino, Italy, September 2017, doi: 10.1109/ISGTEurope.2017.8260208.
- Josep-Andreu Vidal-Clos, Eduard Bullich-Massagué, Mònica Aragüés-Peñaiba, Guillem Vinyals-Canal, Cristian Chillón-Antón, Eduardo Prieto-Araujo, Oriol Gomis-Bellmunt, “Energy management system for islanded microgrids comprising PV systems, diesel generators, energy storage systems: validation in a laboratory environment” in 3rd Hybrid power systems workshop, Tenerife, Spain, May. 2018.

Appendix A

Simulation model of Vanju-Mare PV power plant

This Appendix provides the electrical data of the Vanju Mare PV power plant modelled and described in Chapter 3. For the purpose of readability, PV power plant layout is shown below in Figure A.1.

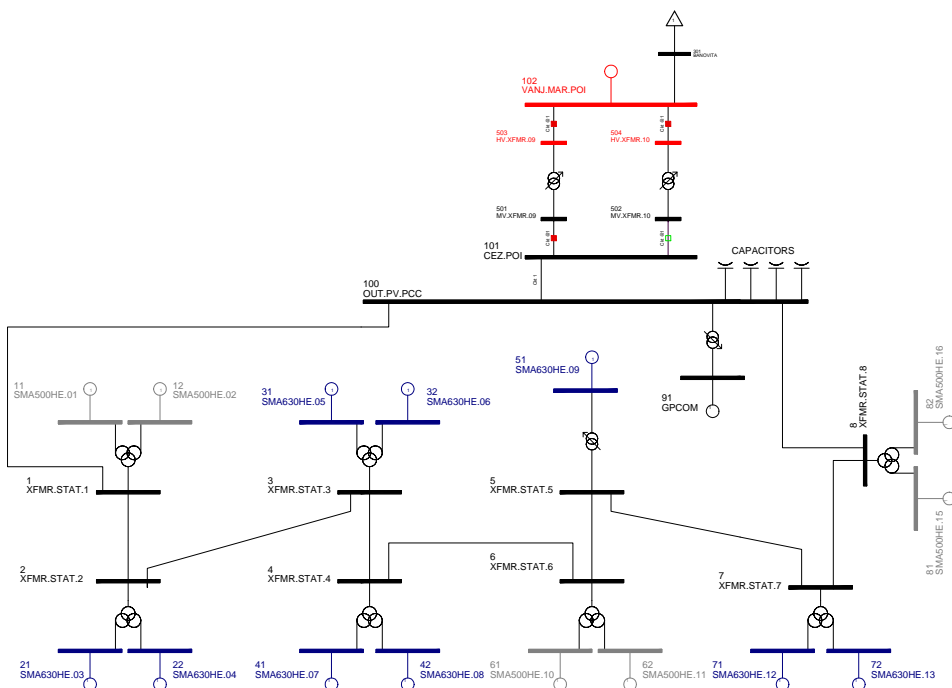


Figure A.1: Scheme of Vanju-Mare PV plant simulation model in PSS/E[®].
Red = 100 kV, black = 20 kV, blue = 0.315 kV, grey = 0.27 kV

A.1 Electrical data

Tables A.1-A.5 summarize the simulation model parameters.

Table A.1: Grid nodes

Node	Name	Voltage [kV]
1	XFMR.STAT.1	20
2	XFMR.STAT.2	20
3	XFMR.STAT.3	20
4	XFMR.STAT.4	20
5	XFMR.STAT.5	20
6	XFMR.STAT.6	20
7	XFMR.STAT.7	20
8	XFMR.STAT.8	20
11	SMA500HE.01	0.270
12	SMA500HE.02	0.270
21	SMA630HE.03	0.315
22	SMA630HE.04	0.315
31	SMA630HE.05	0.315
32	SMA630HE.06	0.315
41	SMA630HE.07	0.315
42	SMA630HE.08	0.315
51	SMA630HE.09	0.315
61	SMA500HE.10	0.270
62	SMA500HE.11	0.270
71	SMA630HE.12	0.315
72	SMA630HE.13	0.315
81	SMA500HE.15	0.270
82	SMA500HE.16	0.270
91	GPCOM	0.700
100	OUT.PV.PCC	20
101	CEZ.POI	20
102	VANJ.MAR.POI	110
301	BANOVITA	110
501	MV.XFMR.09	20
502	MV.XFMR.10	20
503	HV.XFMR.09	110
504	HV.XFMR.10	110

Table A.2: Equivalent grid data

Node	Name	Voltage [kV]	Short circuit power [MVA]	Short circuit ratio (X/R)
102	Vanj.MAR.POI	110	1000	10

Table A.3: Line data

Node 1	Node 2	Line R [Ω]	Line X [Ω]	Line C [μF]
1	2	0.0244	0.0201	0.0597
2	3	0.0863	0.0107	0.2111
3	4	0.0293	0.0241	0.0716
4	6	0.0494	0.0407	0.1209
5	6	0.0244	0.0201	0.0597
5	7	0.0731	0.0603	0.0179
7	8	0.0540	0.0445	0.1322
1	100	0.0423	0.0348	0.1034
8	100	0.1313	0.1082	0.3213
100	101	0.3605	0.2013	1.771
102	301	0.0000	0.0121	0.0000

Table A.4: 3 winding transformer data

Node 1	Node 2	Node 3	V_p [kV]	V_s [kV]	V_t [kV]	S_{nom} [MVA]	$r + jx$ [p.u]
1	11	12	20	0.27	0.27	1 (p)	0.0053+j0.0592 (p-s)
						0.5 (s)	0.0059+j0.0597 (p-t)
						0.5 (t)	0.0055+j0.0592 (s-t)
2	21	22	20	0.315	0.315	1.26 (p)	0.0050+j0.0598 (p-s)
						0.63 (s)	0.0042+j0.0599 (p-t)
						0.63 (t)	0.0051+j0.0598 (s-t)
3	31	32	20	0.315	0.315	1.26 (p)	0.0050+j0.0598 (p-s)
						0.63 (s)	0.0042+j0.0599 (p-t)
						0.63 (t)	0.0051+j0.0598 (s-t)
4	41	42	20	0.315	0.315	1.26 (p)	0.0050+j0.0598 (p-s)
						0.63 (s)	0.0042+j0.0599 (p-t)
						0.63 (t)	0.0051+j0.0598 (s-t)
6	61	62	20	0.27	0.27	1 (p)	0.0053+j0.0592 (p-s)
						0.5 (s)	0.0059+j0.0597 (p-t)
						0.5 (t)	0.0055+j0.0592 (s-t)
7	71	72	20	0.315	0.315	1.26 (p)	0.0050+j0.0598 (p-s)
						0.63 (s)	0.0042+j0.0599 (p-t)
						0.63 (t)	0.0051+j0.0598 (s-t)
8	81	82	20	0.27	0.27	1 (p)	0.0053+j0.0592 (p-s)
						0.5 (s)	0.0059+j0.0597 (p-t)
						0.5 (t)	0.0055+j0.0592 (s-t)

*p - primary; *s - secondary; *t - tertiary

Appendix A Simulation model of Vanju-Mare PV power plant

Table A.5: 2 winding transformer data

Node 1	Node 2	V_P [kV]	V_s [kV]	S_{nom} [MVA]	r [p.u]	x [p.u]
503	501	110	20	16	0.0	0.676
504	502	110	20	10 (out of service)	0.0	0.112
100	91	20	0.69	2	0.0	0.06
5	51	20	0.315	0.63	0.0114	0.0589

Appendix B

Working principle of the measurement filter for improving the ramp rate performance

Let us consider the ramp rate control scheme of Figure 4.4 and the same scheme but filtering the $P_{pcc-meas}(t)$, see Figure 4.5(a). Now, we apply a PV power step and analyse the response of the system in Figures B.1 and B.2 (the response under a real PV profile can be observed above in Figure 4.6).

Figure B.1 shows the performance according to the control scheme without the proposed filter. In this case, once the PV power drops, the controller (executed each $T_s = 100$ ms) detects the ramp event by comparing the actual PV measurement (red) and the previous PCC measurement $P_{pcc-meas}(t-T_w)$ (dashed black) and computes the required setpoint to the battery. Due to the communication delays and plant dynamics, the setpoint is not applied instantaneously. So, The PCC power (blue) drops transiently until the battery reacts. This will be a problem after T_w seconds as the measured power $P_{pcc-meas}(t - T_w)$ will drop despite the PV power remains constant (see the second oscillation in zoomed area). This fact, will be understood as an up-ramp event and a power oscillation will occur. It happens each T_w seconds. So, the result is that PCC power presents power oscillations of a period T_w .

Figure B.2 shows the performance according to the proposed control scheme with filter. As it can be observed, at the beginning of the ramp event the system behaves exactly in the same way. After T_w seconds, the measured power $P_{pcc-meas}(t - T_w)$ (not shown in the plot) drops in the same way. But in this control scheme, the controller uses the power filtered ($P_{pcc-filt}(t - T_w)$, black dashed). So, the initial transient in $P_{pcc-meas}$ is not observed by the controller and the power oscillations during the ramp event are mitigated. Note that as the controlled variable (ΔP_{max} and ΔP_{min}) depends on a time window and the filter adds a delay, it has to be taken into account in the

ramp rate calculation as explained before.

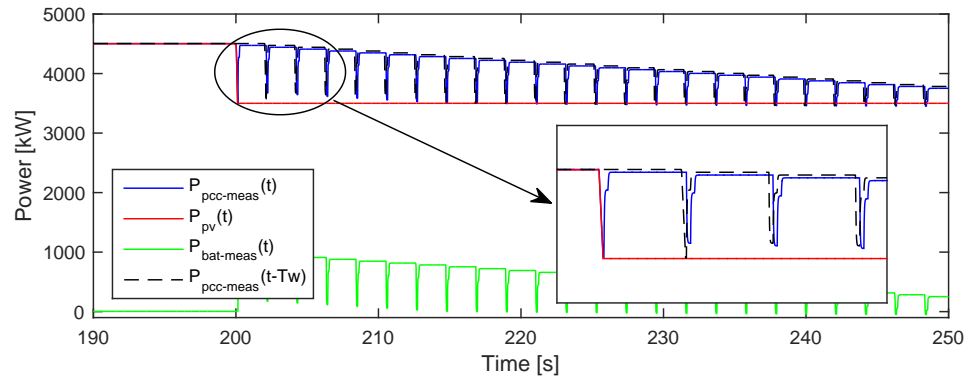


Figure B.1: Ramp rate response after a 1 MW PV power step at second 200. Conventional method without the filter

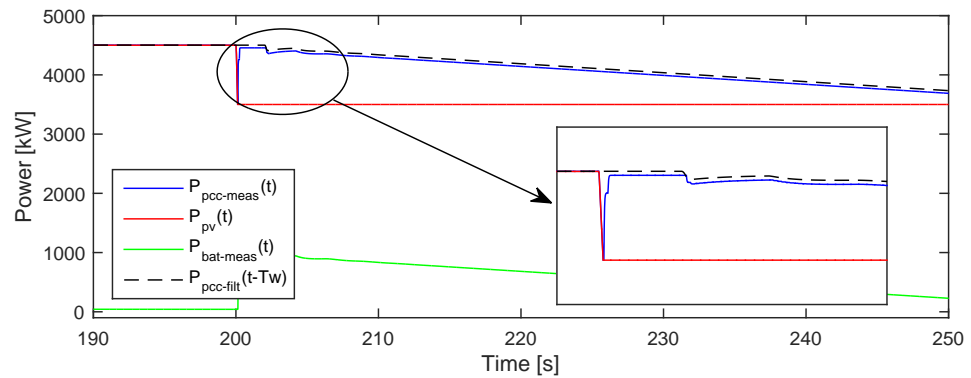


Figure B.2: Ramp rate response after a 1 MW PV power step at second 200. Proposed method: filter applied

Appendix C

Simplified simulation model of Vanju-Mare PV power plant

To be able to simulate several complete days, a simplified model of the PV power plant is used. As only the active power is studied, the model considers an equivalent PV generator and a battery energy storage. The equivalent PV generator represents the PV arrays plus the PV inverters. Based on the observation of SMA PV inverter dynamics, it is modelled as a first order function (Figure C.1), where the input is the PV inverter setpoint α in per unit system. If we consider several PV inverters, each PV inverter i computes its local setpoint according to (C.1), where $P_{nom,i}$ is the nominal power of the inverter i . As we consider an aggregated PV inverter, $P_{nom,i} = P_{plant}$. The output is the PV power P_{pv} , which is limited to a power profile (P_{pv-av} , available PV power obtained from real measurements).

$$P_{pv-set,i}^* = \alpha \cdot P_{nom,i} \quad (\text{C.1})$$

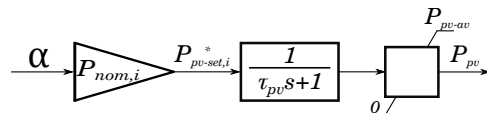


Figure C.1: Simplified PV generator model

The storage model represents a battery and its associated inverter and is also modelled as a first order function to simulate its dynamics. The output of the first order function is saturated according to (C.2) and (C.3). The saturation prevents the model to inject power ($P > 0$) if the $SOC = 0$ and to store power ($P < 0$) if $SOC = 1$ and limits the maximum power to be injected or consumed to its nominal power $P_{bat-nom}$. The SOC of the battery is calculated taking into account its efficiency η_{bat} (see Figure C.2).

$$P_{bat-max} = \begin{cases} P_{bat-nom} & \text{if } SOC > 0 \\ 0 & \text{if } SOC = 0 \end{cases} \quad (\text{C.2})$$

$$P_{bat-min} = \begin{cases} -P_{bat-nom} & \text{if } SOC < 1 \\ 0 & \text{if } SOC = 1 \end{cases} \quad (\text{C.3})$$

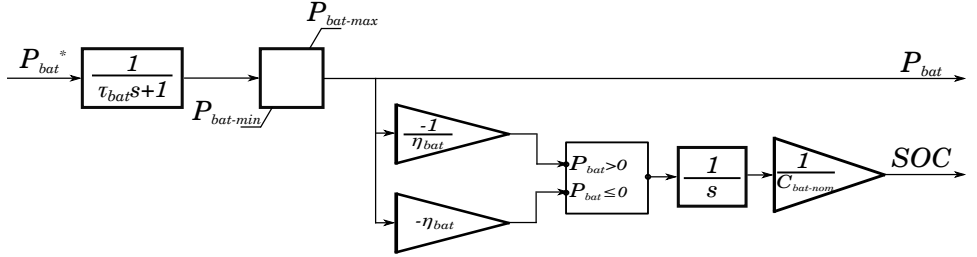


Figure C.2: Simplified Battery model

The model also takes into account communications delays, τ_{com} . Frequency deviations can be simulated by changing f_{meas} in order to test the frequency droop operation. Figure C.3 depicts the complete model including the PPC.

The characteristics of the power plant are shown in Table C.1. The PI controller of the PPC has been tuned empirically. Note that in LS-PVPP projects there are many actors and some information needed for an accurate tuning is often missing. From the available information, the PV plant model has been obtained (see Appendix A). From this model, the proportional gains of the active power and reactive power central controller have been adjusted to obtain a response fast enough to comply with the grid code. Then, the integral gains have been adjusted to ensure a null steady state error.

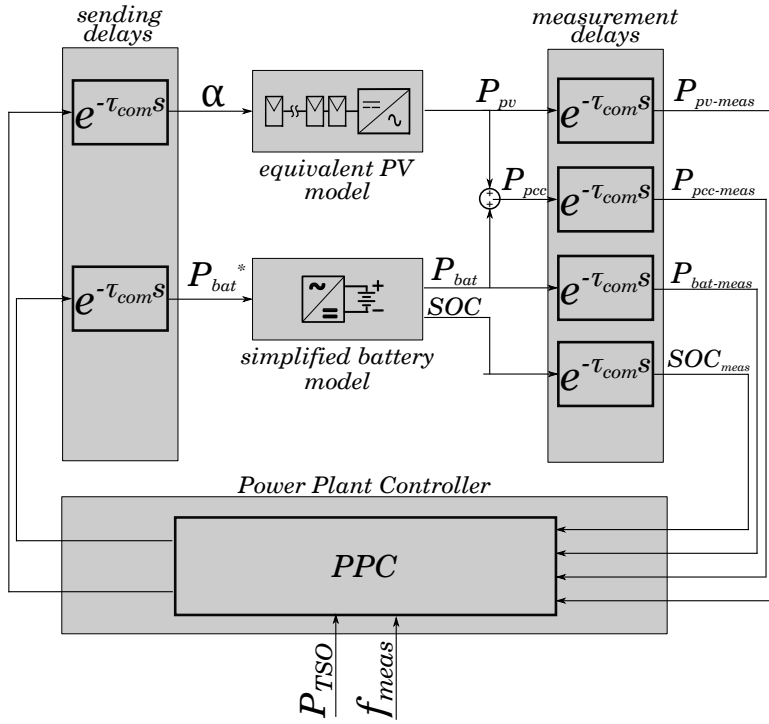


Figure C.3: Simplified model of the hybrid PV-storage power plant

Table C.1: Parameters used in the simulation

Parameter	Value	Parameter	Value
P_{plant}	9.4 MW	τ_{pv}	100 ms
P_{bat_max}	1 MW	τ_{bat}	10 ms
P_{bat_min}	-1 MW	η_{bat}	0.90
C_{bat_nom}	167 kWh	τ_{com}	20 ms
T_w	2 s	T_s	100 ms
RR_{max}	10 %	RR_{min}	-10 %
K_{p-pv}	0.05	K_{i-pv}	1
K_{w-pv}	10	K_{SOC}	1880
τ_{meas}	1 s	f_{min}	47 Hz
f_1	49.5 Hz	f_2	49.8 Hz
f_n	50 Hz	f_3	50.2 Hz
f_4	52 Hz	f_{max}	53 Hz

Appendix D

IEEE 33-Bus distribution system data

The IEEE 33-Bus distribution system data used in Chapter 6 is presented in Tables D.1 and D.2. The rest of the parameters of the base case are shown in Table D.3. The costs of importing energy from the grid (the cost of generator 1, i.e. the slack node) is obtained based on the Spanish market costs at 12.6 kV. It has been considered the energy cost, the grid access tariffs and taxes. For convenience, the grid scheme is reproduced below in Figure D.1.

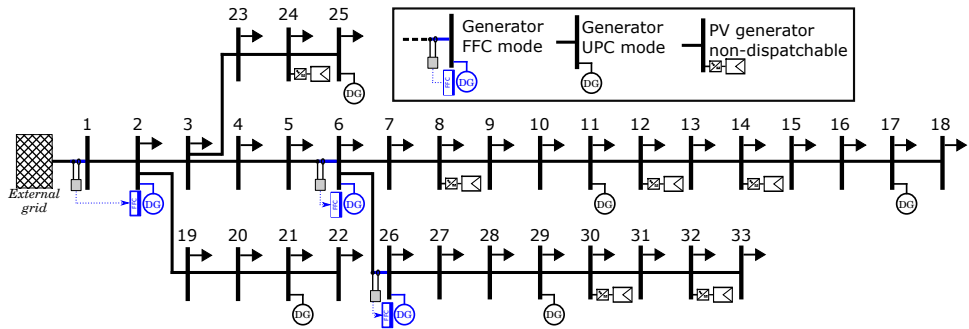


Figure D.1: Scheme of IEEE 33-Bus distribution system

Appendix D IEEE 33-Bus distribution system data

Table D.1: Bus data

Bus Id	P^C [kW]	Q^C [kVar]	P^{Gmax} [kW]	P^{Gmin} [kW]	Q^{Gmax} [kVar]	Q^{Gmin} [kVar]	C^{ag} [€/h]	C^{bg} [€/kWh]
1	0	0	999999	-999999	999999	-999999	0.000	0.103
2	100	60	1500	450	750	-750	14.530	0.083
3	90	40	0	0	0	0	0	0
4	120	80	0	0	0	0	0	0
5	60	30	0	0	0	0	0	0
6	60	20	800	270	400	-400	14.530	0.103
7	200	100	0	0	0	0	0	0
8	200	100	80	0	0	0	0	0
9	60	20	0	0	0	0	0	0
10	60	20	0	0	0	0	0	0
11	45	30	200	70	100	-100	5.080	0.035
12	60	35	30	0	0	0	0	0
13	60	35	0	0	0	0	0	0
14	120	80	90	0	0	0	0	0
15	60	10	0	0	0	0	0	0
16	60	20	0	0	0	0	0	0
17	60	20	250	80	125	-125	5.080	0.035
18	90	40	0	0	0	0	0	0
19	90	40	0	0	0	0	0	0
20	90	40	0	0	0	0	0	0
21	90	40	400	130	200	-200	0.851	0.069
22	90	40	0	0	0	0	0	0
23	90	50	0	0	0	0	0	0
24	420	200	200	0	0	0	0	0
25	420	200	200	70	100	-100	0.851	0.069
26	60	25	700	230	350	-350	14.530	0.103
27	60	25	0	0	0	0	0	0
28	60	20	0	0	0	0	0	0
29	120	70	300	100	150	-150	3.405	0.013
30	200	600	150	0	75	-75	0	0
31	150	70	0	0	0	0	0	0
32	210	100	150	0	0	0	0	0
33	60	40	0	0	0	0	0	0

Table D.2: Line data

From bus	To bus	r [Ω]	x [Ω]	i^{max} [A^2]	From bus	To bus	r [Ω]	x [Ω]	i^{max} [A^2]
1	2	0.0922	0.0470	10^6	17	18	0.7320	0.5740	10^6
2	3	0.4930	0.2511	10^6	2	19	0.1640	0.1565	10^6
3	4	0.3660	0.1864	10^6	19	20	1.5042	1.3554	10^6
4	5	0.3811	0.1941	10^6	20	21	0.4095	0.4784	10^6
5	6	0.8190	0.7070	10^6	21	22	0.7089	0.9373	10^6
6	7	0.1872	0.6188	10^6	3	23	0.4512	0.3083	10^6
7	8	0.7114	0.2351	10^6	23	24	0.8980	0.7091	10^6
8	9	1.0300	0.7400	10^6	24	26	0.8960	0.7011	10^6
9	10	1.0440	0.7400	10^6	6	26	0.2030	0.1034	10^6
10	11	0.1966	0.0650	10^6	26	27	0.2842	0.1447	10^6
11	12	0.3744	0.1238	10^6	27	28	1.0590	0.9337	10^6
12	13	1.4680	1.1550	10^6	28	29	0.8042	0.7006	10^6
13	14	0.5416	0.7129	10^6	29	30	0.5075	0.2585	10^6
14	15	0.5910	0.5260	10^6	30	31	0.9744	0.9630	10^6
15	16	0.7463	0.5450	10^6	31	32	0.3105	0.3619	10^6
16	17	1.2890	1.7210	10^6	32	33	0.3410	0.5302	10^6

Table D.3: Additional parameters

Parameter	Value
v^{max} [p.u.]	1.21*
v^{min} [p.u.]	0.81*
v^* [p.u.]	1
C^{affp}, C^{affq} [€]	0
C^{bfff_p} [€/kW]	2.4
C^{bfff_q} [€/kVar]	2.4
M_1, M_2, M_3	10^{**}
$\Delta C'$ [€]	Depends on the algorithm 1
N_s (number of scenarios)	10
$FFP_n^* _{n=1}$ [kW]	750
$FFQ_n^* _{n=1}$ [kVar]	500

* v^{max} and v^{min} is square voltage. It is equivalent to

$0.9 \leq V \leq 1.1$

** Is large enough considering that the formulation has been done in p.u. $S_{Base} = 1$ [MVA], $V_{base} = 12.66$ [kV]

